Neutrophilic Immune Response against
Pseudomonas aeruginosa and *Staphylococcus aureus*
Skin Wound Infections

By

ALEX VARGAS
DISSERTATION

Submitted in partial satisfaction of the requirements for the degree of

DOCTOR OF PHILOSOPHY

in

Biomedical Engineering

in the

OFFICE OF GRADUATE STUDIES

of the

UNIVERSITY OF CALIFORNIA

DAVIS

Approved:

Scott Simon, Chair

Nicole Baumgarth

Renee Tsolis

Committee in Charge

2024

ACKNOWLEDGEMENTS

I extend my gratitude to Dr. Scott Simon for his mentorship during the past 4 years. I also deeply appreciate the invaluable insight and guidance of my committee members, Dr. Nicole Baumgarth and Dr. Reneé Tsolis, during the preparation for my qualifying exam and through the completion of this dissertation. Their insights have been instrumental in making me a better scientist and in shaping the trajectory of my academic and professional journey.

I also would like to thank all the individuals with whom I had the opportunity to collaborate. Dr. Kevin Francis from PerklinElmer, who helped us during the acquisition of our IVIS Spectrum and during the development of the S1008A-FFLuc mouse line. Stefan Lundgren and Dr. Sean Collings, who helped with the *in vitro* PMN chemotaxis assays. Dr. L. Edward Clemens who collaborated extensively with us on the RP557 studies. Dr. Tomas Gonzales-Fernandez and Evan Cirves who I had the pleasure to work with on the HSPC in GelMA project. Additionally, I would like to thank Dr. Maryam Rahmati and Dr. Augustine Saiz for their indispensable support on histological imaging and analysis.

I also would like to recognize the amazing undergraduate students who I had the opportunity to mentor at one point or another during my PhD, several whom have already graduated and are leading great careers in industry: Alaia Sima, Sita Sanigepalli, Brayden Chipman, and Blanca Osorio. Last but not least, I would like to thank current and former members of the Simon Lab for their support and camaraderie, which significantly enriched my experience at UC Davis. Special thanks to Megan Westerland, Sharon Chen, Gustavo Garcia, Lissette Werba, Jules Madigan, Mable Orser, Vasilios Morikis, and Alfredo Hernandez.

TABLE OF CONTENTS

LIST OF FIGURES

LIST OF ABBREVIATIONS

AMR	Antimicrobial-Resistant
ANOVA	Analysis of Variance
AP-1	Activating Protein-1
BSA	Bovine Serum Albumin
CFU	Colony Forming Unit
CO_2	Carbon Dioxide
CXCL	C-X-C-Motif Ligand (*e.g.* CXCL1, CXCL12)
CXCR	CXC-Motif Chemokine Receptor (*e.g.* CXCR2, CXCR4)
DAMP	Damage-Associated Molecular Pattern
DMSO	Dimethylsulfoxide
DFU	Diabetic Foot Ulcer
dHDP	Designed Host Defense Peptide
DPBS	Dulbecco's Phosphate Buffered Saline
EGFP	Enhanced Green Fluorescent Protein
FFLuc	Firefly Luciferase Reporter
Flt3	Fms-like Tyrosine Kinase 3
fMLP	N-Formylmethionyl-leucyl-phenylalanine (PMN chemotactic factor)
G-CSF	Granulocyte Colony-Stimulating Factor
GelMA	Gelatin Methacrylate
GMP	Granulocyte-Monocyte Progenitor
GR1	Ly-6G/Ly-6C Monoclonal Antibody (RB6-8C5)
HBSS	Hank's Balanced Salt Solution
HSPC	Hematopoietic Stem and Progenitor Cell
IFN	Interferon
IgG1	Rat IgG1 kappa Isotype Control Antibody (eBRG1)
IL-1β	Interleukin-1-beta
IRAK1	IL-1 Receptor-Associated Kinase 1
IRAK4	IL-1 Receptor-Associated Kinase 4
IRFs	Interferon Regulatory Factors
LB	Luria-Bertani Broth
LL-37	Cathelicidin
LPS	Lipopolysaccharide
LRR	Leucine-Rich Repeat

LTB4	Leukotriene B4
MAL	MyD88-Adapter-Like
MAPK	Mitogen-Activated Protein Kinase
MD-2	Myeloid Differentiation Factor 2
MDRPA	Multi-Drug Resistant *Pseudomonas aeruginosa*
MFI	Mean Fluorescence Intensity
MRSA	Methicillin-Resistant *Staphylococcus aureus*
MyD88	Myeloid Differentiation Primary Response 88
NET	Neutrophil Extracellular Trap
NF-kB	Nuclear Factor Kappa B
PA	*Pseudomonas aeruginosa*
Pam_3CSK_4	Pam3CysSerLys4 (TLR2/TLR1 Agonist)
PAMP	Pathogen-Associated Molecular Pattern
PBS	Phosphate-Buffered Saline
PFA	Paraformaldehyde
PI	Propidium Iodine
PMA	Phorbol Myristate Acetate
PMN	Polymorphonuclear Leukocyte
PRR	Pattern Recognition Receptor
Q-VD-OPH	Quinoline-Val-Asp-Difluorophenoxymethylketone (pan-caspase inhibitor)
RBC	Red Blood Cell
RIPA	Radioimmunoprecipitation assay buffer
ROI	Region of Interest
SA	*Staphylococcus aureus*
SCF	Stem Cell Factor
TAB	TAK1/TGF-b-Activated Kinase
TIR	Toll/IL-1 Receptor
TLR	Toll-Like-Receptor (*e.g.* TLR2 is Toll-like Receptor 2; TLR4 is Toll-like Receptor 4)
TNF-a	Tumor Necrosis Factor Alpha
TRAF6	Tumor Necrosis Factor Receptor-Associated Factor 6
TRIF	Toll/IL-1 Domain-Containing Adaptor Inducing Interferon-β
TSB	Tryptic Soy Broth
WT	Wild-Type
αT	Alpha-Toxin (*S. aureus* virulence factor)

ABSTRACT

Neutrophilic response against multi-drug resistant Staphylococcus aureus *and* Pseudomonas aeruginosa *infections in skin wounds*

Antibiotic resistant skin infections are an emerging threat to public health. This is driven by the ubiquitous nature of bacteria, their ability to thrive in hostile environments, and their molecular machinery that allows them to quickly develop mechanisms to render antibiotics ineffective. As a result, there is an urgent need to develop therapeutic approaches to treat bacterial infections without relying on antibiotics. Instead, there should be an emphasis on emerging treatments that rapidly and directly enhance immunity against pathogenic infections. Polymorphonuclear leukocytes (PMN) are the most abundant and important effector cells of the innate immune system and should be a primary target for strategies aimed at enhancing innate immunity. Three PMN-centered approaches are presented in this dissertation. The first one revolves around the development and testing of a designed host defense peptide (dHDP) that acts synergistically with PMN to tackle multi-drug resistant *S. aureus* infection in diabetic mouse wounds. The second approach involves optimizing PMN production and their antibacterial capacity *in vitro* with the objective of subsequently transferring these cells directly into a site of infection to enhance pathogen clearance. The third strategy aims at investigating signaling pathways that govern PMN functions against *S. aureus* and *P. aeruginosa*, with an emphasis on Toll-like receptor signaling and activation of the inflammasome.

Two pathogens of clinical interest are Methicillin-Resistant *Staphylococcus aureus* (MRSA) and Multi-Drug Resistant *Pseudomonas aeruginosa* (MDRPA). These are common sources of hospital and community-acquired skin infections in immunocompromised patients, including the elderly and people with diabetes. *S. aureus* is a gram-positive bacterium capable of forming biofilm and secreting virulence factors that can limit the ability of PMN to be recruited into sites of infection. As a result, therapeutic strategies should amplify PMN quantity and antibacterial functions. Studies presented in Chapter 3 demonstrate that the dHDP RP557 can enhance PMN antibacterial functions *in vitro*, suppress *S. aureus* proliferation, and enhance wound healing. The studies presented in Chapter 4 demonstrate that PMN production and antibacterial capacity can be enhanced through encapsulation of HSPCs in a 3D bone-marrow-like environment. These studies are inspired by previous publications demonstrating that local granulopoiesis driven by HSPC recruitment into an infected wound is part of the immune response against *S. aureus*, and that adoptive transfer of PMN generated *in vitro* from HSPC cultures can enhance bacterial clearance and survival of immunodeficient mice. This response against *S. aureus* involves TLR2/MyD88 signaling and IL-

1β production via activation of the inflammasome. However, the source of IL-1β during this process, the nature of its effects (paracrine or autocrine to HSPC), and whether activation of other TLRs elicits similar IL-1β-dependent local granulopoiesis, remains elusive. Consequently, the studies presented in Chapter 5 demonstrate the early MyD88 activation is required to contain *P. aeruginosa* in wounded skin. In the absence of MyD88, *P. aeruginosa* proliferates and disseminates from the infected wound much faster than *S. aureus.* Compared to wild-type mice, this phenotype correlates with lower levels of IL-1β in wounds of MyD88-/- mice, as well as impaired PMN movement, and their ability to undergo pyroptosis and NETosis. Thus, suggesting that MyD88 is essential for survival against *P. aeruginosa* by regulating PMN antibacterial functions via IL-1β signaling. Combined, these studies point to the development of antibacterial strategies that target these key adaptors to amplify the immune response to infection.

CHAPTER 1: BACKGROUND AND SIGNIFICANCE

Antibiotic-resistant skin infections are an emerging threat to human health and pose a significant burden on the healthcare system. People who suffer from diabetes, AIDS, cystic fibrosis, and other immunodeficiencies are at higher risk of experiencing intractable infections that can result in sepsis or severe tissue necrosis if left untreated. The current standard of care against these infections is delivery of antibiotics that directly kill bacteria or disrupt their ability to proliferate. However, this strategy comes with significant challenges as some antibiotics are only effective against a limited number of bacterial strains and, more concerning, bacteria are equipped with an array of molecular mechanisms that allows them to rapidly evolve and become resistant to antibiotics. As a result, there is a need to develop alternative, antibiotic-free approaches to combat bacteria and promote tissue repair. Polymorphonuclear leukocytes (PMN) are the most important and abundant effector cells of the innate immune system that play a critical role in controlling bacteria within hours following infection. Thus, enhancing PMN function should be a primary target in the development of immune therapies against pathogenic bacteria. Three PMN-centered approaches to tackle skin wound infections are discussed in this dissertation: 1) The use of a novel designed host defense peptide that acts synergistically with PMN to combat *Staphylococcus aureus* in diabetic mouse wounds; 2) the enhancement of PMN antibacterial and proliferative capacity *in vitro* via encapsulation in a 3D bone marrow-like structure; and 3) the role of Toll-like receptor- and MyD88-dependent signaling pathways that regulate PMN antibacterial functions critical to contain *Pseudomonas aeruginosa* during the early stages of infection. This chapter describes key concepts and the overall significance for the research presented in this dissertation.

1.1: Pathogenesis and Clinical Overview of P. aeruginosa *and* S. aureus *Infections*

Staphylococcus aureus and *Pseudomonas aeruginosa* are two leading causes of pathogenic infections in health care settings [1–13]. *S. aureus* is a gram-positive bacterium that can be both, commensal and pathogenic, by being responsible for soft tissue and skin infections [1–6]. Specifically, Methicillin-Resistant *S. aureus* (MRSA) was first observed in clinical settings in the 1960s and has rapidly become a source of community-acquired infections since the 1990s [1–6, 12]. MRSA virulence is driven by toxins such as hemolysins, leukocidins, protein A, and hyaluronidase that work to evade host immune responses and promote pathogen persistence [1–6]. *P. aeruginosa,* on the other hand, is a gram-negative bacterium characterized by its flagellar motility and ability to rapidly form biofilm, making it also very difficult to treat [7–11, 13]. *P. aeruginosa* infections are commonly seen in individuals with

burn wounds or with respiratory disorders, such as cystic fibrosis or chronic obstructive pulmonary disorder [8]. The human toll caused by *S. aureus* and *P. aeruginosa* is staggering. In 2017 alone, more than 100,000 people suffered from intractable bloodstream infections of *S. aureus* and more than 20,000 people died as a result [12]. In that same year, *P. aeruginosa* caused more than 32,000 infections and 2,700 deaths among hospitalized patients [13]. This epidemic is on the rise and primarily driven by antibiotic resistance [14].

The current standard of care against bacterial infections is direct application or systemic administration of antibiotics. These antimicrobial agents disrupt bacterial viability or capacity to proliferate by interfering with cell membrane structures, inhibiting protein or nucleic acid synthesis, or inactivating metabolic enzymes [15]. However, this strategy is becoming increasingly ineffective, because bacteria have wired-in mechanisms to quickly alter their molecular machinery to circumvent the effects of antibiotics [16]. *S. aureus*, for example, quickly became resistant to penicillin in the 1940s [1]. Resistance mechanisms involve enzymes that directly degrade the antibiotic, modify antibiotic target sites, or change the cell membrane structure to decrease antibiotic influx or induce antibiotic export via efflux pumps [16]. In addition, the number of newly discovered antibiotics has been decreasing since its peak in the 1950s [17]. All of this has led to an increasing number of multi-drug resistant bacterial infections. According to a global survey, it was estimated that in 2019 close to 2 million people died from illnesses attributed to antimicrobial-resistant (AMR) infections, with *S. aureus* and *P. aeruginosa* ranking among the top six causes [18]. The proportion of bacteria strains resistant to antibiotics is on the rise. It is estimated that by 2050 these could cause as many as ten million deadly infections each year [18]. From 2019 to 2020 alone, the number of drug-resistant, hospital-acquired deaths and infections rose by 15%, which was likely exacerbated by the COVID-19 pandemic [19]. The risk of MRSA and *P. aeruginosa* infections is significantly higher in children, the elderly, people with HIV, individuals who suffer from cystic fibrosis, diabetics, health-care workers, and institutionalized populations [1, 8, 12–13, 18–19]. Because of this, there is an urgent need to develop alternative, antibiotic-free treatments against multi-drug resistant infections. One way to do this is to enhance the host's own immunity by targeting and enhancing polymorphonuclear leukocyte (PMN) antimicrobial functions. Studies aimed at better understanding PMN mechanisms against infections will facilitate the development of therapeutic interventions to combat pathogens such as *S. aureus* and *P. aeruginosa*. The skin is the largest and most important immune barrier and provides an ideal model to study innate immunity.

1.2: Overview of Innate Immunity in Skin

Bacteria are ubiquitous single-cell microorganisms approximately 0.5-3 micrometers in size [20]. The vast majority are harmless and can have positive, symbiotic relationships with humans and other mammals. Some bacterial strains found in the human lower gastrointestinal tract, for example, help with food digestion and in some cases are even required for proper immune development and function [21, 22]. There are bacteria strains, however, that can cause tissue necrosis, nutrient depravation, and severe disease if left unchecked [23]. As a result, mammals have evolved several defense mechanisms to quickly control and eradicate pathogenic bacteria. The first layer of defense consists of physical barriers, such as the outmost layer of the skin, the mucus-layered surfaces of the respiratory tract, or the low-pH environment of the gastrointestinal tract [24]. However, when these physical barriers are breached, for example when the skin is wounded, a cascade of immune responses is immediately triggered to clear any potential invading pathogens and to promote tissue repair [24, 25]. In humans, the skin is the largest organ and contains a variety of resident immune cells ready to act against invading bacteria, when wounding and infection occurs [26].

The skin is one of the most important barriers against bacterial infections. It is composed of two primary layers: the epidermis and the dermis. The epidermis is the outermost layer and is itself composed of various sublayers known as corneal, granular, spinous, and basal [26, 27]. The corneal sublayer is the outmost part of the skin and is composed of terminally differentiated keratinocytes that lack organelles and are composed of highly crosslinked keratin fibers. The remaining sublayers beneath the corneal sublayer are also composed of keratinocytes but at various earlier stages of differentiation. Keratinocytes are constantly being turned over from the basal up to the corneal sublayer, where they are eventually shed off [27]. Beneath the epidermis is the dermis, which is primarily composed of collagen and elastin fibers bordering capillary vessels. Several cell types of the immune system reside in the epidermis and the dermis, enabling the skin to play a critical role in early immune responses to wounding and infection [27]. When *S. aureus* enters an open wound, it can form biofilm and engage in hemolysis, which is thought to be a mechanism for nutrient acquisition [27]. Skin resident cells must quickly respond to infection by initiating a cascade of inflammatory events to mitigate pathogen dissemination within the wound and into the circulation. Keratinocytes, for example, secrete antimicrobial and pro-inflammatory peptides during cutaneous injury and infection [27]. Macrophages can also secrete similar mediators, in addition to engaging in phagocytosis and in the production of reactive oxygen species (ROS). Other resident skin cells include dendritic cells, natural killer cells, plasma cells, and T and B lymphocytes [27]. These cells work collectively and in conjunction with

polymorphonuclear leukocytes (PMN or neutrophils) that recruited from circulation–and are the most abundant cells of the immune system–to elicit immune responses upon pathogen recognition that ultimately lead to infection resolution and tissue repair [27].

The immune responses to infection can be categorized as either *innate* or *adaptive.* The innate immune system, also called *nonspecific,* refers to the collection of complement proteins, soluble factors, and immune cells (polymorphonuclear leukocytes, mast cells, macrophages, natural killer cells, and dendritic cells) that respond within minutes or hours after pathogen encounter [25, 28]. The adaptive immune system, also known as *specific*, refers to antibody, B cell, T cell responses that are characterized by antigen specificity and memory from prior pathogen exposure, and requires days to activate and develop [28]. While the innate and adaptive immune systems work in concert to eradicate infections, and the differences between innate and adaptive immunity have become less distinct in recent years [28], this dissertation is focused on the indispensable, early immune responses by polymorphonuclear leukocytes (PMN) following bacteria detection in an infected wound [27, 28].

1.3: Toll-like Receptors Facilitate Pathogen Detection and Initiation of Immune Responses

Innate immune responses are initiated in part because of the ability to distinguish between self and pathogens through an array of evolutionarily conserved molecular patterns. These motifs, known as PAMPs (pathogen-associated molecular patterns), are identified in microbes by cells of the innate immune system and include bacterial DNA, proteins, membranes, and cell wall components [29, 30]. Cells of the innate immune system, including PMNs, are equipped with an array of pattern recognition receptors (PRRs) that enable recognition of PAMPs in addition to DAMPs (damage-associated molecular patterns) upon skin injury and infection [30]. Studies on *S. aureus* and *P. aeruginosa* have identified key PRRs that can activate certain inflammatory pathways [8, 31–36]. These include Toll-Like-Receptors (TLRs) that are activated upon recognition of certain bacterial structures at the early stages of infection. For example, TLR2 binds to peptidoglycan, a cell wall component of *S. aureus* [31,32, 33]. Similarly, TLR4 binds to lipopolysaccharides (LPS), a cell wall component of gram-negative bacteria such as *P. aeruginosa* [8, 34, 35].

TLRs are conserved structures with similar domain organization and downstream signaling pathways. *Toll* was first discovered in *Drosophila melanogaster* and homologues were later discovered in mammals [30, 36]. Today, it is believed that nearly all organisms express TLRs, suggesting that these are one of the most ancient classes of PRRs [36, 37, 38]. In humans and mice at least 10 and 12 different TLRs have

been identified, respectively [30, 36]. TLRs are considered type I transmembrane proteins with three primary structural components: 1) Leucine-rich repeats (LRRs), which facilitate pathogen recognition; 2) a transmembrane domain; and 3) a cytoplasmic Toll/IL-1 receptor (TIR) domain that initiates signaling by engaging with transduction adaptors [30–38, 41]. After ligand recognition and dimerization, TLR activation responses can be classified as either MyD88-dependent or TRIF-dependent [38, 39]. In humans and mice, MyD88 (myeloid differentiation primary response protein 88) is an adaptor molecule recruited following activation of all TLRs, except TLR3, and binds directly to the TIR domain. Thereafter, IRAK4 (IL-1 receptor-associated kinase 4) binds to the death-domain of MyD88, forming a Myddsome complex [38, 40]. This leads to autophosphorylation of IRAK1 (IL-1 receptor-associated kinase 1) and activation of TRAF6 (tumor necrosis factor receptor-associated factor 6). This subsequently leads to the activation of the TAB (TAK1/TGF-b-activated kinase) complex via K-63-linked polyubiquitination of TAK1 and TRAF6 [38]. The inhibitor IkBa (I kappa B alpha) is then degraded, allowing for the nuclear translocation of NF-kB (nuclear factor kappa B), which in turn initiates transcription of genes that encode for inflammatory cytokines [38]. On the other hand, TRIF-dependent pathways are specific to only a handful of TLRs, including TLR3 and TLR4 in mammals [38], but also result in the activation of NF-kB in addition to AP-1 (activating protein-1) and IRFs (IFN [interferon] regulatory factors). TRIF-dependent pathways also result in the production of inflammatory and antiviral cytokines, including type 1 interferons [38].

The MyD88- and TRIF-dependent pathways downstream of TLR4 are relevant in studies aiming to understand the immune response to *P. aeruginosa*. In mammals, TLR4 and MD-2 (myeloid differentiation factor 2) form a heterodimer that recognizes various LPS structures found in the cell wall of gram-negative bacteria [50]. The TLR4-MD2-LPS complex induces early-phase NF-kB and MAPK (mitogen-activated protein kinase) activation following MyD88 and MAL (MyD88-adapter-like) recruitment [38]. The TLR4-MD2-LPS assembly can also enter the cell via endocytosis, where it interacts with TRIF and TRAM adaptors (TRAM is also known as TICAM2, TIR domain-containing adapter molecule 2). The TRIF-dependent pathway results in the production of IFN1 (type 1 interferons) and in the activation of IRF7 and late-phase NF-kB [38]. Overall, TLR activation results in the production of cytokines that regulate inflammatory responses, including PMN recruitment and antibacterial functions [57–59]. This dissertation is primarily focused on the innate immune response following activation of TLR2 during *S. aureus* infection and TLR4 and TLR5 during *P. aeruginosa* infection and their effects on PMN production, recruitment, and antibacterial capacity.

1.4: The Role of Polymorphonuclear Leukocytes (PMN) in Innate Immunity against S. aureus *and* P. aeruginosa

Polymorphonuclear leukocytes (PMN) are the most abundant and important effector cells of the innate immune system [59–72]. PMN encompass granulocytes that can be classified as basophils, eosinophils, and neutrophils. Neutrophils comprise more than 70% of all circulating leukocytes [63], and thus, the terms 'neutrophil' and 'PMN' are used interchangeably in this dissertation. PMN are produced in the bone marrow from self-renewing hematopoietic stem cells (HSC) through a process termed granulopoiesis [63]. During granulopoiesis, cells undergo various stages of differentiation [63]. HSCs give rise to MPPs (multipotent progenitors), which in turn give rise to GMPs (granulocyte-monocyte progenitors). GMPs give rise to mature PMNs under the influence of the cytokine G-CSF (granulocyte colony-stimulating factor) [63, 64]. Mature PMN are released from bone marrow into the circulation through CXCR2 and CXCR4 interactions [63]. CXCR4-expressing PMN are kept in the bone marrow by stromal cells that produce CXCL12. Release of PMN into circulation involves G-CSF-mediated CXCR2 ligand production by endothelial cells outside the bone marrow. These ligands reduce the expression of CXCL12 and CXCR4 in the bone marrow, resulting in PMN release. In the absence of infection or disease (i.e. homeostatic conditions) only 1-2% of bone marrow and marginated PMN in humans are found in blood [63]. Still, PMN comprise the vast majority of immune cells. Humans release more than 10^{11} PMN from the bone marrow every day [63]. During homeostatic conditions, PMN in circulation are short-lived, with an average lifetime of typically less than 24 hours [63, 65]. However, following skin wounding and infection, several PMN-mediated mechanisms are mounted by the innate immune system that alter PMN lifetime, production, and antibacterial phenotype in order to quickly eradicate invading pathogens and promote wound healing.

PMN are critical for mounting an immune response that leads to resolution of infection in wounded skin. Following tissue injury and bacterial breach into an open wound, skin resident cells produce cytokines and chemokines that are detected by the PMN in circulation [62–64, 78]. PMN then roll, arrest, and transmigrate across the walls of endothelial vessels [62, 63, 78]. These mechanisms are triggered by cytokines, including TNF-α and IL-1β, that upregulate chemokines and adhesion receptors on inflamed venular endothelium [62, 78]. Once at the site of infection, PMN engage in a variety of antimicrobial functions that include degranulation, phagocytosis, elaboration of reactive oxygen species, and release of extracellular traps (NETosis) [66–71, 79, 80]. These antibacterial functions are marked by L-selectin shedding from the cell surface [72–74] and upregulation of CD11b expression [75–77, 152]. At the site of

infection, PMN can undergo cell death as a result of pathogen virulence factors or as part of their programmed antibacterial functions [71, 78, 79]. α-toxin and γ-toxin, for example, are virulence factors produced by *S. aureus* that cause lysis of immune cells, including PMN and resident macrophages [79–82]. Similarly, during NETosis, PMN deliberately release their DNA and intracellular components–including antibacterial peptides, histones, elastase, and DAMPs such as calprotectin (S100A8/A9) and cathelacidin (LL37)–in an attempt to contain and kill invading pathogens [71, 83–86]. As a matter of fact, NETosis is believed to be an important host mechanism against *P. aeruginosa* and other gram-negative bacteria that may help enable pathogen containment and prevent dissemination into vital tissues [87–89]. However, as a result of this constant cell turnover, PMN production and release from the bone marrow is also increased during infection as a way to provide a sufficient cell quantity needed to combat bacteria, which is in and of itself a process known as 'emergency granulopoiesis' [62, 69].

Studies involving *S. aureus* infections in full-thickness mouse wounds have uncovered key host strategies that govern PMN recruitment into an infected wound [90]. These studies involve longitudinal, *in vivo* imaging of LysM-EGFP mice that produce green-fluorescent granulocytes [90]. These mice undergo dorsal wounding and inoculation with bioluminescent *S. aureus*, which allows for measurement of PMN recruitment and bacterial abundance over the course of several days after infection (Figure 1.1) [90–94]. In this model, the bioluminescent signal produced by *S. aureus* clearly correlates with a rise in fluorescence generated by recruited PMN into the wound [90]. These studies show that PMN recruitment continuously rises until its peak on Day 6 [90]. This marked by a continuous decrease in bacterial abundance, which is then followed by a decrease of EGFP signal [90]. After Day 6, the decrease in bacterial abundance and PMN numbers correlates with a decrease in wound size [90], which is indicative of healing. Furthermore, the number of PMN in bone marrow and circulation is also increased in mice infected with *S. aureus* compared to those inoculated with saline [90]. This suggests that emergency granulopoiesis and PMN recruitment from circulation is part of the innate immune response to infection. In addition to that, PMN are also able to extend their lifetime for up to five days at the site of infection, while the average lifetime of PMN in uninfected wounds is closer to one day [90]. This suggest that extended PMN lifetime is an additional strategy to combat *S. aureus*. Interestingly, it has also been demonstrated that PMN can be produced from HSPC directly at the site of *S. aureus* infection, which is a process termed 'local extramedullary granulopoiesis' [90, 93, 94]. This is evident in studies in which circulating PMN are depleted from mice before and after infection [90]. Mice that are depleted before infection with *S. aureus* still show EGFP fluorescence at the site of infection, which continuously rises from Day 1 up to Day 12 [90]. Surprisingly 80% of these PMN-depleted mice survive and are presumably able to defeat the *S.*

aureus infection [90]. In contrast, less than 50% of mice that are depleted of both PMN and HSPC survive. Adoptive transfer studies of HSPC from LysM-EGFP mice into C57BL6 infected mice also show granulopoiesis at the site of infection, indicated by an increase in EGFP fluorescence [90]. Thus, local production of PMN at the site of infection, extended PMN lifetime, and recruitment from circulation are three key strategies deployed by the innate immune system to clear *S. aureus* in wounded skin (Figure 1.2).

The mechanism of local granulopoiesis in response to *S. aureus* in wounded skin involves TLR2 and MyD88 signaling, in addition to the virulence factor alpha toxin and the cytokine IL-1β [93, 94]. As discussed earlier, alpha-toxin is secreted by *S. aureus* and causes lysis of immune cells, including PMN and resident macrophages. This results in attenuated PMN recruitment into the site of infection. Mice infected with *S. aureus* have lower PMN numbers in the wounded skin during the first three days of infection compared to mice infected with an *S. aureus* mutant lacking α-toxin (ΔAT) or mice inoculated with only saline [94]. As a result of this disruption to PMN trafficking, mice appear to have evolved a response mechanism that involves trafficking of HSPC from bone marrow into the site of infection. In fact, HSPC transmigration is not affected by α-toxin [94]. Once at the site of infection, HSPC undergo granulopoiesis to provide sufficient PMNs to clear the infection [91, 93, 94]. This response appears to be regulated by the cytokine interleukin 1β (IL-1β) [94]. *In vitro* granulopoiesis studies show that production of PMN from HSPC involves synergistic stimulation of TLR2 and IL-1β [94]. Enumeration of HSPC in *S. aureus*-infected wounds shows that the number of HSPC at the site of infection is significantly lower in mice lacking TLR2 or MyD88 [93]. In fact, MyD88-/- mice that are infected with *S. aureus* experience mortality within 5 to 10 days after infection due to the inability to clear the infection [94]. Mortality, however, can be prevented via adoptive transfer of HSPC directly into the site of infection [94]. Interestingly, IL-1β-/- HSPC do not elicit rescue of MyD88-/- mice infected with *S. aureus* [94]. Thus, HSPC recruitment and local granulopoiesis is an important defense mechanism against *S. aureus* α-toxin that involves TLR2 and MyD88 activation in addition to secretion of IL-1β. However, key questions remain regarding the source of IL-1β and whether its production is paracrine or autocrine of PMN and HSPC, and whether similar mechanisms are observed in response to activation of other TLRs, such as TLR4 in response to *P. aeruginosa*.

1.5: Dissertation Objectives

One of the key objectives of this dissertation is to better understand the link between TLR and inflammasome activation that leads to IL-1β production and the effect on PMN fate during infection. As

discussed earlier, a key host defense mechanism in response to *S. aureus* infection is TLR2 activation that leads to production of IL-1β [94, 95]. IL-1β modulates several pro-inflammatory effects, including myeloid expansion of HSPC at the site of infection [94]. IL-1β is also involved in PMN recruitment and abscess formation to mitigate pathogen dissemination [95]. PMN are the main producers of IL-1β during *S. aureus* skin infection [95] and *P. aeruginosa* corneal infection [96]. When immunodeficient MyD88-/- mice infected with *S. aureus* undergo adoptive transfer of HSPC, the production of PMN at the site of infection is necessary and sufficient for survival and is a rescue mechanism dependent on IL-1β [95]. HSPC can produce PMN *in vitro* via either TLR2 or IL-1β stimulation, but PMN production is highest when both TLR2 and IL-1β agonists are present [95]. This suggests that TLR2 and IL-1β signals act in synergy *in vitro* and likely in a wound to drive HSPC granulopoiesis. However, it is currently unknown if a similar mechanism can be elicited via activation of other TLRs, or whether it's possible to use HSPC to rescue MyD88-/- mice infected with gram-negative bacteria such as *P. aeruginosa*, which elicits TLR4 and TLR5-dependent responses.

The link between TLR2 activation and IL-1β release during *S. aureus* infection involves activation of the NLRP3 inflammasome [97]. Following TLR2 activation, translocation of NF-kB into the cell nucleus leads to generation of pro-IL-1β, which is the non-active form of IL-1β. IL-1β is such a potent pro-inflammatory regulator that its activation requires a second signal in addition to TLR2. The second signal can be induced by virulence factors, such as α, β, and γ gamma hemolysins that are shed by *S. aureus* [97]. This leads to assembly of the NRLP3 inflammasome, which in turn activates caspase-1. Caspase-1 then cleaves pro-IL-1β to generate active IL-1β [97]. Interestingly, IL-1β generation has also been found to be involved in cell pyroptosis, which is a form of programmed cell death. The release of IL-1β occurs through pores on the cell membrane formed by Gasdermin D [100]. Gadermin D has also been implicated in NETosis, another form of programmed cell death that mediates *P. aeruginosa* killing and containment, as discussed earlier [104]. Thus, a key advancement of this dissertation is to bridge the understanding between TLR and MyD88 activation and IL-1β generation as they relate to PMN generation, survival and antibacterial functions.

One key antibacterial function against *P. aeruginosa* is PMN's release of extracellular traps (NETs). NETs are composed of nucleic acids, histones, and elastase that can entrap and facilitate killing against bacteria [84]. This process is mediated by peptidyl arginine deaminase 4 (PAD4) [71, 106, 107]. Scientists have long believed that NETosis results in PMN death ('suicidal NETosis'), though recent research suggests that NETosis can also occur without resulting in cell death ('vital NETosis') [84, 85]. In fact, non-cell death

NETosis can take place *in vivo* during infection caused by gram-positive bacteria, like *S. aureus* [83]. Vital NETosis allows PMN to quickly release NETs while also phagocytosing live bacteria [84]. However, the role of NETosis, especially lytic NETosis, in innate immunity remains controversial and many questions remain about the mechanisms that regulate this process. Some researchers believe that lytic NETosis is a beneficial immune response that facilitates capture and killing of pathogens, while others have suggested that lytic cell death is a pathogen strategy to evade the host immune response [84]. Studies on psoriasis, a chronic inflammatory disease characterized by the formation of itchy, red, and thick patches on the surface of the skin, suggest that skin resident cells and PMN act in synergy to induce cell-death NETosis via TLR4 and MyD88 [108]. Similarly, Gasdermin-D pores, which mediate IL-1β release, also appear to mediate release of NETs. An objective of this dissertation is to examine the relationship between TLR4 activation and NET formation via MyD88 in response to *P. aeruginosa* infection in wounded skin.

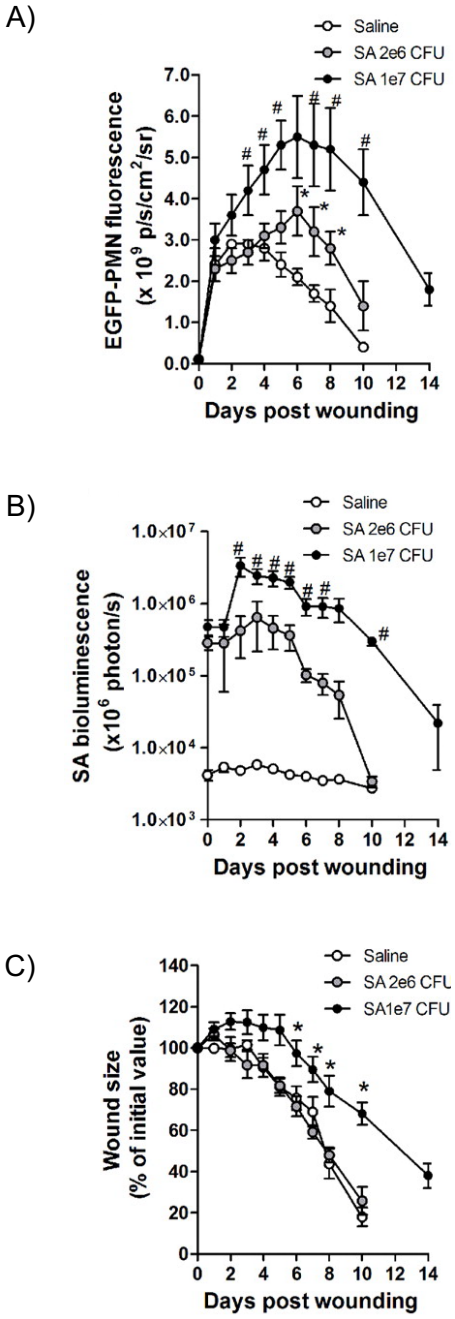

Figure 1.1: Response to S. aureus infection on LysM-EGFP mice. LysM-EGFP mice inoculated with bioluminescent S. aureus are useful in understanding PMN recruitment and their role in bacterial clearance and wound healing. This is accomplished via *in vivo*, whole-animal, longitudinal imaging.
Data are derived from n=6–8 mice per group.
* denotes p-value ≤0.05 compared to saline group. # denotes p-value ≤0.05 compared to SA-2e6 CFU group.

This research was originally published in Blood. Kim et al. PMN survival and c-kit+-progenitor proliferation in *Staphylococcus aureus*-infected skin wounds promote resolution. *Blood*. 2011; 117:3343-3352.

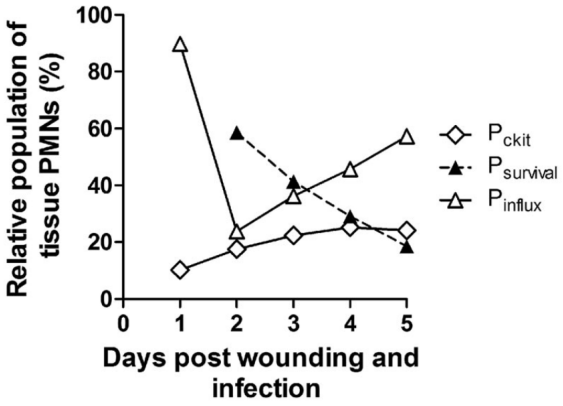

Figure 1.2: Contributions to PMN numbers measured in mouse wounds infected with *S. aureus*. Three key host mechanisms contribute to PMN quantity during S. aureus infection: recruitment from circulation (P_{influx}), prolonged survival ($P_{survival}$), and local extramedullary granulopoiesis (P_{ckit}).

This research was originally published in Blood. Kim et al. PMN survival and c-kit+-progenitor proliferation in *Staphylococcus aureus*-infected skin wounds promote resolution. *Blood*. 2011; 117:3343-3352.

CHAPTER 2: MATERIALS AND METHODS

2.1: List of Materials and Reagents

Name	Vendor	Catalog Number
EasySep™ Buffer	StemCell Technologies	20144
70um Sterile Cell Strainer	Fisher Scientific	22363548
EasySep™ Mouse Hematopoietic Progenitor Cell Isolation Kit	StemCell Technologies	19856
EasySep™ Mouse CD117 (cKIT) Positive Selection Kit	StemCell Technologies	18757
StemSpan™ SFEM II	StemCell Technologies	09655
Recombinant Murine SCF (Stem Cell Factor)	PeproTech Inc.	25003
Recombinant Murine Flt3-Ligand	PeproTech Inc.	25031L
Recombinant Murine G-CSF (Granulocyte Colony-Stimulating Factor)	PeproTech Inc.	25005
Recombinant Murine IL-3	PeproTech Inc.	21313
Recombinant Murine IL-6	PeproTech Inc.	21616
Recombinant Murine IL-1β	PeproTech Inc.	21111B
Pam3CSK4 Synthetic triacylated lipopeptide - TLR1/2	Invivogen	Tlrl-pms
Lipopolysaccharide (LPS) eBioscience	ThermoFisher	00-4976-03
Trypan Blue Solution (0.4% w/v) in PBS	Corning Inc	25-900-CI
OneComp eBeads™ Compensation Beads	Thermo Fisher	01-1111-42
APC/Fire 750 anti-mouse CD45 Antibody	Biolegend Inc.	147714
Brilliant Violet 421 anti-mouse CD117 (c-Kit) Antibody	Biolegend Inc.	105828
Brilliant Violet 711 anti-mouse/human CD11b Antibody	Biolegend Inc.	101242
Alexa Fluor 700 anti-mouse Ly-6C Antibody	Biolegend Inc.	128024
Alexa Fluor® 488 anti-mouse Ly-6C Antibody 100ug	Biolegend Inc.	128022
APC anti-mouse Ly-6G Antibody	Biolegend Inc.	127614
PE anti-mouse/human CD282 (TLR2) Recombinant Antibody	Biolegend Inc.	153004
PE anti-mouse CD284 (TLR4) Antibody	Biolegend Inc.	145404
Zombie Yellow™ Fixable Viability Kit	Biolegend Inc.	423104
PE anti-mouse CD117 (c-Kit) Antibody	Biolegend Inc.	105808
PE anti-mouse Ly-6G/Ly-6C (Gr-1) Antibody	Biolegend Inc.	108408
LIVE/DEAD™ Fixable Far Red Dead Cell Stain	ThermoFisher	L34974
LB Agar (Miller) w/ 10ug/ml Tetracycline Plate	VM Biological	SPECIAL
BHI Agar w/ 5% Cow-Bld Plate	VM Biological	1092
Tryptic Soy Broth (TSB)	Thomas Scientific	C838N78
LB Broth	ThermoFisher	10855021
Kanamycin sulfate	Sigma Aldrich	K1377-5G
Tetracycline	Sigma Aldrich	87128-25G
Glycerol	ThermoFIsher	17904
Buprenorphine Hydrochloride, 0.3mg/ml	MWI Veterinary	7292
Sodium Chloride for Injection, 0.9%	Pfizer Inc/Medline	ABB048881010Z
FlurisoTM, Isoflurane, 250mL	MWI Veterinary	502017
Povidone-Iodine Solution	Geneseesci	72-478
Biopsy punch, 6mm, disposable	Fisher Scientific	124-604-12
Syringe, Insulin, BD, Lo-Dose, 0.5cc, 28G x 0.5 in.	Fisher Scientific	14-826-79
Mouse neutrophil enrichment kit	StemCell Technologies	19762
CellROX™ Deep Red Reagent	ThermoFisher	C10422
N-Formyl-Met-Leu-Phe (fMLP)	Sigma Aldrich	47729-10MG-F
RBC Lysis Buffer (10X)	Biolegend Inc.	420302
Q-VD-OPH, 1mg	Cayman Chemical	15260
Luminol	Sigma Aldridch	123-072-5G

Acuderm Biopsy Punch, 10mm, Sterile	Fisher Scientific	NC9236770
16% Paraformaldehyde Aqueous Solution	Fisher Scientific	50-980-487
RIPA Buffer	Sigma Aldrich	R0278-50ML
Mouse IL-1 beta/IL-1F2 Quantikine ELISA Kit	R&D Systems	MLB00C
Halt™ Protease and Phosphatase Inhibitor Cocktail	ThermoFisher	78444
Ly-6G/Ly-6C Monoclonal Antibody (RB6-8C5), eBioscience™	ThermoFisher	14-5931-85
Rat IgG1 kappa Isotype Control (eBRG1), eBioscience™	ThermoFisher	14-4301-85
Albumin from Bovine Serum (BSA), Alexa Fluor™ 594 conjugate	ThermoFisher	A13101
Albumin from Bovine Serum (BSA), Alexa Fluor™ 680 conjugate	ThermoFisher	A34787
Sodium azide 0.1M solution	MiliporeSigma	08591-1ML-F
Annexin V Fluor 647	ThermoFisher	A23204
Propidium Iodine	ThermoFisher	P1304MP
SYTOX Green Nucleic Acid Stain - 5 mM Solution in DMSO	ThermoFisher	S7020
SYTOX™ Orange Nucleic Acid Stain - 5 mM Solution in DMSO	ThermoFisher	S11368
pHrodo™ Red Phagocytosis Particle Labeling Kit	ThermoFisher	A10026
pHrodo™ Red *S. aureus* Bioparticles™ Conj. for Phagocytosis	ThermoFisher	A10010
XenoLight D-Luciferin - K+ Salt	Perklin Elmer	122-799

2.2: Mouse Husbandry

Animal studies were approved by the Institutional Animal Care and Use Committee of the University of California, Davis, under protocol numbers 19922, 21790, and 23428. Animal studies were performed following the guidelines of the Animal Welfare Act and the Health Resource Extension Act.

Mice used in these studies were on a C57BL/6, FVB.129 or hybrid genetic background and between the ages of 8 and 26 weeks old. Both male and female mice were used in animal experiments. All mouse colonies were bred under specific pathogen-free conditions in the Genome and Biomedical Sciences Facility (GBSF) Vivarium at the University of California, Davis.

List of mouse strains

The following mouse colonies were bred and maintained at the University of California, Davis:

Wild-type (WT) LysM-EGFP: B6;129-lysEGFP

MyD88-/- LysM-EGFP: B6;129-lysEGFP x MyD88-/-

The following mouse strains were initially purchased from the Jackson Laboratories and colonies were subsequently bred at the University of California, Davis:

Wild-type (WT): C57BL6/J

TLR4-/- : B6(Cg)-Tlr4tm1.2Karp/J

The following mouse strains were purchased directly from the Jackson Laboratories:

MyD88-/-: B6.129P2(SJL)-Myd88tm1.1Defr/J Stock: 009088

Cas1-/-: B6.Cg-Casp1em1Vnce/J Stock: 032662

For studies involving topical application of anti-bacterial peptides against diabetic wounds infected with *S. aureus*: Ten-week-old male diabetic TALLYHO/JNGJ mice were obtained from Jackson Laboratories (Stock No: 005314) and maintained on LabDiet 5K52 feed (Item 15502, Newco Distributors Inc., Hayward, CA, USA, MFG 5K52C3P) at the University of California, Davis. These mice were a model of type 2 diabetes, which confirmed by measures of blood hyperglycemia (i.e., glucose level of >300 mg/dL).

To generate the MRP8-FFLuc line, the following mouse strains were obtained from the Jackson Laboratories (Bar Harbor, Maine) and cross-bred at the University of California, Davis: B6.Cg-Tg(S100A8-cre,-EGFP)1Ilw/J (Jax Strain #021614)[44] and STOCK Gt(ROSA)26Sortm1(Luc)Kael/J (Jax Strain #034320)[45]. To identify and select offspring mice expressing the firefly luciferase reporter, mice were subcutaneously administered 250mg/kg of D-Luciferin (Cat#: 122799, Perkin Elmer, Waltham, Massachusetts) and imaged in an IVIS Spectrum (Perkin Elmer, Waltham, Massachusetts).

2.3: Isolation of Hematopoietic Stem Cells (HSCs) from Murine Bone Marrow

Mice, at least 8 weeks old, were humanely euthanized by CO_2 asphyxiation in accordance with IACUC guidelines at the University of California Davis. Following euthanasia, mouse femurs and tibias were extracted, cleared of any muscle and tissue ligands, and crushed using a mortar and pestle while being submerged in EasySep™ Buffer (StemCell Technologies, Cat # 20144). The extracted cell solution was filtered through a 70um sterile cell strainer (Fisher Scientific, Cat # 22-363-548) and centrifuged at 1200 RPM for 10 minutes. C-kit$^+$ (CD117) cells were isolated via a two-step magnetic enrichment using a EasySep™ Mouse Hematopoietic Progenitor Cell Isolation Kit (StemCell Technologies Cat #19856) followed by an EasySep™ Mouse CD117 (cKIT) Positive Selection Kit (StemCell Technologies Cat #18757), adhering to the manufacturer's instructions. Isolation purity was confirmed to be >80% using an Attune NxT flow cytometer (ThermoFisher, Waltham, MA) (Figure 4.7A shows a representative flow cytometry plot after isolation).

2.4: Production of PMN from Murine Hematopoietic Stem Cells (HSCs)

C-kit^{+} cells extracted from murine bone marrow via magnetic isolation were seeded in 48-well plates (Falcon® Cat # 353230) at a density of 10,000 to 20,000 cells/mL in StemSpan™ SFEM II media (StemCell Technologies, Cat # 09655), supplemented with the following growth factors (PeproTech Inc.):

Name of Reagent	Concentration
Recombinant Murine SCF (Stem Cell Factor) (Cat # 250-03)	100ng/mL
Recombinant Murine Flt3-Ligand (Cat # 250-31L)	100ng/mL
Recombinant Murine G-CSF (Granulocyte Colony-Stimulating Factor) (Cat # 250-05)	10ng/mL
Recombinant Murine IL-3 (Cat # 213-13)	10ng/mL
Recombinant Murine IL-6 (Cat # 216-16)	10ng/mL
Recombinant Murine IL-1β (Cat # 211-11b)	25ng/mL

Media was changed every 48 hours and cells were extracted from their wells and analyzed for surface marker expression via for flow cytometry using an AttuneNxT cytometer at various timepoints post-seeding (*i.e.* days 0, 1, 3, and/or 7).

2.5: Cell Phenotype Characterization by Flow Cytometry

For surface marker analysis, cells were prepared at a density of $1x10^6$ cells/mL. $1x10^5$ cells in 100uL were stained with antibodies of interest at a 1:100 – 1:20 concentration (based on optimal Staining Index). Compensation and Fluorescence-Minus-One (FMO) samples were prepared accordingly. Cell samples were analyzed in an AttuneNxT flow cytometer (ThermoFisher, Waltham, MA). All flow cytometry data was analyzed using FlowJo™ (FlowJo™ Software for Windows, Version 10.8.2. Ashland, OR: Becton, Dickinson and Company; 2020–2014).

2.6: S. aureus Bacterial Culture

Single colonies of bioluminescent MRSA NRS384/USA300 [109] were grown on Brain Heart Infusion (BHI) agar plates with 5% cow blood (VMBS, UC Davis), followed by cultured in a shaking incubator (VWR, Avantor, Radnor, PA) at 300 RPM, 37 °C in 6mL of Tryptic Soy Broth (TSB) medium with chloramphenicol (100μg/mL) and/or kanamycin (50ng/mL). This bacteria culture was diluted in 6mL of TSB the next day, and further grown to an optical density of 0.02–0.04, which corresponded to 10^7 CFU in 50μL, measured

with a NanoDrop spectrophotometer device (ThermoFisher, Waltham, MA, USA). This culture was then centrifuged at 3750–3850 RPM for 10–15 min at 4°C (Beckman Coulter, Brea, CA, USA), decanted, and finally brought to a volume of 1mL in DPBS (Dulbecco's Phosphate Buffered Saline) (Gibco, Waltham, MA, USA). A volume of 50μL from this final culture was inoculated into the mouse wounds of infected cohorts.

2.7: P. aeruginosa Bacterial Culture

Pseudomonas aeruginosa bacteria (PA-xen41, PerklinElmer PN: 119-229, Xenogen Corp., USA) [110], were grown on Luria-Bertani broth (LB) agar plates with 10μg/mL Tetracycline (VMBS, UC Davis) and then cultured in 6mL of LB medium supplemented with Tetracycline and on a shaking incubator at 300 RPM, 37°C. This culture was thoroughly vortexed and diluted in 6mL of LB medium the next day, and further cultured at 37°C, 300 RPM until it reached an optical density of 0.015–0.030, which corresponded to 10^7 CFU in 50μL, measured using a NanoDrop spectrophotometer device (ThermoFisher, Waltham, MA, USA). Bacteria were centrifuged at 3750–3850 RPM for 10-15 min at 4°C (Beckman Coulter, Brea, CA, USA), decanted, and brought to a final volume of 1 mL with DPBS (Gibco, Waltham, MA, USA). 50μL from this final 1mL suspension were inoculated into the dorsal wounds of infected mouse cohorts.

2.8: Mouse Wounding, Infection, and In-Vivo Longitudinal Imaging

Mice were prepared for wounding, infection, and imaging as previously described [91–94, 157]. 20–30 min before wounding, all mice received an intraperitoneal, 100uL dose of 0.03 mg/mL of buprenorphine hydrochloride (NDC 12496-0757-5CN) in NaCl (NDC 63323-186-01). Mice were subsequently anesthetized with 2–4% isoflurane (Vet One® Fluriso™ NDC 13985-528-60) for 10–15 min until loss of movement and sensation was observed. Mouse dorsal areas were shaven and sanitized with gauze in povidone-iodine solution (Cat # 3955-16, Ricca Chemical Company, Arlington, TX, USA), followed with gauze in 70% isopropanol. Subsequently, mice received a full-thickness dorsal wound with a 6mm biopsy punch (Integra™ Miltex™, Fisher Scientific, Cat # 12-460-412,). Wounds were immediately subcutaneously inoculated with 50uL of bacteria or vehicle control (saline). Wounds were photographed using a Nikon D3300 camera (Nikon Inc., Melville, NY) and wound size was measured using ImageJ (Fiji) [236]. Wounds were also scanned for bioluminescence and fluorescence using an IVIS Spectrum. Wound size and scan measurements were performed starting from the day of the inoculation (denoted as “Day

0 Post-Wounding"), unless otherwise noted. Bioluminescence and fluorescence flux from the wounds was calculated using LivingImage® software (Version 4.7.3, Perklin Elmer, Waltham, MA, USA) as total flux (photons/second or p/s) or average radiance (p/s/cm^2/sr), as noted on figure axes, by drawing a region of interest (ROI) onto the wound image.

2.9: RP557 Peptide Preparation and Administration

Solid phase synthesis was used to synthesize RP557 (AmbioPharm, North Augusta, SC, USA) and purity was assayed via high-performance liquid chromatography and mass spectroscopy by scientists at RIPTIDE Inc [120, 157]. RP557 was received at UC Davis in powder form and a sterile-filtered solution of 20 mg/mL (2%) of RP557 (molecular weight of 2135 g/mol) was prepared in sterile DPBS (Gibco, Waltham, MA, USA). 50uL (1mg) of this RP557 solution was topically applied onto dorsal mouse wounds once a day after imaging, or as otherwise noted. Mice were kept under anesthesia after imaging and very closely monitored for 30–40 min until the peptide was fully absorbed into the wound [157].

2.10: Detection of Reactive Oxygen Species in vivo *via Luminol*

Luminol (Cat #123072-5G, Sigma-Aldrich) solution was prepared in DMSO (4-X, ATCC) at a concentration of 100mg/mL. To measure ROS production at the site of infection, mice were administered 100uL of 100mg/mL of Luminol in DMSO by intraperitoneal injection or directly into the site of infection. Mice were then imaged for bioluminescence inside an IVIS Spectrum under 2% isoflurane. Sequential imaging was performed for 1 hour (1 minute exposure, 2-4 binning, and 1 minute delay for a total of 30 segments).

2.11: IL-1β Cytokine Measurements from Wound Tissues

To measure IL-1β cytokine concentration from infected wounds, mice were euthanized by CO_2 asphyxiation in accordance with IACUC guidelines. Wounds were then excised using a 10mm biopsy punch and immediately submerged in liquid nitrogen. Wounds were then weighted and minced with tweezers and scissors before being placed in 2mL of digestion buffer. Digestion buffer consisted of RIPA (Radio-Immunoprecipitation Assay) buffer (Cat # R0278, Sigma Aldrich Inc, Milwaukee, WI) supplemented with 1x Halt Protease and Phosphatase Inhibitor Cocktail and 1x EDTA solution (Cat #

78444, ThermoFisher). Tissues were briefly placed on ice for 30 seconds and then incubated in digestion buffer for 40 minutes at room temperature under slight vortexing every 10-15 minutes. Digested tissues were then centrifuged at 3000 RPM for 15 minutes and supernatants were collected for protein analysis. IL-1β cytokine measurements were performed using R&D ELISA kits (Cat # MLB00C-1, R&D Systems Inc, Minneapolis, MN) in accordance with the manufacturer's instructions.

2.12: Wound Tissue Preparation for Histological Analysis

For histopathological wound analysis, mice were euthanized by CO_2 asphyxiation in accordance with IACUC guidelines and had their wounds excised with a 10mm biopsy punch. Wound were then submerged in 4% PFA (EMS, Cat # 60-980-487, Fisher Scientific, Pittsburg, PA) dissolved in DPBS (Gibco, Cat # 14040133, ThermoFisher, Waltham, MA, USA) and stored at 4°C for 24 hours. Wounds were rinsed and resuspended in DPBS (Gibco, Waltham, MA, USA). Some wound embedding in paraffin blocks and slide sectioning was performed by the Anatomic Pathology Department at the UC Davis Veterinary Teaching Hospital. H&E staining, imaging, and analysis were performed by the Comparative Pathology Laboratory at UC Davis.

2.13: PMN Isolation and Enumeration from Murine Blood and Bone Marrow

To isolate PMN from bone marrow, mice were euthanized by CO_2 asphyxiation and had their femurs and tibias removed. Bones were cleared of any muscle and ligands and crushed in Flow Buffer (Cat # 20144, StemCell Technologies), followed by filtration through a 70μm sterile mesh. Isolation of PMN, specifically, was performed using a StemCell mouse PMN isolation kit (EasySep™, Cat #19762, StemCell Technologies, Vancouver, BC) in accordance with the manufacturer's instruction manual. Flow cytometry revealed >80% cell purity. Enumeration of bone marrow LysM-EGFP PMN was calculated using an AttuneNxT flow cytometer with known inputted cell volumes and densities (from cell cultures directly isolated from bone marrow) followed by gating on EGFP+ cells. To isolate cells from blood, heart puncture was performed on euthanized mice using an insulin syringe and recording the volume collected, followed by blood incubation in 10x RBC (Red Blood Cell) lysis buffer (Cat # 420302, Biolegend) for 15 minutes at room temperature. Blood was centrifuged at 1200 RPM for 10 minutes and incubated again in lysis buffer for a total of two incubations before the cells being resuspended in 1mL of flow buffer. PMN were enumerated using an AttuneNxT cytometer as described above.

2.14: Systemic PMN Depletion in Mice

To deplete circulating PMN, LysM-EGFP mice received 100uL of 1mg/mL of anti-Gr1 monoclonal IgG1 rat antibody (mAb, RB6-8C5) or rat IgG1 control by intraperitoneal injection (0.1mg in 100uL) one day prior to wounding and infection. Mouse wounds were imaged for EGFP fluorescence 12-16 hours after infection to confirm PMN depletion, indicated by decreased EGFP recruitment in mice that had received the anti-Gr1 antibody treatment.

2.15: PMN Adoptive Transfer and Measurement of Lifetime During Wound Infection

To measure PMN lifetime in infected wounds after *P. aeruginosa* infection, C57BL6 (non-LysM-EGFP) mice received PMN via tail-vein injection. Isolation of PMN was performed using a StemCell mouse PMN isolation kit (EasySep™, Cat #19762, StemCell Technologies, Vancouver, BC) in accordance with the manufacturer's manual. Recipient mice received a 50uL bolus i.v. tail-vein injection with $3x10^6$ PMN in HBSS+/+. Two hours later, these C57BL6 mice were dorsally wounded and inoculated with either saline or *P. aeruginosa*. This procedure was also performed on MyD88-/- mice receiving WT or MyD88-/- PMN. Mice were imaged in an IVIS Spectrum for bacterial load (bioluminescence) and recruitment of the transferred PMN (EGFP fluorescence) at the site of infection. To measure PMN lifetime, an exponential decay function was fitted into the fluorescence curve from peak PMN-EGFP fluorescence. To measure PMN lifetime upon immediate encounter with *P. aeruginosa*, C57BL6 mice were dorsally wounded and inoculated with either saline or *P. aeruginosa*. Immediately after wounding and infection, a 50μL bolus with $1x10^6$ PMN isolated from LysM-EGFP mice was transferred directly into the site of infection. Mouse wounds were then imaged every 4-6 hours for bioluminescence and fluoresceine using an IVIS Spectrum. To measure PMN lifetime as a function of MyD88 signaling, C57BL6 mice were systemically depleted of their circulating PMN via anti-Gr1 mAb administration. Mice then received LysM-EGFP PMN from wild-type or MyD88-/- mice ($6x\ 10^6$ PMN in 50μL) via i.v. tail vein injection. Two hours later, mice were dorsally wounded and infected with *P. aeruginosa*, followed by subsequent wound imaging for bioluminescence and EGFP fluorescence.

2.16: Wound Permeability Assay

To assess wound permeability as a result of infection with *P. aeruginosa* and MyD88 signaling, wounded mice were placed under 2-4% isoflurane anesthesia for 5 minutes and injected i.v. via the tail-vein a 50μL dose of 1.0mg/mL BSA-Alexa 680 conjugate (Cat # A34787, ThermoFisher) (dissolved in sterile DPBS) at 12-14 hours after infection. Mice were then immediately placed inside an IVIS Spectrum and wounds were imaged for Alexa-680 fluorescence (680 Ex, 700 Em, 1s exposure, 1 segment per minute, for a total of at least 45 segments). Barrier permeability at the wound site was measured as fold-change fluorescence flux from t=0 to t=45 min.

2.17: PMN Functionality Assays

Pyroptosis

PMN were isolated from bone marrow and matured for four hours at 37°C, 5%CO_2 in StemSpan™ SFEM II media (StemCell Technologies, Cat # 09655), supplemented with the following growth factors (PeproTech Inc.):

Name of Reagent	Concentration
Recombinant Murine SCF (Stem Cell Factor) (Cat # 250-03)	100ng/mL
Recombinant Murine G-CSF (Granulocyte Colony-Stimulating Factor) (Cat # 250-05)	10ng/mL
Recombinant Murine IL-3 (Cat # 213-13)	10ng/mL
Recombinant Murine IL-6 (Cat # 216-16)	10ng/mL

Cells were incubated with *P. aeruginosa*, PMA, or control. After four hours, cells were extracted and stained with Staining Buffer containing Annexin Binding Buffer (1x), Propidium Iodine (1mg/mL at 1:500), Zombie Yellow (1:100), anti-Ly6G mAb (1:100), and Annexin V (1:16). After staining, flow cytometry analysis was performed in an AttuneNxT flow cytometer (ThermoFisher, Waltham, MA, USA). Live, Ly6G+ cells were analyzed for AnnexinV and Propidium Iodine staining using FlowJo.

NETosis

PMN isolated from murine bone marrow or generated from HSPC *in vitro* were seeded into a 96 well plate in HBSS +/+ (Hank's Balanced Salt Solution supplemented with Ca^{2+}) at a density of 1 x 10^5cells/ml and in the presence of *P. aeruginosa* (1x 10^8 CFU), PMA, or vehicle control. Plates were then incubated

overnight at 37°C then stained with 20uL of 5uM SYTOX Orange and incubated a room temperature for 15 minutes. Plates were then imaged on the IVIS Spectrum for SYTOX orange to measure NET output.

Phagocytosis

Phagocytosis was induced on PMN (that were either produced from HSPC *in vitro* or isolated from murine bone marrow using a pHrodo *S. aureus* BioParticle Phagocytosis kit (Cat # A10026, ThermoFisher, Waltham, MA, USA) according to the manufacturer's instructions. pHrodo MFI was measured on EGFP+ cells using an AttuneNxT flow cytometer.

2.18: Firefly Luciferase Preparation and Administration

Mice received a daily subcutaneous dose of 250 mg/kg of D-Luciferin (Cat # 122799, PerklinElmer) (dissolved in DPBS and sterile-filtered) 5 minutes prior to imaging in an IVIS Spectrum to quantify MRP8-luciferase activity *in vivo.*

2.19: Transfer of GelMA Constructs with HSPC into Mouse Wounds

Seven days after HSPC from S100A8-FFLuc mice were grown in either 3D hydrogels or 2D suspension cultures, cells were transplanted into C57BL6 mice in either suspension form or encapsulated in GelMA. 20–30 minutes prior to surgery, mice received a 100uL intraperitoneal injection of 0.03 mg/mL Buprenorphine Hydrochloride (Cat # 7292, MWI Veterinary Supply, Los Angeles, CA). Mice were then placed in 2-4% Isoflurane (Cat # 502017, MWI Veterinary Supply, Los Angeles, CA). Dorsal area of each mouse was shaven and aseptically sterilized with gauze in povidone iodine, followed with gauze in 70% isopropanol. One hydrogel per mouse was transplanted into a dorsal, intradermal pouch [156]. To quantify S100A8-luciferase activity at the site of transplantation, mice received a subcutaneous dose of 250 mg/kg of D-Luciferin (Cat # 122799, PerklinElmer, Waltham, MA, USA) and then placed under 2-4% Isoflurane for 5 minutes prior to being imaged under an IVIS Spectrum (PerklinElmer). Imaging was performed once a day as previously described [156].

2.20: Statistical Analysis

Data from animal studies are presented as Mean ± SEM unless otherwise stated. For *in vitro* studies, data are presented as Mean ± Standard Deviation unless otherwise noted. Statistical analysis was done

using one-way ANOVA test, two-way ANOVA with multiple comparisons test, or multiple or single Student's t-test. *, **, ***, and **** denote *p*-values of ≤0.05, ≤0.01, ≤0.001, and ≤0.0001, respectively. Unless otherwise noted, all statistical analysis and plots were generated in GraphPad Prism Version 10.2.1 (GraphPad Software, Boston, Massachusetts USA, www.graphpad.com). Illustrations accompanying data plots were created with BioRender.com under an Academic License.

CHAPTER 3: A DESIGNED HOST DEFENSE PEPTIDE FOR THE TOPICAL TREATMENT OF DIABETIC WOUNDS INFECTED WITH *STAPHYLOCOCCUS AUREUS*

3.1: Introduction

People with diabetes suffer from impaired immune responses as a result of poor cell metabolism and cellular senescence caused by insulin resistance [111,112]. At the same time, these individuals have elevated levels of inflammatory cytokines and chemokines released from visceral fat that in turn prematurely activate PMN and other immune cells during what should otherwise be homeostatic conditions [113, 114]. This leads to an inability to mount an effective immune response when pathogens breach the skin barrier, which leads to biofilm formation and chronic, intractable wound infections [115]. This typically manifests in the form of foot ulcers (DFUs), often seen in diabetic individuals as a result of impaired oxidative stress that disrupts pathogen clearance and tissue repair [113, 157]. This means that a diabetic foot ulcer (DFUs) is an environment where pathogens proliferate unimpeded, which often results in severe tissue necrosis, bone damage, and amputation [116]. Because this problem is only exacerbated by the rise in antibiotic-resistant bacteria, it is imperative to develop treatments for diabetic infections that directly target and improve host innate immunity [117–119]. The studies presented in this chapter evaluate the potential of a relative novel designed host defense peptide (dHDP), known as RP557, to act in synergy with PMN to suppress bacterial proliferation and accelerate healing of diabetic mouse wounds infected with Methicillin-Resistant *S. aureus*. The concepts, findings, methods, and figures that are part of this chapter were previously published in The International Journal of Molecular Sciences. This work was done in collaboration with Dr. L Edwards Clemens, Dr. Katherine Woodburn, Gustavo Garcia, and Kathryn Rivara and under the supervision of Dr. Scott I Simon at the University of California, Davis.

3.2: Designed Host Defense Peptide RP557

As discussed earlier, antimicrobial peptides (AMPs) are found in the dermis layer of the skin and play a critical role in defeating bacteria in wound infections [27, 97]. Their mechanism of action involves a β-sheet structure or amphipathic α-helix that has a net positive charge and disrupts the barrier function of negatively-charged bacterial cell walls [27, 97, 157]. Designed host defense peptides (dHDPs) are direct analogs to AMPs [120]. While AMPs serve as a line of defense against bacterial infections in healthy individuals [121–124], AMP activity is severely impaired in people with diabetes [125]. Thus, dHDPs present a promising strategy to restore AMP antibacterial capacity in diabetic individuals.

AMPs and dHDPs can directly and quickly eradicate bacteria, including MRSA and *P. aeruginosa* [126, 157]. This led to the development of the dHDP RP557 through several cycles of peptide design and synthesis [157]. RP557 has already been evaluated for antimicrobial activity both *in vitro* and *in vivo* [127, 128]. This includes its evaluation against *S. aureus* and *P. aeruginosa* in porcine burn wounds, where it was shown that bacteria were quickly eradicated after direct application of a single dose of RP557 [129]. The studies presented in the following sections build on these previously published reports on RP557 by assessing its potential to resolve diabetic infections and enhance PMN antibacterial functions *in vitro*.

3.3: RP557 Enhances PMN Effector Functions in vitro

One of the first host responses against MRSA and other pathogenic bacteria strains is PMN recruitment from circulation into the site of infection. This process involves PMN extravasation and activation characterized by upregulation of adhesion receptors such as CD11b and production of reactive oxygen species (ROS) [71–77]. Once recruited into the site of infection, PMN can phagocytose bacteria and undergo NET formation to stop pathogen proliferation and survival [130]. Therefore, PMN are key in the host's battle against pathogenic infections. Given that PMN are rapidly recruited and present at infection sites, the effect of RP557 directly on human PMN phenotype and function was evaluated *in vitro.* PMN viability, CD11b and CD18 expression, L-selecting shedding, migratory capacity, and ROS production were measured following cell incubation with RP557 in a dose-dependent manner. At a RP557 concentration of 156μg/mL, PMN remained more than 90% viable. Viability decreased to nearly 60% at 625μg/mL, and was nearly zero at 1mg/mL concentration of RP557 (Figure 3.1A). This suggests that higher RP557 concentrations may fasten PMN programmed apoptosis that follows PMN activation. To test the effect of RP557 on PMN activation, CD11b expression was measured. RP557 indeed upregulated surface CD11b expression nearly three-fold at a concentration of 312μg/mL of RP557 compared to 0μg/mL (Figure 3.1B) (at 312μg/mL, PMN still remained nearly 85% viable). These changes in CD11b upregulation correlated with a nearly six-fold increase in expression of high-affinity CD18 at a concentration of 312μg/mL of RP557 compared to 0μg/mL (Figure 3.1C). This phenomenon also correlated with measurements of L-selectin, CD62L shedding. L-selectin is expressed on PMN but is cleaved during PMN activation following pathogen encounter or stimulation with a chemotactic agent such as fMLP [72, 131, 157]. Therefore, lower levels of L-selectin expression correlate with a more activated and mature PMN state. PMN incubation with RP557 at a concentration of 16μg/ml resulted in

negligible L-selectin shedding compared to the 0μg/mL concentration. However, at 156μg/mL, shedding was nearly 60% and at 312μg/mL, RP557 elicited L-selectin shedding to more than 90% compared to 0μg/mL (Figure 3.2A). The next step was to evaluate the effect of RP557 on PMN migratory capacity. PMN migration in response to 10nM IL-8 alone served as a positive control, which was then compared to various concentrations of RP557 (Figure 3.2B). At 78μg/mL, the percentage of migratory cells was similar to the 0μg/mL condition but increased nearly two-fold from that at 156μg/mL. At 312μg/mL, migratory capacity was more than half than what was measured with IL-8 (Figure 3.2B). As discussed earlier, once PMN transmigrate into a site of infection, they perform a variety of antibacterial function such as ROS production (61–70). Therefore, ROS release was measured as a function of RP557 concentration. ROS production was induced by RP557 alone at concentrations as low as 156μg/mL and increased at 312μg/mL to a level >25% higher than what was observed with 10nM IL-8 alone (Figure 3.2C). Synergistic stimulation with fMLP further increased ROS levels also in an RP557 dose-dependent manner four- to eight-fold of what was measured from baseline. At a 312μg/mL concentration, RP557 stimulated more ROS production than 10nM IL-8 in the presence of fMLP (Figure 3.2C). Thus, RP557 can directly enhance PMN activation and antibacterial state *in vitro*.

3.4: RP557 Mitigates S. aureus Proliferation and Promotes Closure of Infected Diabetic Mouse Wounds

While RP557 may show promising potential for use as an antibacterial agent in a clinical setting, it must also be evaluated for potential cytotoxic effects that could be elicited on host cells and tissues. To examine whether RP557 altered the normal would healing process, sterile full-thickness dorsal wounds were performed on LysM-EGFP mice that produce granulocytes tagged with EGFP, which enables measurement of PMN recruitment into dorsal wounds via fluorescence imaging [90–94]. These wounds were treated daily with RP557 or vehicle control (saline) starting on Day 1 after wounding. RP557 did not alter the normal rate of wound healing over the course of the experiment (Figure 3.3A). Wounds treated with RP557 healed at similar rates as those treated with saline. Furthermore, EGFP imaging of these wounds showed that RP557 had negligible effects on PMN migration into the wound sites, measured as percent change in fluorescence intensity relative to Day 1 post-wounding (Figure 3.3B). This demonstrated that RP557 is likely not cytotoxic *in vivo* as it did not seem to alter the inflammatory processes that regulate PMN recruitment and tissue repair in the absence of infection.

A clinical application of interest is to employ RP557 to treat Diabetic Foot Ulcers (DFUs). To evaluate the antimicrobial potential in the context of diabetes disease, RP557 was applied directly into type 2 diabetic mouse wounds inoculated with bioluminescent MRSA [157]. Suppression of bacterial proliferation, measured by percent change in bioluminescent signal from the infected wounds, and wound healing, measured by percent changes in wound size, were the two primary readouts during these studies. SEM scanning of these wound tissues obtained at 24 hours post-infection revealed that MRSA had formed biofilm by that timepoint (Figure 3.4A), which is a contributing factor to DFU morbidity in people with diabetes [112]. Thus, daily topical treatment with RP557 on infected wounds started at 24 hours post-wounding to assess the ability of the dHDP to tackle biofilm-prone infections. Bioluminescence flux from these wounds was measured once daily using an IVIS spectrum to quantify bacterial growth over time. By Day 3 post-wounding (*i.e*. at 48 hours after the first application of RP557), bacterial proliferation was suppressed and lower on mice treated with RP557 compared to those treated with only vehicle control ($p<0.01$). (Figure 3.4B). Subsequent applications of RP557 continued to mitigate bacterial growth, while the control group increased, peaking at Day 3 post-infection, and remaining elevated on Day 4 ($p=0.069$) and slightly elevated on Day 5 ($p=0.14$).

The effect of RP557 on wound closure was also examined on infected and uninfected diabetic mouse wounds. Wound sizes were measured once daily following mouse imaging and computed as percent change relative to Day 1. Uninfected mice were studied to confirm that RP557 did not alter the normal healing process of diabetic sterile wounds. Uninfected wounds treated with either RP557 or vehicle control closed at similar rates (Figure 3.5A), meaning that RP557 did not alter the wound healing process on uninfected mice. However, RP557 did have an effect on closure of diabetic wounds infected with MRSA. Wounds treated with RP557 were smaller than those treated with vehicle control as early as 24 hours after the first dose (Figure 3.5B). Wound closure continued to accelerate with each subsequent daily dose of RP557, while wounds treated with vehicle control steadily increased in size until peaking at Day 6 post-wounding. Further analysis of the impact of RP557 on the rate of wound closure, performed by calculating the slope of the linear regression fit on wound size data from Day 1 to Day 5 post-wounding, revealed that RP557 significantly increased the rate of closure of infected wounds (Figure 3.C). In fact, MRSA-infected wounds treated with RP557 healed at a rate similar to that of uninfected wounds, suggesting that RP557 indeed inhibited bacterial proliferation within the wound bed.

3.5: Conclusions and Future Directions

As discussed throughout this dissertation, PMN recruitment into a site of infection is essential for bacterial clearance and resolution of infected wounds [61–71, 82, 90–95]. *In vitro*, RP557 significantly enhanced a variety of PMN markers indicative of activation and antibacterial phenotype. *In vivo*, daily topical application of RP557 suppressed bacterial proliferation and accelerated tissue repair on diabetic mice. Therefore, RP557 appears to act in two ways: 1) by reducing MRSA growth, biofilm production and the associated inflammatory response; and 2) by enhancing PMN chemotactic and antibacterial activity, such as ROS production. At the same time, RP557 also did not alter PMN recruitment or healing of non-infected wounds, suggesting that it was non-cytotoxic and specifically active in the presence of bacteria. What remains elusive is the mechanism of action by which RP557 elicits upregulation of CD11b, CD18, L-selectin shedding, migration, and ROS production. Future studies will examine the effects of RP557 on TLR binding and other surface receptors that are engaged before activation, such as G-protein coupled receptors. Future studies will also assess PMN state *in vivo* following infection and treatment with RP557 via histology and cytokine measurements from wound tissues, such as TNF-α and IL-1β.

Diabetic infections are characterized by weakened immune responses as a result of cellular senescence and insulin resistance [137, 157]. PMN are impaired, leading to dysfunctional bacterial killing and an increase in bacterial growth [82, 138]. As a result, pathogens that breach the skin barrier, such as *S. aureus* or P. aeruginosa have an opportunity to proliferate and form biofilm in diabetic wounds [82, 94, 97, 112]. Antibiotic resistance developed by *S. aureus* and other bacterial strains, combined with a decrease in the discovery and development of novel and effective antibiotics, further complicates bacterial infections in diabetic individuals, and exacerbates the burden on the health care system [1–6, 12]. Therefore, there is an urgent need to develop therapeutic approached that suppress bacterial growth and enhance the immune system to promote resolution and tissue repair. The dHDP RP557 present a promising viable alternative based on the mouse studies presented in this chapter. These studies showed that by Day 3 post-infection, daily topical treatment with RP557 mitigated MRSA proliferation in subcutaneously-infected diabetic wounds, while MRSA burden steadily increased in wounds treated with only vehicle control. Furthermore, no resistance to RP557 has been known to develop by bacteria strains like MRSA or *P. aeruginosa* [120]. This is a key advantage over antibiotic treatments, where antimicrobial resistance complicates the treatment of diabetic foot ulcers and infected wounds. With that being said, the bacteria burden data shows that there is room for

improvement to further and more rapidly diminish bacterial abundance in diabetic mouse wounds. For that end, additional SEM analysis of wound tissues should be performed in future studies at Day 3 post-wounding and later to confirm that MRSA is fully and evenly eradicated at the wound surface and deep into the tissue. In addition, alternative routes of RP557 delivery, such as systemic or subcutaneous injection should also be explored. Lastly, the long-term application of RP557 to treat DFUs and diabetic wound infections in a clinical patients will need to be performed in conjunction with other strategies that tackle disease morbidity, including plasma glucose level regulation, adoptive cell transfer from healthy donors, and the use of multifunctional wound dressings, additional dHDPs, virulence factor neutralizers, off-loading devices, superparamagnetic iron oxide nanoparticles, and growth factors that exert healing effects [82, 94, 112, 117–119, 135–139, 157].

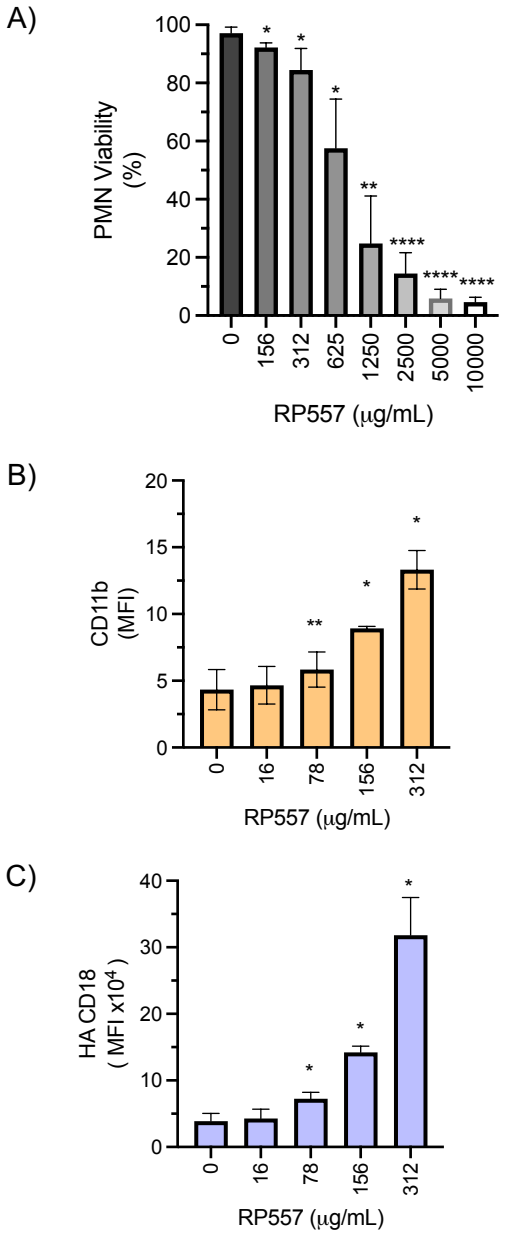

Figure 3.1: Effect of RP557 on PMN viability and integrin expression. A) Viability of human PMNs that were incubated for 30 minutes with different concentrations of RP557. Viability was determined using propidium iodine staining B) Measurement of CD11b and C) CD18 via flow cytometry from human PMNs that were incubated with the indicated concentrations of RP557 for 20 min at 37 °C. Paired Student's t-tests were performed comparing the average value of a given condition to the control condition (e.g. 0 μg/mL) of the same donor.
Data are derived from n = 4 replicates per group.
*, **, ***, and **** denote p-values of ≤0.05, ≤0.01, ≤0.001, and ≤0.0001, respectively.
MFI = Mean Fluorescence Intensity.

Data were first published in *MDPI International Journal of Molecular Sciences* by Vargas et al., 2023.

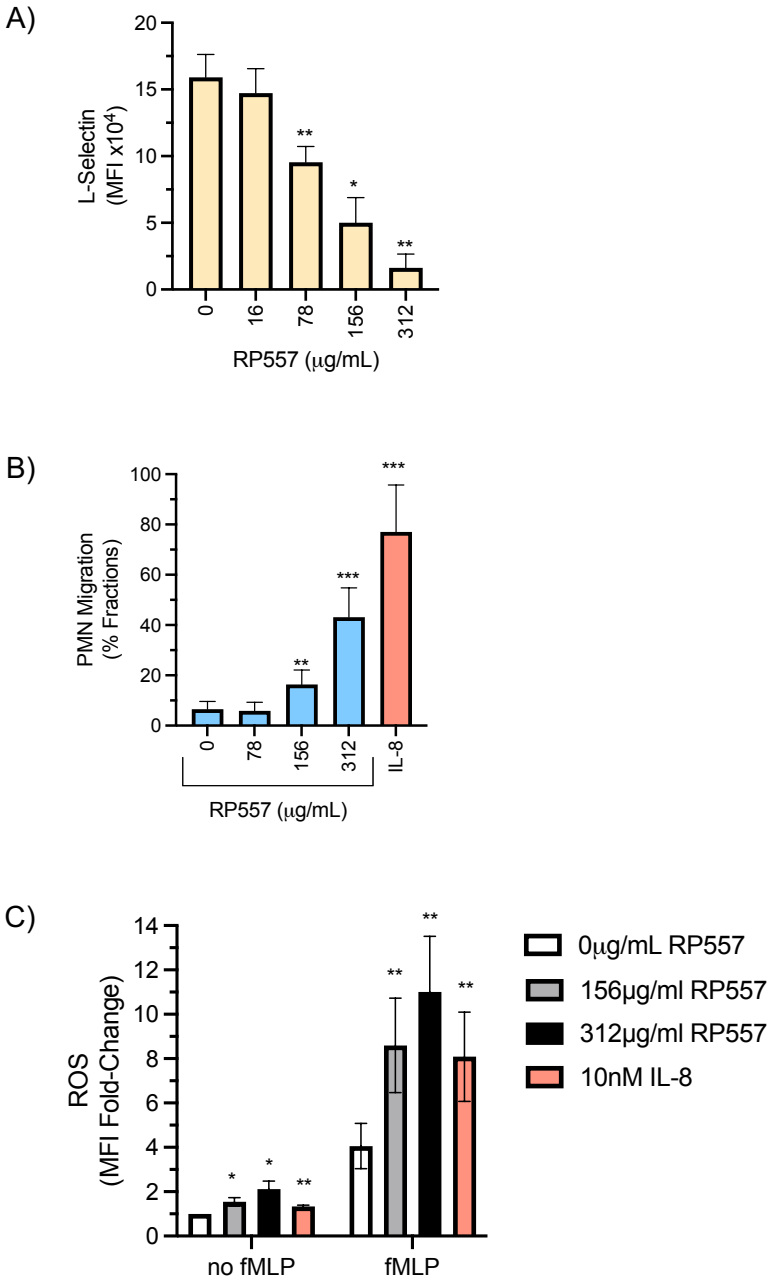

Figure 3.2: Effect of RP557 on PMN effector functions. A) L-Selectin (CD62L) expression, B) migratory capacity, and C) ROS elaboration by human PMNs after being incubated with varying concentrations of RP557.
Data are derived from n=3 replicates per group.
*, **, *** denote *p*-value ≤0.05 ≤0.01, and ≤0.001, respectively.
MFI = mean fluorescence intensity.
ROS = Reactive Oxygen Species
fMLP = N-Formylmethionyl-leucyl-phenylalanine (PMN chemotactic factor)

Data were first published in *MDPI International Journal of Molecular Sciences* by Vargas et al., 2023.

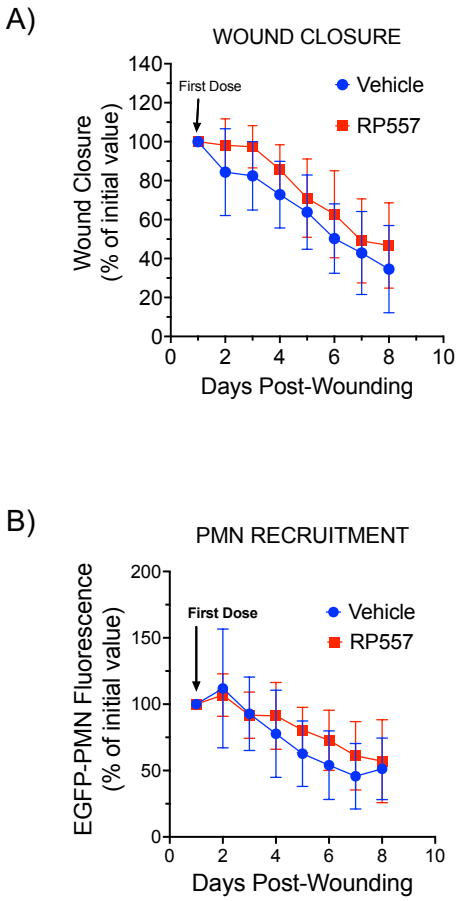

Figure 3.3: Effect of RP557 on PMN recruitment and would healing of wild-type, uninfected wounds. Nondiabetic LysM-EGFP mice that produce EGFP-tagged granulocytes were dorsally wounded and treated with RP557 or vehicle control. A) PMN recruitment into the wound was measured using an IVIS spectrum as a function of fluorescence flux. B) Wound closure measured as changes in wound size over time.
Data are derived from *n* = 11 mice per group.

Data were first published in *MDPI International Journal of Molecular Sciences* by Vargas et al., 2023.

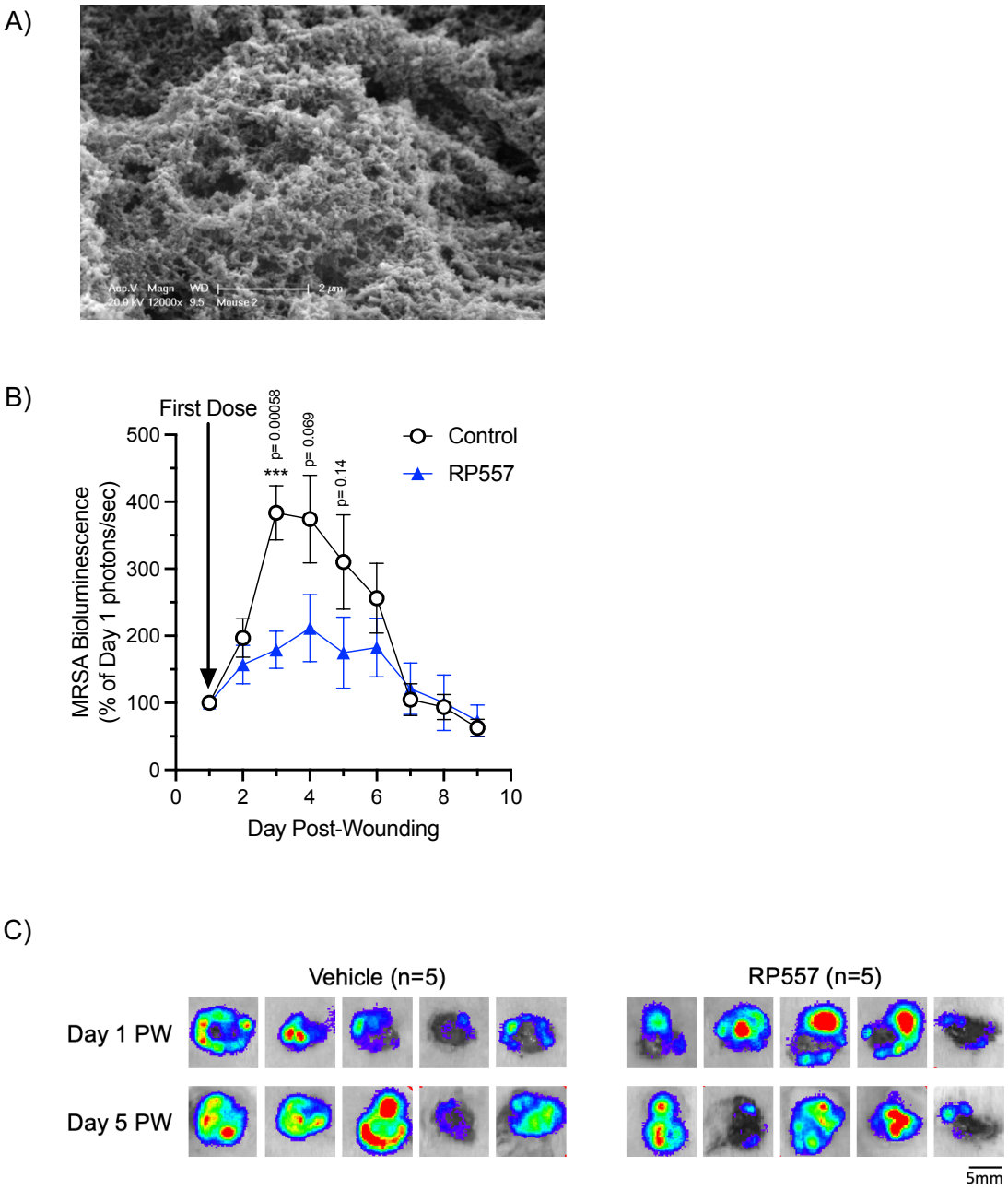

Figure 3.4: RP557 prevents *S. aureus* proliferation in infected, diabetic mouse wounds. Diabetic (TALLYHO) mice received a full-thickness dorsal wound that was immediately inoculated with bioluminescent MRSA USA300 (this timepoint is denoted as "Day 0"). Starting at 24 hours after bacterial inoculation (i.e. "Day 1"), mouse wounds were treated once daily with either saline (control) or RP557. A) SEM scan of wound tissue extracted at 24 hours post-inoculation showing that MRSA had proliferated and underwent biofilm formation. B) Measurements of bioluminescence flux from the wound acquired with an IVIS machine as photons/second and normalized to their value on "Day 1." C) Representative bioluminescence scans of mouse wounds acquired on "Day 1" and "Day 5." Data are derived from n = 5–10 mice per group.
*, **, *** denote *p*-value ≤0.05 ≤0.01, and ≤0.001, respectively. Scale bar is 5mm.

Data and figures were first published in *MDPI International Journal of Molecular Sciences* by Vargas et al., 2023.

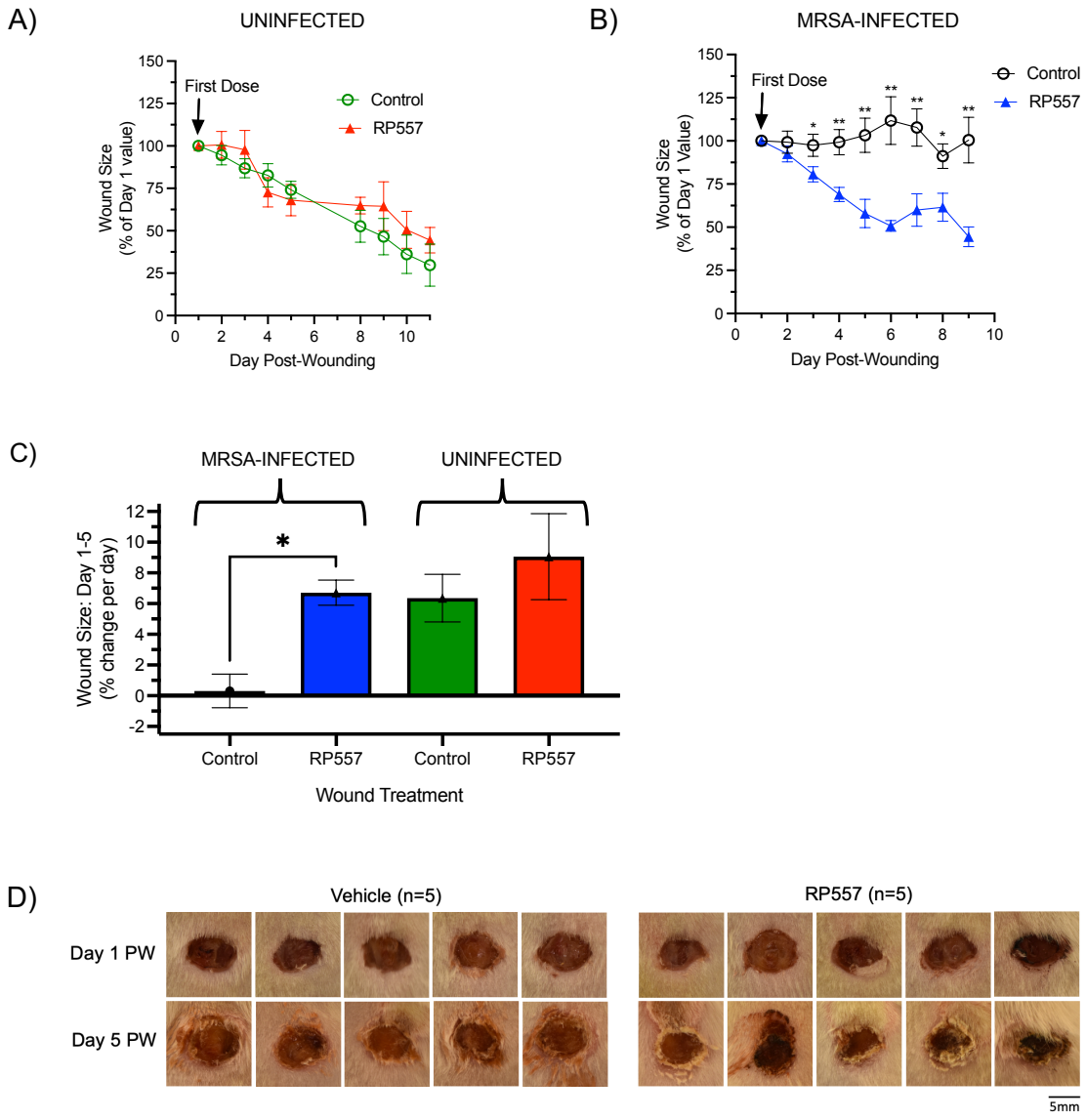

Figure 3.5: RP557 accelerates closure of diabetic mouse wounds infected with S. aureus. Diabetic (TALLYHO) mice received a full-thickness dorsal wound on Day 0. Starting on Day 1 (*i.e.* 24 hours after wounding), wounds were treated at each timepoint with either control treatment (saline or FBS) or RP557. A) Change in wound size of uninfected diabetic (TALLYHO) wounds relative to wound size on Day 1 (these wounds were treated from Day 1 to Day 5 and from Day 8 to Day 11. Data are from one experiment (n = 3–5 mice per group). B) Change in wound size of MRSA-infected diabetic (TALLYHO) wounds relative to wound size on Day 1. Data are from two independent experiments (n = 5 to 10 animals per group). C) Slope value of the simple linear regression fit of the data shown in A and B, from Day 1 to Day 5, expressed as a positive value. D) Representative images of mouse wounds from the uninfected and infected groups (vehicle control-treated vs RP557-treated). Scale bar is 5mm.
*, **, *** denote p-value ≤0.05 ≤0.01, and ≤0.001, respectively.

Data and figures were first published in *MDPI International Journal of Molecular Sciences* by Vargas et al., 2023.

CHAPTER 4: PMN EXPANSION FROM HEMATOPOIETIC STEM CELLS VIA ENCAPSULATION IN 3D GELATIN MICROGELS TO ENHANCE INNATE IMMUNITY AGAINST *STAPHYLOCOCCUS AUREUS*

4.1: Introduction

Methicillin-resistant *Staphylococcus aureus* (MRSA) is a common source of hospital-acquired infections that can result in severe pain and tissue damage. Individuals who suffer from cancer, diabetes, or HIV, or are otherwise immunocompromised, often experience severe infections [1–6]. MRSA infections can become chronic and intractable because of its resistance to a wide range of antibiotics, including methicillin, penicillin, linezolid, and daptomycin [140]. An alternative approach to treat MRSA infections is via delivery of PMN produced from hematopoietic and pluripotent stem cells (HSPC) directly into the site of infection. PMN are the most important and abundant effector cells of the immune system, and previous studies have shown that a single dose of HSPC transferred into immunodeficient mice enhances the immune response and increases overall survival rates [94]. However, the signaling mechanisms that govern PMN production from HSPC as well as strategies to optimize cell number production and antibacterial function remain at large. The following studies employ porous hydrogels for HSPC encapsulation to optimize PMN proliferation and antibacterial function for the potential use in adoptive transfer studies in the future.

Recent studies have shown that hematopoietic stem and pluripotent cells (HSPC) traffic into the site of MRSA infection and are essential for full bacterial clearance. To demonstrate this, in previous studies, PMN were depleted from the circulation of LysM-EGFP mice with mAb Gr-1, an anti-PMN mAb, either before (pre-Gr1) or after (post-Gr1) bacterial inoculation (Figure 4.1A) (The term “Pre-Gr1” denotes antibody administration one day before infection and “Post-Gr1” denotes antibody administration one day after infection. This experimental overview is shown on Figure 4.1A) [90]. In the pre-Gr1 group, the number of PMN detected at the site of infection still increased over time (Figure 4.1B SA-pre Gr-1) despite receiving anti-Gr1 antibody one day prior to infection and on days 1 and 3 post-infection, and surprisingly, the majority of these mice survived the infection [90]. At the same time, in the post-Gr1 cohort, the number of PMN began to decrease after day 1 as expected, but it began to increase again on day 4 despite continuing Gr1 treatments (Figure 4.1B SA-post Gr-1) [90]. In order to show that the source of EGFP-PMN at the site of infection was indeed from HSPC, an adoptive transfer of HSPC from LysM-EGFP mice was performed into the tail-vein of ‘dark’ (non-LysM-EGFP) C57BL6 mice (Figure 4.2A)

[90]. HSPC were labeled with Qtracker 705 and observed migrating from circulation into the wound site in mice inoculated with Saline and in mice inoculated with *S. aureus*. (Figure 4.2B) [90]. EGFP signal, indictive of PMN differentiation, continuously rose for eight consecutive days on mice infected with *S. aureus* wounding (Figure 4.2C) [90]. Combined, these studies demonstrate that HSPC migrate into a wound, undergo extramedullary granulopoiesis, and play a critical role in providing sufficient PMN numbers at the site of a MRSA infection [90].

Furthermore, previous studies have shown that it is possible to rescue immunodeficient MyD88-/- mice infected with *S. aureus* via adoptive transfer of PMN expanded from HSPC *in vitro*. MyD88 is a key adaptor molecule necessary to launch an effective immune response against *S. aureus*. MyD88-/- mice are more likely to show an inability to defeat the infection. Kim et al., proposed that hematopoietic stem cells are recruited to and experience granulopoiesis at the site of infection via a MyD88-dependent pathway [90]. As discussed earlier, MyD88 is recruited following Toll-like Receptor 2 (TLR2) activation by peptidoglycan and lipoteichoic acid from the cell wall of *S. aureus* [62]. Survival rates of MyD88-/- mice infected with *S. aureus* are lower compared to those of wild-type mice [94]. Falahee et al., also showed that mortality due to sepsis is partially reversed when HSPC are transferred into MyD88-/- mice infected with *S. aureus* [94]. This inspires the development of methods to enhance PMN production from HSPC *in vitro* as a potential strategy to enhance the immune response against drug-resistant infections via adoptive cell transfer into sites of infection.

This chapter presents a series of studies demonstrating that PMN production can be enhanced *in vitro* by encapsulating HSPC in a 3D hydrogel-based microenvironment. Previous studies have shown that cell survival can be prolonged within collagen-based 3D hydrogels compared to 2D suspension cultures [141], which is critical for HSPC granulopoiesis during bacterial infection that often leads to lysis of immune cells due to pathogen virulence factors [94]. Previous studies have demonstrated that gelatin methacrylate (GelMA) hydrogels can maintain stem and progenitor cell populations [142]. The studies presented herein show that 3D GelMA hydrogels increase PMN production without resulting in loss of cell functionality against pathogenic bacteria. The ultimately goal is to use these hydrogels as a delivery vehicle in PMN transplantation studies to enhance the immune response to infection. Some of the figures, ideas, and methods presented as part of this chapter were previously published in Advanced Healthcare Materials [156] as noted in the figure legends. This work was done in collaboration with Dr. Tomas Gonzalez-Fernandez and Evan Cirves under the supervision of Dr. Scott I Simon at the University of California, Davis.

4.2: Encapsulation of HSPC in 3D GelMA Hydrogels Increases Production of GMP and PMN

One of the main objectives of this chapter is to address whether a 3D microenvironment can enhance HSPC survival, proliferative capacity, and overall granulopoiesis. It is known that cell mechano-transduction plays an important role in stem cell differentiation, but whether a 3D microenvironment can enhance or sustain HSPC survival and PMN production is still an active area of research [142, 156]. To fill in this gap in knowledge, HSPC were extracted from LysM-EGFP mice and maintained either inside 3D GelMA constructs or in 2D suspension culture. LysM-EGFP mice produce granulocytes that are tagged with the green fluorescent protein, while undifferentiated HSPC are not [94, 143]. This easily enables detection and quantification of PMN production via flow cytometry, especially when used in conjunction with other PMN markers such as CD11b and Ly6G. In this experiment, cells were cultured for three days and then quantified and analyzed via flow cytometry. The results showed that there were similar total number of cells in both suspension and GelMA gels. However, closer analysis revealed that there were more GMP ($LysM^{hi}Ly6C^{hi}$ cells) and PMN ($LysM^{hi}Ly6G^{hi}CD11b^{hi}$ cells) detected in the 3D cultures (Figure 4.3A-C). Furthermore, fold-expansion measurements, calculated as the total number of cells divided by the initial HSPC cell density [94], show that the 3D hydrogels produce more GMP and PMN cells per input HSPC compared to the 2D suspension cultures (Figure 4.3D). Combined, this data shows that the 3D GelMa hydrogels significantly enhance the production of PMN from HSPC relative to the 2D suspension cultures.

The ability of the cells to exit or remain inside the 3D hydrogels was also examined. The results show that cells can “escape” out of the 3D hydrogel microenvironment (Figure 4.4A). In these studies, cells were cultured in either 3D hydrogels or 2D suspension culture for 7 days. The rationale for this longer culture period was to allow for more cells to escape the hydrogel so they could be then analyzed via flow cytometry and compared with the cells inside the hydrogel (In-GelMA) and those grown in suspension. At 7 days, the GelMA hydrogels showed slightly more cells with an LSK phenotype, but this was not statistically significant when compared to the suspension group (Figure 4.4B). The phenotype of the cells that remained specifically inside the gel (In-GelMA) was then directly compared with the phenotype of the cells that escaped. The cells grown in suspension served as a positive control. There were fewer total cells outside the hydrogels (Escaped) compared to inside the hydrogels (In-GelMA) (Figure 4.4C). However, inside the hydrogel there was a higher fraction of LSK cells. This fraction was also higher than what was measured in suspension cultures (Figure 4.4D). This suggests that LSK cells

underwent self-renewal at higher rates inside the hydrogel, meaning that the 3D GelMA constructs maintained HSPC survival and proliferative capacity. Outside the hydrogel, the majority of cells exhibited a GMP phenotype, which was also a higher fraction than what was measured from suspension cultures (Figure 4.4D). Although the number of PMN was similar both inside and outside the GelMA hydrogels, the EGFP Mean Fluorescence Intensity (MFI) was higher on the cells found inside the hydrogel (Figure 4.4E). Higher EGFP MFI is indicative of more mature granulocytes, meaning that cells inside the GelMA were at later stages of differentiation [143]. It is possible, however, that once outside the hydrogel, mature PMN undergo programmed cell death at faster rates, resulting in overall similar PMN fractions when compared to the other groups. It is also unclear whether cell release is marked by increased cell migratory capacity, another indication of a more mature cell state, or by cell enzymes that degrade collagen and other ECM components [144–145, 156].

4.3: Evaluation of Antibacterial Function of PMN Produced in 3D Hydrogels vs 2D Culture

While PMN production measured as cell number or percent fraction is a key indicator on the promising potential of GelMA hydrogels to serve as cell culture microenvironments, it is equally important to confirm that any cells generated are competent and can act against pathogenic bacteria. As a result, it was important to assess antibacterial capacity of cells grown in 3D hydrogels and in suspension culture. Two main functions were assessed in these studies: phagocytosis against *S. aureus* bioparticles and NETosis against live *P. aeruginosa* (Figure 4.5A). HSPC were cultured in equal numbers in either a 3D hydrogel culture or in a 2D suspension culture for three days. Cells isolated from bone marrow served as a control. To measure NETosis, cells in equal numbers were either exposed to live *P. aeruginosa*, PMA or vehicle control and then extracellular DNA was quantified with SYTOX staining. When exposed to *P. aeruginosa*, cells from suspension cultures and GelMA cultures showed nearly similar levels of extracellular DNA as cells from bone marrow (Figure 4.6B). Although the signal from cells in bone marrow was statistically higher, it is noteworthy to highlight that the cells cultured *in vitro* from HSPC and exposed to live *P. aeruginosa* still possessed the capacity to release NETs at higher rates than the control group and the PMA group (Figure 4.6B). Similarily, the results from the phagocytosis assay showed that cells from both suspension and GelMA had higher antibacterial capacity than cells from bone marrow when exposed to *S. aureus* bioparticles in equal numbers (Figure 4.6C). The cells from suspension had similar but statistically higher activity than those from the GelMA hydrogels (Figure 4.6C). Taken together, these studies demonstrate that HSPC grown *in vitro* can lead to the production of

functionally active granulocytes that could be adoptively transferred into immunodeficient hosts to tackle bacterial infections.

4.4: Potential of 3D GelMA Hydrogels to Enable PMN Transplantation

The ultimate goal of these studies is to employ the 3D GelMA hydrogels not only as an environment to grow functional PMN from HSPC but also to use as a delivery vehicle to transplant PMN into infected wounds to enhance pathogen clearance and healing. To track these cells *in vivo* under the skin, a mouse line, herein known as S100A-FFLuc, with higher imaging sensitivity was developed. These S100A8-FFLuc mice have the firefly luciferase (FFLuc) reporter inserted in the myeloid related protein 8 (MRP8/S100A8) promoter region. This reporter enables PMN imaging deeper in tissue and at a high sensitivity (*i.e.*, detection of luciferase signal relative to background can be achieve with 10^4 PMN, which is a lower cell number compared to cells from to LysM-EGFP mice) [91] (Figure 4.6, Supplemental Figure 5.1). There is in fact a linear correlation between increasing PMN number seeded *in vitro* and increasing Firefly signal measured using an IVIS Spectrum (Figures 4.6 and 4.7).

To determine the effects of the 3D hydrogel environment alone on granulopoiesis, HSPC from S100A8-FFLuc mice were cultured in suspension or GelMA in either basal media (denoted *CTLR*) or in media supplemented with myeloid-inducing factors (denoted *DIFF*). Luciferase activity was not observed in HSPC immediately after their extraction from bone marrow and seeding (Day 0), indicating that any firefly signal was produced solely by maturing PMN (Figure 4.7). Firefly signal was started to be detected in both 2D (suspension) and 3D (GelMA) cultures as early as Day 3 (Figure 4.7C). By Day 7, the firefly signal was significantly higher from cells cultured in DIFF media, suggesting more granulocyte maturation by this timepoint (Figure 4.7D). Interestingly, cells cultured inside the GelMA hydrogel in the absence of differentiation factors (CTRL) still produced firefly signal at a higher rate than what was measured on Day 3 (Figure 4.7D). When cultured in CTRL media, luciferase activity was only detected from cells grown in the 3D GelMA hydrogels and not in the 2D suspension cultures (Figure 4.7C-D), suggesting that the 3D GelMA microenvironment was sufficient to induce granulopoiesis likely via a mechano-transduction pathway. Flow cytometry analysis of these cells showed that the number of LSK, GMP, and PMN was higher in cell groups grown in DIFF media compared to those grown in CTLR media (Figure 4.8). Cells cultured in GelMA also had higher numbers of GMP and PMN compared to their suspension counterparts (Figure 4.8B-C), even when grown in CTRL media. All of this data reaffirms that

the 3D GelMA hydrogels serve as an environment that is better at producing PMN compared to 2D cultures.

To assess the ability of the GelMA construct to maintain cell survival *in vivo,* cells were transplanted directly into the dorsal area of C57BL6 mice. HSPC were extracted from S100A8-FFLuc mice and grown in either suspension or in 3D hydrogels in differentiation for 7 days before transplantation. Mice were then imaged daily under an IVIS Spectrum. Mice that received a GelMA transplant showed luciferase signal at Day 5 post-transplantation, while those that received cells from suspension cultures did not (Figure 4.9). Quantification of this signal showed 40% less luciferase flux from the mice with cells from suspension compared to mice with GelMA hydrogels [156]. The signal from the GelMA hydrogels was also more localized, highlighting the potential to use these constructs for controlled cell transplantation into specific wound infection sites. More replicates will need to be performed in future studies to confirm these observations and optimize the hydrogel transplantation process.

4.5: Conclusions and Future Directions

PMN are the first line of defense against bacterial infections. In response to *S. aureus* infection in skin, Hematopoietic Stem and Progenitor Cells (HSPC) traffic to the site of infection and undergo extramedullary granulopoiesis to produce PMN in sufficient quantity necessary to resolve infection. Furthermore, MyD88-/- mice that lack sufficient granulopoiesis are able to boost their immune response against *S. aureus* via adoptive transfer of wild-type PMN and HSPC into the site of infection. However, the ability to scale up production of functional PMN remains elusive. There is currently a need to address challenges of *in vitro* PMN production from HSPC as a way to provide sufficient functional PMN to immunodeficient individuals, such as those who are undergoing chemotherapy, for example. Previous studies have shown that delivery of a single dose of PMN generated from HSPC *in vitro* via 2D suspension culture was sufficient to enhance the survival of immunodeficient mice that had been dorsally wounded and infected with *S. aureus* [94]. The studies presented in this chapter demonstrate the ability to produce functional PMN in a 3D microenvironment that enhances HSPC granulopoiesis compared to 2D suspension cultures. Furthermore, these 3D constructs have the potential to be implanted into specific sites of infection to boost granulocyte counts and overall innate immune function.

One of the main objectives in the cell adoptive transfer studies presented in this chapter is to ensure that the survival and self-renewal capacity of HSPC populations that are critical for sustained production of PMN is both maintained and enhanced [156]. A strategy to achieve this is to build a 3D

microenvironment with similar mechanical properties as the bone marrow, such as porosity and stiffness. 4% GelMA constructs have been shown to maintain LSK populations at up to 20% frequency after one week following encapsulation [142]. In the studies presented in this chapter, 5% GelMA constructs resulted in the highest expansion efficiency compared to other GelMA concentrations, including 10% and 20% [156]. A 5% GelMA was shown to maintain HSPC populations and increase GMP and PMN production over suspension cultures at Day 3 post-HSPC encapsulation. These results are consistent with previous studies reporting that 3D collagen substrates can enhance HSC proliferation [141] and show that a 5% GelMA 3D hydrogel is a suitable environment to maintain HSPC survival and self-renewal capacity and leads to increased production of PMN and GMP [156].

The effect and efficacy of 3D GelMA hydrogels to generate and maintain GMP and PMN populations from HSPC was examined. $CD117^{hi}$ HSPC were isolated from the femurs and tibias of LysM-EGFP mice. These mice produce granulocytes that are tagged with the green fluorescence protein, while HSPC are not [143]. The HSPC were either cultured in suspension culture or encapsulated into 3D GelMA hydrogels on the same day they were isolated from mice. The process of encapsulation involved polymer UV-crosslinking and resulted in the production of hydrogels with desired sizes and mechanical properties [156]. HSPC were cultured in media factors that promoted differentiation towards a PMN phenotype (see section 2.4 in Chapter 2). After three or seven days after culture, cells were analyzed via flow cytometry to assess GMP and PMN phenotype. The results show that HSPC encapsulation and culture in 3D GelMA hydrogels leads to higher numbers of GMP and PMN compared to HSPC cultures grown in 2D (suspension). Although the total cell expansion between 3D GelMA and 2D suspension cultures remained similar, when the phenotype of these cell populations was further classified via flow cytometry analysis, it was clear that the 3D GelMA microenvironment had promoted production of more GMP and PMN cell populations than the 2D suspension cultures. It remains unclear whether the media growth factors that promote PMN production can reach the cells inside the 3D hydrogel at similar concentrations as the cells grown in suspension culture, as suggested by previous studies [146, 147]. Future studies will examine fluid dynamics to optimize and adjust media growth factor concentration to cells inside a 3D environment and whether this further optimizes cell survival, HSPC renewal capacity, and PMN production.

The ability of cells to exit the 3D GelMA microenvironment was also observed. By Day 7 after encapsulation, nearly 40% of all cells were found outside the 3D constructs, with the majority of the cells exhibiting a GMP phenotype [156]. Interestingly, the majority of the cells that remained inside the

3D construct exhibited an LSK phenotype, as measured via flow cytometry analysis. This supports the notion that the 3D GelMA hydrogels can maintain HSPC survival and possibly self-renewal capacity. Although the differences in PMN frequency were not significant between inside and outside the GelMA construct, it is possibly that mature PMN produced inside the GelMA undergo cell release similar to what occurs *in vivo* when PMN exit the bone marrow and enter the circulation, which is a continuous process during both inflammation and during homeostatic conditions that is followed by programmed cell death via apoptosis [71]. It is possible that once cells exit the GelMA construct, more mature PMN undergo programed cell death, resulting in similar PMN numbers measured both inside and outside the 3D microenvironment. Future studies will further examine the apoptotic state of cells inside and outside the GelMA hydrogels and compare with those grown in suspension. It is also unclear if cell escape is mediated by increased PMN/GMP migratory capacity or by secretion of collagenase enzymes that degrade or otherwise alter the 3D environment, as some studies have suggested [148]. Future studies will examine the mechanisms governing this cell escape out of the 3D constructs and how this phenomenon can be optimized to enable controlled delivery of GMPs and PMNs into infected skin wounds.

The capacity to activate and perform antibacterial functions was also investigated in cells grown in GelMA and suspension. This involved measuring CD11b expression, phagocytosis, and NETosis. CD11b is an integrin that is key in mediating PMN recruitment into sites of infection [150–152, 156]. Since one of the ultimate objectives is to deliver PMN grown *in vitro* to sites of inflammation *in vivo*, measuring CD11b expression was a critical marker indicative of not only cell maturity but also activation and antibacterial capacity. Cells grown in the 3D GelMA constructs were capable of more upregulation of CD11b expression than cells grown in suspension cultures following stimulation with PMA [156]. This highlights the superiority of the GelMA constructs at producing not only more mature but also more competent PMN. This is further supported by phagocytosis assays performed on cells from GelMA and suspension cultures. Flow cytometry-based assays using *S. aureus* bioparticles revealed that PMN from suspension and GelMA cultures were capable of performing phagocytosis, both groups at higher levels than PMN directly isolated from bone marrow. Another indicator of PMN maturation and competency is their ability to undergo NETosis in response to infection [83–87, 103, 104, 107]. When exposed to live *P. aeruginosa* or PMA, equal numbers of cells from the suspension group and the GelMA group produced NETs at similar levels to each other, but both to a lesser extent in comparison to cells that were directly isolated from bone marrow. This still demonstrates, however, that the 3D GelMA constructs lead to the production of functional, competent PMN. Taken together, this data supports the conclusion that HSPC

encapsulated in a 3D GelMA hydrogel microenvironment can generate functional PMN that could be use to combat pathogenic infections caused by bacterial strains of clinical interest, including *P. aeruginosa* and *S. aureus*.

To further assess expansion efficiency and the potential to transplant GelMA constructs into sites of bacterial infection to provide sustained PMN numbers, a mouse line expressing the firefly luciferase reporter on granulocytes was developed. This line was generated by cross-breeding mice expressing a Cre-MRP8 promoter with mice expressing a FFLuc-Lox reporter. The resulting mice produced granulocytes expressing Firefly luciferase in the S100A8 protein that could be imaged and quantified through skin tissue. This S100A8-FFLuc reporter acted as a mature PMN tracker that could be imaged and quantified *in vivo* at higher sensitivity and tissue penetration compared to the LysM-EGFP reporter mouse line (compare Figure 4.6 and Supplemental Figure 5.1). The use of S100A8-FFLuc cells made it possible to observe cell maintenance under the skin of C56BL6 mice following transplantation of the GelMA constructs or cells grown in suspension form into the dorsal area. Cells transplanted inside the 3D hydrogel retained bioluminescence signal for up to 5 days. On the other hand, cells transplanted in suspension form dissipated and their FFLuc signal was diminished throughout the course of the study [156]. This highlights the potential to use GelMA hydrogels for targeted and possibly controlled delivery of self-renewing HSPC and mature PMN into specific, desired sites of infection. HSPC from S100A8-FFLuc mice were also grown in both 2D and 3D culture with and without differentiation growth factors, denoted CTRL (without) and DIFF (with). The purpose of this was to assess the direct biomechanical effects of the 3D GelMA microenvironment on HSPC self-renewal capacity and PMN differentiation. Cell phenotype analysis and classification of these cells via flow cytometry showed that the number of both GMP and PMN populations were higher in the 3D GelMA constructs than in the 2D suspension cultures. The results also showed that cells grown inside the GelMA constructs produced FFLuc signal, and thus mature PMN, even when cultured without any differentiation growth factors. This was observed only on cells cultured inside the 3D hydrogels and not on those grown in suspension form. Therefore, the 3D environment alone was sufficient to promote cell renewal and expansion. This interesting discovery highlights the effects and the importance of a 3D microenvironment and its mechanical properties that influence cell proliferation and granulopoiesis.

Future work will focus on optimizing PMN production and delivery in the GelMA environment to evaluate its therapeutic potential to combat antibiotic-resistant wound infections. Part of this optimization will involve examining the signaling pathways that govern and could be targeted to

enhance HSPC granulopoiesis *in vitro*. For example, TLR2 and IL-1β have been shown to synergistically increase PMN proliferation from HSPC in suspension cultures. This is further supported by the fact that TLR2-/- and MyD88-/- HSPC undergo granulopoiesis less effectively than HSPC from wild-type mice [93]. As a result, MyD88-/- mice infected with *S. aureus* become septic [93, 94]. Therefore, future studies should examine the effect TLR and IL-1 agonists on PMN production from HSPC. Adoptive transfer studies into transgenic and chimeric MyD88-/-, TLR-/-, and IL-1-/- mice would also guide our understanding of signaling pathways that govern HSPC expansion and the role of hematopoietic and non-hematopoietic cells alike in this process. Furthermore, when HSPC from LysM-EGFP mice are directly transferred into the wounds of C57BL6 mice two hours after infection with *P. aeruginosa*, there was a significant increase in EGFP fluorescence emanating from these wounds (Figure 4.10), suggesting that local production may also be induced in response to gram-negative bacteria. Therefore, future studies should also focus on understanding and enhancing the immune response to gram-negative bacteria like *P. aeruginosa* that induce TLR4-dependent immune responses. Lastly, the safety regarding the use 3D hydrogels to transplant and deliver immune cells into a patient should also be investigated. For example, these studies should examine whether transplanted PMN could be rejected by the immune system of a recipient patient, the optimal transplantation dose and dosing schedule, as well as any side effects caused as a result of hydrogel degradation following transplantation [153-156].

A)

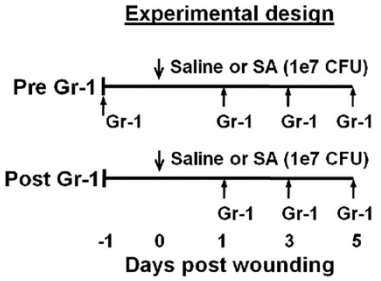

B)

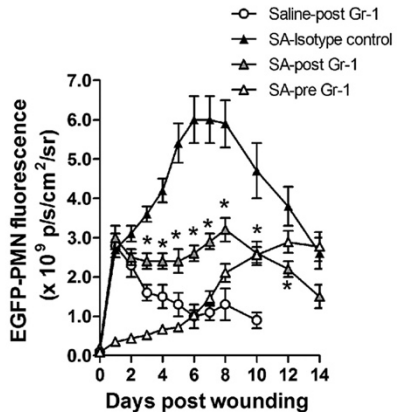

C)

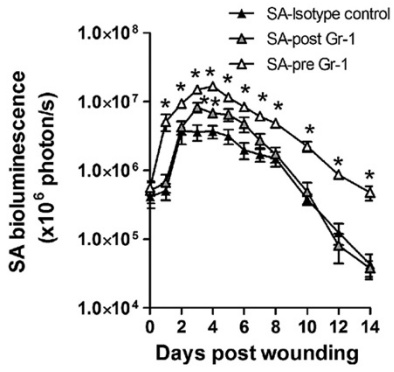

Figure 4.1: PMN depletion via mAb Gr-1 administration showing that HSPC recruitment and extramedullary granulopoiesis in an infected wound is an important tactic against *S. aureus* infection. A) Experimental design noting timepoints of anti-Gr1 administration. B) EGFP-PMN recruitment showing that even mouse that undergo depletion show recruitment/granulopoiesis at the site of S. aureus infection. C) Bacterial abundance showing that depleted mice are still able to combat the infection. "Post" denotes mAB Gr1 treatment after SA infection and "Pre" denotes mAB Gr1 treatment before SA infection.
Data are derived from n=5–6 mice per group. * denotes *p*-value ≤0.05 compared to IGG1-isotype control.
EGFP = Enhanced Green Fluorescent Protein | SA = *Staphylococcus aureus*

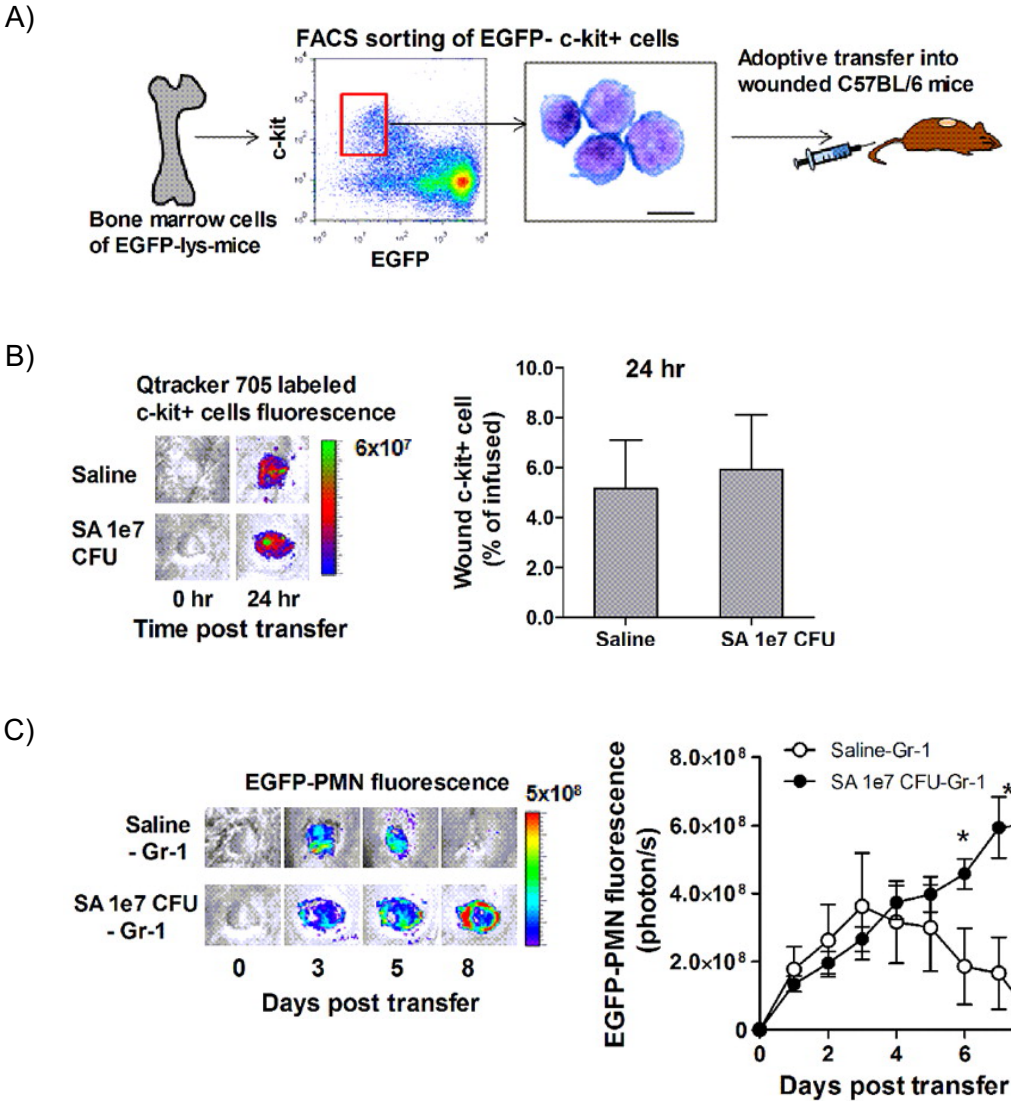

Figure 4.2: Adoptive transfer studies of HSPC from LysM-EGFP mice into 'dark' C57BL6 mice showing recruitment and extramedullary granulopoiesis. A) Experimental design of isolation and adoptive transfer of HSPC from LysM-EGFP mice into C57BL6 mice. B) Labeling and tracking of HSPC into *S. aureus* wounds denoting recruitment. C) Extramedullary granulopoiesis at the site of infection of the aforementioned transferred and recruited HSPC denoted by an increased in EGFP fluorescence at the site of infection.
Data are derived from n=3–5 mice per group
* denotes *p*-value ≤0.05 compared to saline control.

This research was originally published in Blood. Kim et al. PMN survival and c-kit+-progenitor proliferation in *Staphylococcus aureus*-infected skin wounds promote resolution. *Blood*. 2011; 117:3343-3352.

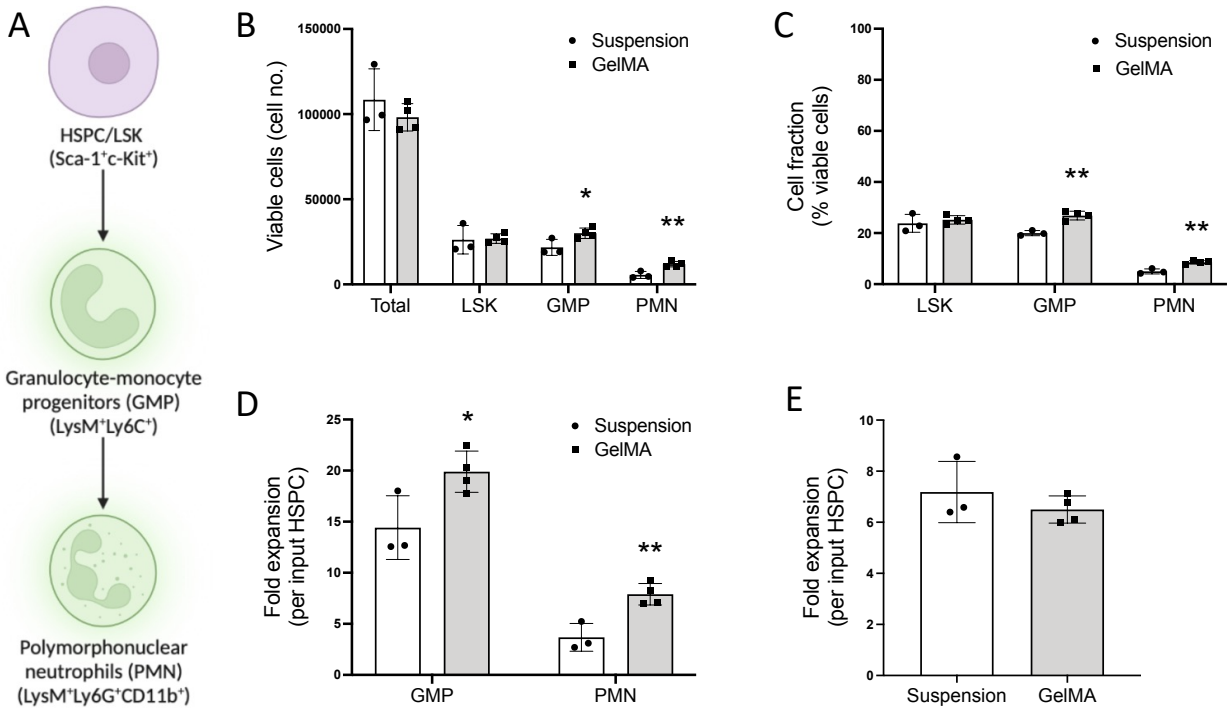

Figure 4.3: Effect of HSPC encapsulation on granulopoiesis and proliferative capacity. A) HSPCs were isolated from murine bone marrow and cultured in 3D hydrogels or 2D suspension and stained with various markers of interest to assess PMN production. B) After 72 hours of *in vitro* culture in either 2D suspension or 3D GelMA hydrogels, cells were isolated, and the total number of viable cells was measured via flow cytometry. C) Cell fractions of LSK, GMP and PMN populations were also quantified. D) GMP or PMN production per input HSPC and E) the total fold expansion of all enumerated cells per input HSPCs were also determined.
Data are derived from n = 3–4 replicates per group.
* and ** denote *p*-value ≤0.05 and ≤0.01 respectively (relative to the suspension group).
HSPC = Hematopoietic Stem and Progenitor Cell
LSK = Lineage-negative, Sca-1-positive, and c-kit-positive cells
GMP = Granulocyte-Monocyte Progenitor defined as Ly6C-positive and c-kit-positive cells
PMN = Polymorphonuclear Leukocyte defined as CD11b-positive and Ly6G-positive cells

Data and figure were first published in *Advanced Healthcare Materials* by Cirves and Vargas et al., 2024.

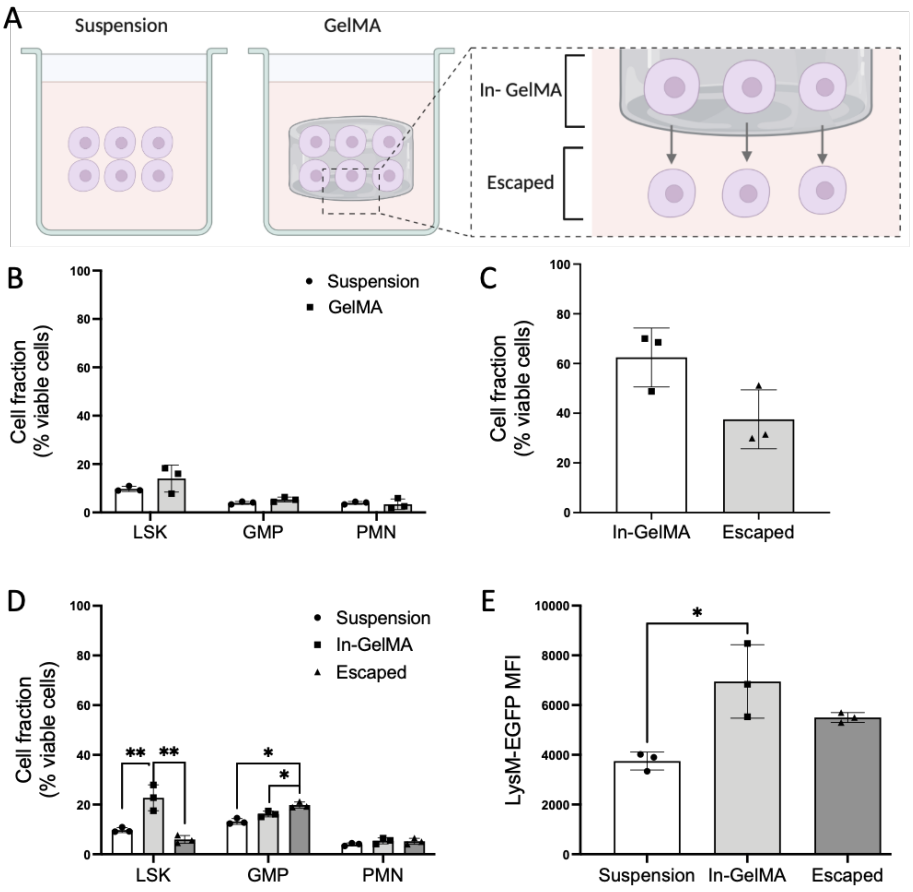

Figure 4.4: Flow cytometry characterization of cells that remained inside the 3D hydrogels, escaped the hydrogel, or were grown in 2D culture. A) Graphical representation of analyzed cell populations defining the cells that remained encapsulated in the GelMA gels (In-GelMA) versus cells that escaped the hydrogel (Escaped). B) Percentage of LSK, GMP and PMN cells in suspension or GelMA (Escaped + In-GelMA cells) after 7 days. C) Total cell viability of the population inside the hydrogel vs outside ("escaped"). D) Percentage of LSK, GMP and PMN cells in suspension, in-GelMA and escaped after 7 days of differentiation culture. E) Median Fluorescence Intensity (MFI) of LysM-EGP+ cells after 7 days of differentiation culture.
Data are derived from n=3 replicates per group.
* and ** denote *p*-value $\leq$0.05 and $\leq$0.01, respectively.
EGFP = Enhanced Green Fluorescent Protein
LSK = Lineage-negative, Sca-1-positive, and c-kit-positive cells
GMP = Granulocyte-Monocyte Progenitor defined as Ly6C-positive and c-kit-positive cells
PMN = Polymorphonuclear Leukocyte defined as CD11b-positive and Ly6G-positive cells

Data and figure were first published in *Advanced Healthcare Materials* by Cirves and Vargas et al., 2024.

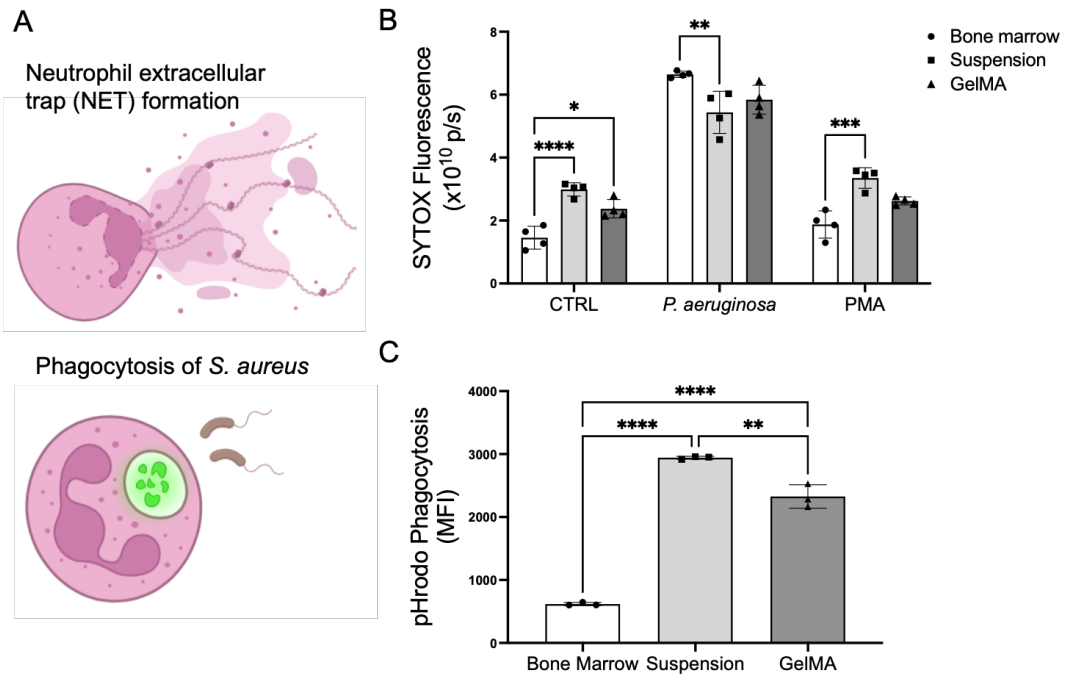

Figure 4.5: Functionality assessment via NETosis and Phagocytosis of PMN derived from HSPC cultures.
A) Biological abstract of the performed assays. B) Average fluorescence of SYTOX Orange (an analog for NETosis) following stimulation with either P. aeruginosa or PMA. SYTOX Orange is a cell-impermeant, nucleic-acid stain measured on the IVIS spectrum. C) Average fluorescence pH-reactive S. aureus bioparticles phagocytosed by EGFP+ cells and measured via AttuneNxT flow cytometer. Cells in both experiments were seeded and expanded for 7 days.
Data are derived from n=3–4 replicates per group.
*, **, ***, and **** denote *p*-value ≤0.05, ≤0.01, ≤0.001), and ≤0.0001, respectively.
MFI = Mean Fluorescence Intensity

Data and figure were first published in *Advanced Healthcare Materials* by Cirves and Vargas et al., 2024.

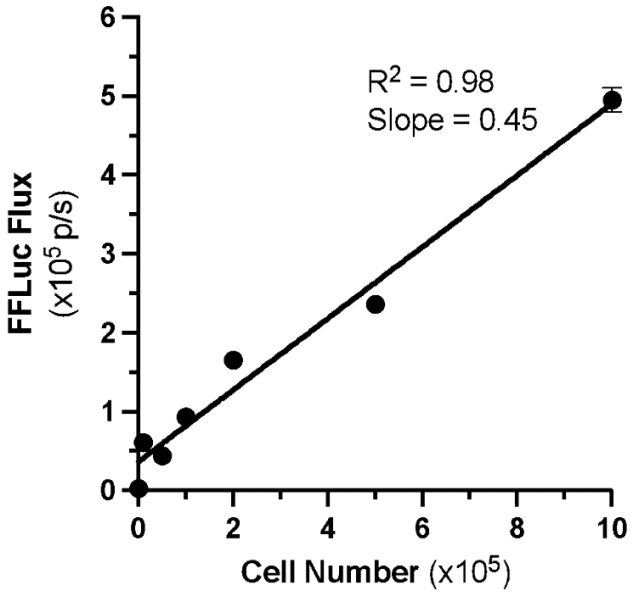

Figure 4.6: *In vitro* correlation between PMN number and Firefly (S100A8-FFLuc) signal flux.
Mice expressing a Cre MRP8-EGFP promoter (Tg(S100A8-cre,-EGFP)1Ilw) were cross-bred with mice expressing a ffLuc-Lox reporter (Gt(ROSA)26Sortm1(Luc)Kael/J) to generate mice expressing Firefly luciferase (FFLuc) in granulocytes. Offspring received a subcutaneous dose of 5mg/mL of D-Luciferin and imaged in an IVIS Spectrum to identify mice expressing the FFLuc reporter (FFLuc+). Bone marrow neutrophils (CD11bhi Ly6Ghi confirmed by flow cytometry) were isolated from FFLuc+ mice and a known number of cells were placed in a 96-well plate containing 5mg/mL D-Luciferin. The plate was imaged in an IVIS Spectrum to correlate FFLuc total flux (p/s) with neutrophil number.
Data are derived from n=3 replicates per group.
FFLuc = Firefly Luciferase (reporter)

Data and figure were first published in *Advanced Healthcare Materials* by Cirves and Vargas et al., 2024.

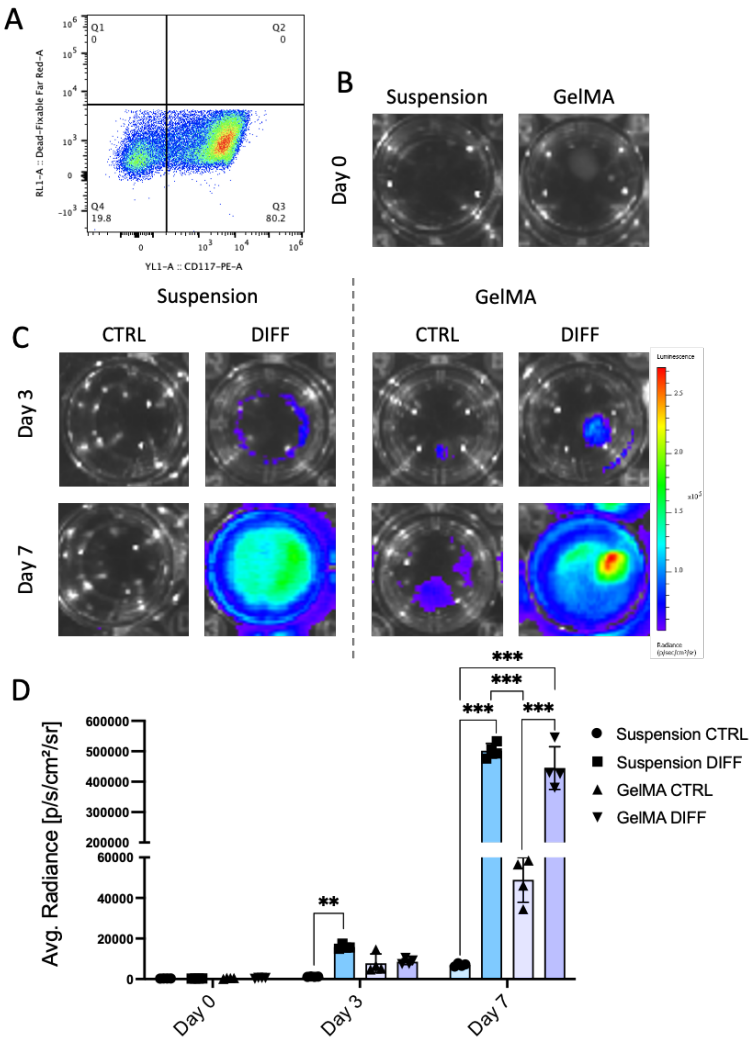

Figure 4.7: PMN production from HSPC in 2D or 3D culture measured by luciferase activity. A) Confirmation of >80% of CD117+ HSPCs after cell isolation from the bone marrow of MRP8-FFLUC mice. (B) Luciferase activity at day 0 after isolation in cells in suspension or encapsulated in 5% GelMA gels. (C) Luciferase activity after 3 and 7 days of *in vitro* culture in cells cultured in suspension or encapsulated in GelMA gels and maintained in basal (CTRL) or differentiation (DIFF) media. (D) Quantification of luciferase activity.
Data are derived from n=4 replicates per group.
** and *** denote *p*-value ≤0.01 and ≤0.001, respectively.
CTRL = Basal Media (i.e. no addition of myeloid differentiation factors noted in Section 2.4)
DIFF = Media supplemented with myeloid differentiation factors (noted in Section 2.4)

Data and figure were first published in *Advanced Healthcare Materials* by Cirves and Vargas et al., 2024.

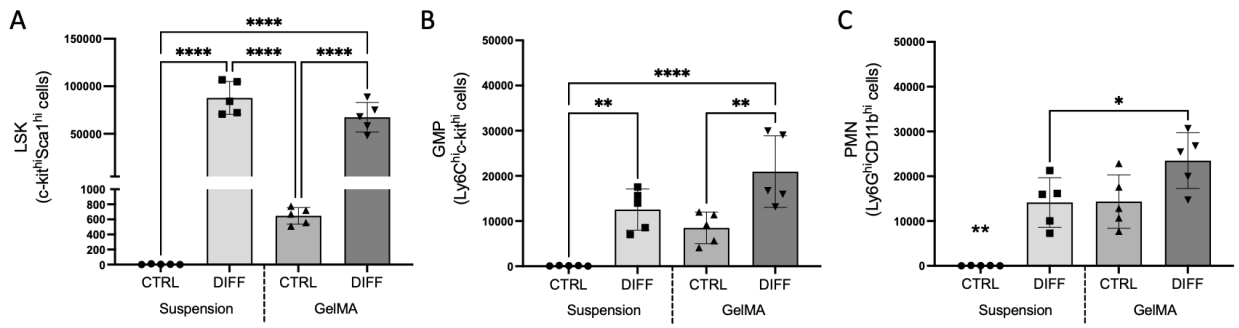

Figure 4.8: Flow cytometry characterization of HSPC-derived cells grown in 2D vs 3D cultures in non-supplemented (CTRL) vs PMN-differentiation (DIFF) media. HSPC derived from S100A8-FFLuc mice were grown in 2D (Suspension) or 3D culture (encapsulated in GelMA hydrogel) in the absence (CTRL) or presence (DIFF) of granulopoiesis-inducing growth factors. Data shows the number of A) LSK (Sca-1+c-kit+), B) GMP (Ly6C+c-kit+) and C) PMN (Ly6G+CD11b+) after 7 days of culture.
Data are derived from n=5 replicates per group.
*, **, and **** denotes *p*-value ≤0.05, ≤0.01, and ≤0.0001, respectively.
LSK = Lineage-negative, Sca-1-positive, and c-kit-positive cells
GMP = Granulocyte-Monocyte Progenitor defined as Ly6C-positive and c-kit-positive cells
PMN = Polymorphonuclear Leukocyte defined as CD11b-positive and Ly6G-positive cells

Data and figure were first published in *Advanced Healthcare Materials* by Cirves and Vargas et al., 2024.

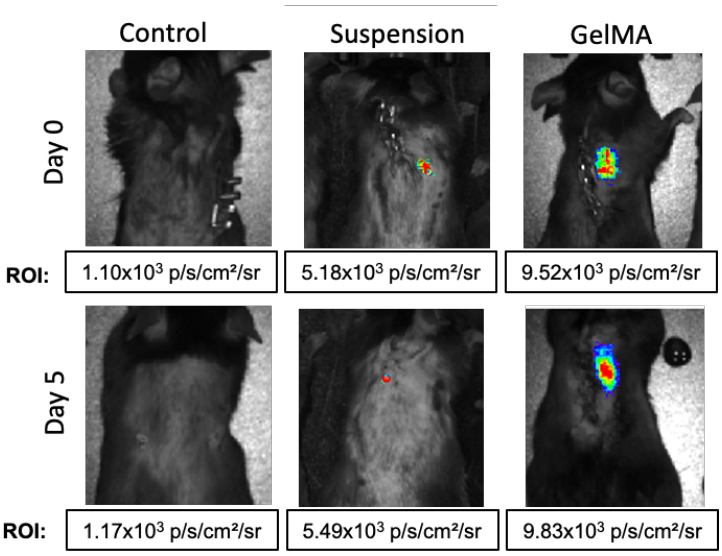

Figure 4.9: S100A8-FFLuc HSPC-derived PMN transplantation into C57BL6 mice. Luciferase activity of cells in suspension or in GelMA at days 0 and 5 after transplantation into C57BL/6J mice. Bioluminescence flux was obtained as radiance average (p/s/cm^2/sr) by drawing a region of interest (ROI) on top of the site of transplantation.
Data are derived from n=1 mouse per group.

Data and figure were first published in *Advanced Healthcare Materials* by Cirves and Vargas et al., 2024.

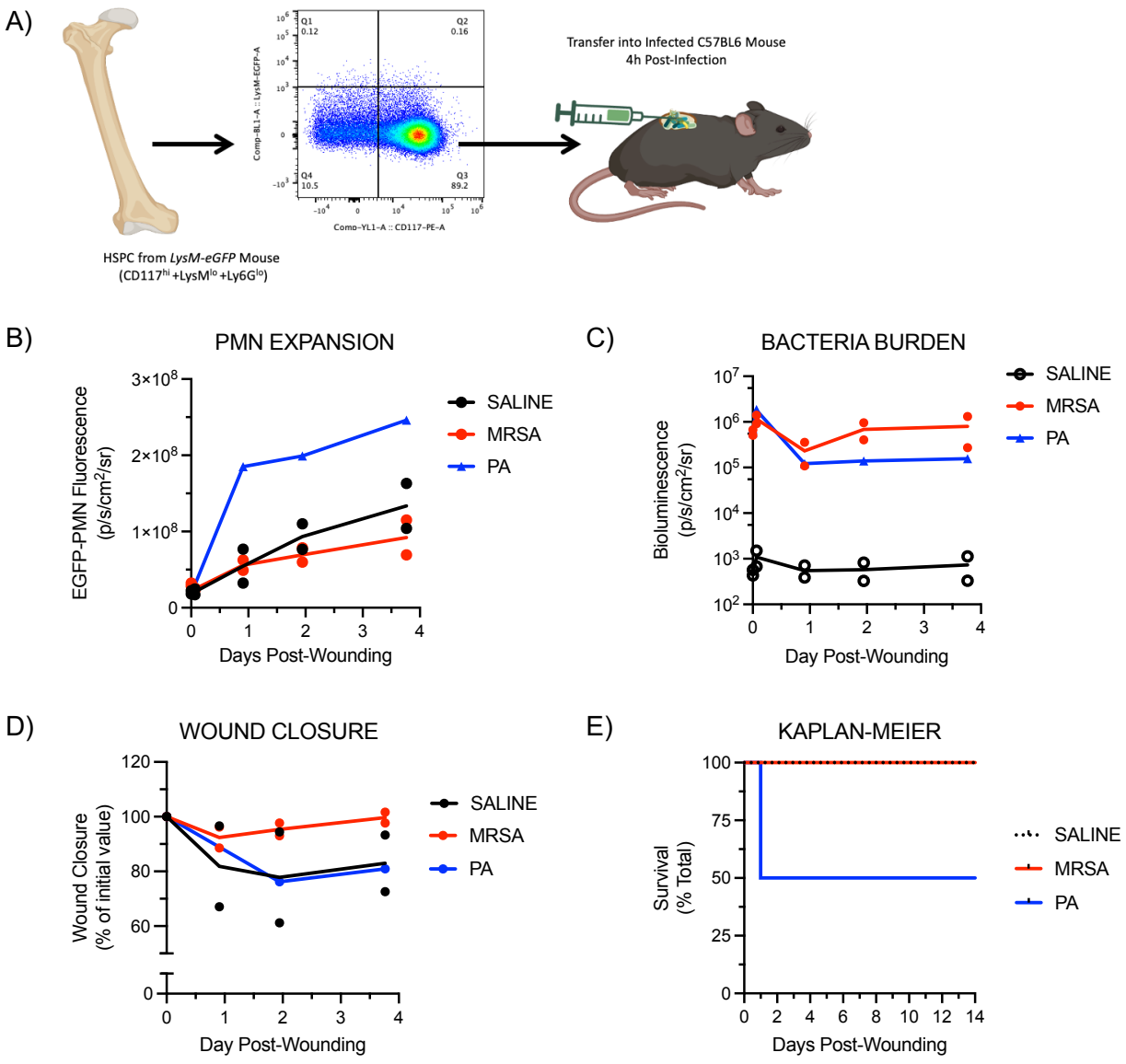

Figure 4.10: Production of PMN from HSPC delivered into *P. aeruginosa*-infected mouse wounds. C57BL6 mice were dorsally wounded and inoculated with S. aureus or P. aeruginosa followed with subcutaneous transfer of HSPC isolated from LysM-EGFP mice at 2-4h after infection. EGFP fluorescence was measured on an IVIS spectrum to quantify production of PMN from HSPC. A) Experimental design schematic of HSPC isolated from LysM-EGFP mice and then transferred into 'dark' C57BL6 mice 2 hours after these were wounded and infected. *Illustration was created with BioRender.com*. B) EGFP fluorescence from C57BL6 mice showing local production of PMN from HSPC at the site of infection. C) Bioluminescence flux from bacteria at the wound site. D) Wound closure over time. E) Kaplan-Meier curve showing animal survival.
Data are derived from n=2 mice per group.

CHAPTER 5: ROLE OF MYD88 SIGNALING IN PMN-MEDIATED IMMUNITY AGAINST *PSEUDOMONAS AERUGINOSA* INFECTION IN WOUNDED SKIN

5.1: Introduction

Antibiotic resistance to community and hospital-acquired infections is a major threat to public health [1–19]. As a result, there is an urgent need to better understand the mechanisms mounted by the innate immune system against infection and to develop host-based therapies that enhance bacteria clearance and tissue repair. Polymorphonuclear leukocytes, or PMN, are the most abundant and one of the primary effector cells of the innate immune system [60–71]. During the early stages of infection, PMN are quickly recruited from circulation into sites of infection, where they launch an array of antibacterial functions to eliminate bacteria [27, 62, 63, 66–71, 90, 94, 97]. These functions are governed by a complex series of signaling pathways that are initiated by pathogen recognition via conserved molecular patterns that activate toll-like receptors (TLR). These signals tightly regulate PMN production in bone marrow, release into the circulation, and transmigration from blood vessels at the site of tissue insult [51–75]. TLR stimulation prime PMNs for enhanced responses against pathogens via potentiation of chemokine signaling of antibacterial functions, including reactive oxygen species production, phagocytosis, and formation of PMN extracellular traps (NETosis) [27, 61–71, 78, 83–86, 90–95, 97]. Mutations that dysregulate TLR signaling and activation of the inflammasome lead to impaired pathogen killing, severe tissue damage, and sepsis [59–71]. Persistent, chronic infections often require antibiotic treatments for bacterial clearance [1–19]. One major obstacle to this is the ability of bacteria to rapidly develop mechanisms that render antibiotics ineffective [15–19]. As a result, alternative therapeutic approaches need to be developed that rely on enhancing PMN numbers and their antibacterial capacity. In fact, previous studies have shown that tuning the number and function of PMN at the site of skin infections can improve host prognosis [94]. However, key signaling molecules that govern PMN production, recruitment, and antibacterial functions during the early stages of infection remain elusive [90, 93, 94].

Previous studies on mouse wounds have shown that discrete populations of PMN mount an effective response to bacterial virulence factors. *S. aureus* in wounded skin elicits prolongation of PMN lifetime within the wound. They also induce local granulopoiesis by HSPC that traffic into the infected wound to generate and maintain sufficient PMN numbers for clearing the infection [27, 90, 93, 94, 97]. These mechanisms are regulated through host pathways that signal via MyD88 through TLR2 and IL-1β, and

are a direct response to virulence factors such as Hematoxylin A, which impairs PMN extravasation by lysing perivascular macrophages in mouse skin [94]. In the absence of MyD88, the host response to infection is severely impaired as noted by decreased PMN recruitment, increased bacterial dissemination, and mortality within 5 to 10 days after infection [82,93,94]. We chose to further investigate the role of MyD88 on PMN-mediated host defense in response to *P. aeruginosa*, a flagellated gram-negative pathogen that induces TLR4- and TLR5-dependent immune responses [7–11]. Although *P. aeruginosa* infections are common in pneumonia patients suffering from cystic fibrosis, it can also cause invasive and life-threatening infections in skin, particularly in individuals with diabetes [82, 157–161]

P. aeruginosa is a primary cause of opportunistic infections and sepsis in immunocompromised populations [7–11, 13]. These infections are notoriously difficult to treat because *P. aeruginosa* has a remarkable capacity to readily proliferate, form biofilm, and resist antibiotic treatments [7–11]. One of the main mechanisms of host defense against infectious bacteria is infiltration of circulating PMN produced in the bone marrow into the site of infection [27, 61–71, 94, 97]. Quick and sufficient PMN recruitment and activation of their antibacterial functions is necessary to contain and subsequently clear pathogenic bacteria [61–-71, 87, 90, 94, 95, 97]. These mechanisms are triggered by TLR4 activation of MyD88 that signals via MAPK and NF-kB inducing production of cytokines, including IL-1β and TNFα [27, 82, 94, 95, 97]. This ultimately results in PMN production, recruitment, and activation of antibacterial functions at the site of infection. However, the rate at which PMN and produced and recruited into an infected wound, and whether local granulopoiesis induced by TLR4 stimulation is a host tactic to control *P. aeruginosa,* remains unknown. Similarly, the direct role of TLR4 and MyD88 on PMN functions like migration, phagocytosis, and NETosis during the critical first 24 hours of infection, that can mitigate pathogen dissemination, is unclear. Furthermore, during inflammation, PMN undergo programmed cell death via mechanisms that involve TLR detection of pathogen-associated molecular patterns (PAMPs) and virulence factors that lead to inflammasome and resident macrophage activation [6-12]. Whether these programmed cell mechanisms are beneficial for the host to be able to contain and defeat the infection remains unclear [84–86, 100, 101, 103–105]. In the studies presented here, we use a mouse wounding model to show that MyD88 activation is required for an effective immune response within hours after infection with *P. aeruginosa,* through IL-1β generation and sufficient PMN migration, pyroptosis, and NET formation. In the absence of MyD88, *P. aeruginosa* quickly proliferates and disseminates from the infected wound and into vital tissues, resulting in severe sepsis. The phenotype correlates with lower levels of IL-1β production in MyD88-/- wounds, as well as impaired PMN movement and inability to undergo pyroptosis and NETosis *in vitro*. Taken together, these studies

suggest that MyD88 activation in PMN is essential for host survival from *P. aeruginosa* infection by regulating lifetime and antibacterial functions regulated by IL-1β.

The data in Figure 5.15 were collected in collaboration with Dr. Maryam Rahmati at UC Davis. The data and figures in 5.16 were obtained in collaboration with Stefan Lundgren from the Collins Lab at UC Davis. All histopathological H&E images and analysis were performed in collaboration with the Comparative Pathology Lab at UC Davis.

5.2: Early PMN Recruitment is Essential to Control P. aeruginosa *Cutaneous Infection*

LysM-EGFP mice were employed to measure PMN recruitment into an infected wound. These mice express the enhanced green fluorescent protein (EGFP) downstream of the *lysM* gene, which enables the quantification of granulocyte recruitment into a dorsal wound using an IVIS Spectrum device [90, 91, 94, 143]. To validate this model, a known number of PMN isolated from LysM-EGFP mice were inoculated subcutaneously into the dorsal wounds of non-LysM-EGFP, C57BL6 mice. We found a direct, linear correlation between the number of PMN and the EGFP flux measured from the wound (Supplemental Figure 5.1). To characterize the role of PMN during the innate immune response to infection, LysM-EGFP mice were dorsally wounded and inoculated with *S. aureus*, *P. aeruginosa*, or saline control (Figure 5.1). In response to *S. aureus*, the number of PMN recruited into the site of infection by day one post-wounding were 70% lower than those in Saline or *P. aeruginosa* wounds. This is consistent with previous findings showing that *S. aureus* virulence factor alpha-toxin attenuates PMN recruitment by lysing immune cells at the site of infection [82, 94]. These studies also demonstrated that PMN local granulopoiesis and prolonged PMN lifetime are host mechanisms that augment the cell count within the wound that is needed to reduce *S. aureus* abundance [90, 94]. On the other hand, *P. aeruginosa* exhibited two-fold higher PMN numbers at the site of infection by day one post-wounding and continued to rise to a maximum at day five post-infection that was 25% above saline and 160% above *S. aureus*. This higher number correlated with lower bacterial abundance and faster wound closure than *S. aureus* wounds. Furthermore, PMN enumeration in bone marrow and circulation at 16 hours after wounding revealed that *P. aeruginosa*-infected mice have 60% less PMN in bone marrow and more than 10-fold higher PMN counts in circulation compared to mice only inoculated with saline (Figure 5.2). Taken together, this suggests that rapid PMN production in bone marrow and recruitment from circulation is necessary to defeat *P. aeruginosa* in an infected wound.

A strategy to further evaluate the importance of early PMN release from bone marrow and recruitment to the site of infection is to deplete circulating PMN in LysM-EGFP mice via intraperitoneal administration of anti-Gr1 mAb one day before wounding and inoculation with *P. aeruginosa*. Within 16 hours of infection PMN production was increased in bone marrow in both IgG control and anti-Gr1 cohorts. This resulted in PMN release into circulation that correlated with their rapid recruitment into infected wounds in the IgG control group but not the PMN-depleted mice (Figure 5.3A-C). *P. aeruginosa* infected and PMN depleted mice were unable to contain the infection and survived for less than 24 hours after infection (Figure 5.3D). These mice were also more likely to exhibit higher levels of *P. aeruginosa* abundance in blood than the IgG control (Figure 5.3E). Histopathological analysis revealed the presence of *P. aeruginosa* in lung, liver, and spleen. These studies indicate that within 24 hours of detection of *P. aeruginosa* at the site infection, rapid bone marrow production and recruitment of sufficient numbers of PMN from circulation is critical to prevent pathogen dissemination and fatal sepsis. This differed from the response to *S. aureus,* where PMN depleted mice were still able to defeat the infection via a mechanism that involved HSPC recruitment from bone marrow and PMN production directly at the site of infection through TLR2 and IL-1β signaling [91–94].

5.3: PMN that Encounter P. aeruginosa Undergo Rapid Cell Death

To characterize PMN recruitment as a function of initial *P. aeruginosa* abundance, mice were wounded and inoculated with 10^4 or 10^7 CFU of bacteria, or saline control. Previous studies of *S. aureus* infected wounds revealed that PMN infiltrated the wound bed most rapidly over the first 24 hours and that a five-fold increase in *S. aureus* inoculant correlated with a 100% increase in the rate and extent of PMN recruitment [90]. In contrast, in the case of *P. aeruginosa* an increase in inoculant correlated with a decrease in PMN recruitment, especially over the initial 48 hours and this was accompanied with a significant decrease in survival of 25% of infected mice (Figure 5.4A-C).

We hypothesized that following recruitment to infected wounds, PMN undergo rapid cell death proportional to bacterial abundance, which is responsible for the 50% lower rate and extent of PMN numbers in wounds inoculated with 10^7 versus 10^4 CFU of *P. aeruginosa*. To assess whether PA interfered with phagocyte recruitment from the circulation and contributed to depletion within infected compared with saline control wounds, PMN from LysM-EGFP mice were isolated and injected directly into wounds, or delivered via tail vein injection, into non-LysM-EGFP mice inoculated with *P. aeruginosa*. Within 6 hours of injection into circulation, equivalent numbers (~$5x10^5$ PMNs) were recruited into PA

and saline wounds. However, over the ensuing 24 hours only 25% of PMN remained within infected wounds compared with 75% in wounds inoculated with saline (Figure 5.5A). This indicates that PMN undergo rapid lysis in the presence of *P. aeruginosa*. This is consistent with published studies demonstrating that NETosis is a primary PMN response to *P. aeruginosa* and is necessary to control biofilm formation and subsequent vascular dissemination [87]. Similarly, when PMN from LysM-EGFP mice were placed into the tail vein of C57BL6 mice, 2 hours before wounding and inoculation with either Saline or *P. aeruginosa*, fewer PMN were detected in infected wounds over the course of the first 24 hours post-wounding, compared to wounds that had only been inoculated with saline. PMN in wounds inoculated with saline followed a linear increase in the number of PMN measured, consistent with the recruitment data shown in Figure 5.1. In infected wounds, on the other hand, recruitment kinetics formed a "zig-zag" pattern characterized by rapid increase followed by a flattened slope. By 28 hours post-wounding, *P. aeruginosa* wounds had only 25% of the number of PMN observed in saline wounds, further supporting the conclusion that 75% of PMN recruited within the first 24 hours post-wounding undergo cell death (Figure 5.5B).

Three distinct mechanisms act in concert to maintain sufficient numbers of PMN for host defense in *S. aureus* infected wounds. These include: 1) sustained mobilization of PMN produced in the bone marrow that correlated with infection burden, 2) prolonged survival within the wound, and 3) local proliferation of PMN produced from hematopoietic progenitor stem cells that traffic to the wound and undergo myeloid differentiation [91,94]. Previously, it was reported that PMN extended their lifetime within *S. aureus* infected wounds by up to six days once recruited into the site of infection [91-94. In the case of *P. aeruginosa*, the half-life of the 25% of PMN remaining after 24 hours post-infection was closer to 3 days compared with 1 day for saline control (Figure 5.6B). This further supports the conclusion that PMN have shorter survival in *P. aeruginosa*-infected wounds.

MyD88 is a key mediator of TLR signaling. It also determines cell fate via pyroptosis and apoptosis upon stimulation of proinflammatory signals like IL-1β and TNF-α [95, 162–164]. To further assess the mechanisms underlying PMN survival within *P. aeruginosa* wounds, PMNs were isolated from the bone marrow of wild-type and MyD88-/- mice expressing LysM-EGFP and cultured *in vitro* in the presence of basal media (control) or media with *P. aeruginosa* or PMA (Figure 5.7). 24 hours after culture, cells were analyzed via flow cytometry for relative expression of EGFP as a marker indicative of cell viability. Only 10% of wild-type PMN incubated with *P. aeruginosa* remained viable after 24 hours compared to 40% of those incubated in basal media. This means that *P. aeruginosa* induced a 75% decrease in wild-type

PMN viability (i.e. from 40% in CTRL group to 10% in *P. aeruginosa* group). This further confirms that in the presence of *P. aeruginosa*, nearly 75% of PMN undergo cell death within hours of pathogen encounter. On the other hand, nearly 25% of MyD88-/- remained viable after 24 hours, indicative of impaired cell death in response to *P. aeruginosa*.

5.4: Early MyD88 Signaling is Required to Contain P. aeruginosa *and Avert Sepsis*

Previous studies with *S. aureus* infections have shown that MyD88 signaling downstream of TLR2 mediates IL-1β production, which is necessary to elicit PMN production and antibacterial functions to clear the bacteria [94, 95]. LysM-EGFPxMyD88-/- that lack MyD88 and have the capacity to produce EGFP-tagged granulocytes were dorsally wounded and inoculated with bioluminescent *P. aeruginosa*. In contrast to wild-type mice, none of the MyD88-/- mice survived beyond 24 hours after infection. By 16 hours post-infection, bioluminescence revealed 10-fold higher levels of *P. aeruginosa* abundance and dissemination in MyD88-/- mice. In contrast, wild-type mice exhibited a continuous drop in bacterial abundance that was contained within the wound bed (Figure 5.8A). Interestingly, imaging of eGFP fluorescence from the wound tissue, which is indicative of PMN abundance at the site of infection, were not significantly different between MyD88-/- and wild-type mice during the 24-hour duration of the study (Figure 5.8B). Further analysis of PMN numbers in the bone marrow and blood between PA infected wild-type and MyD88-/- mice revealed equivalent levels, consistent with whole animal fluorescence imaging.

Histopathological analysis of organs obtained post-mortem at 14 hours post-infection of MyD88-/- mice revealed that *P. aeruginosa* exited the wound and was detected in blood, liver, kidney, and lung, while bacterial dissemination did not occur in wild-type mice (Figure 5.9). To evaluate whether a breach in microvascular barrier function at 24 hours correlated with dissemination of PA into vital organs of MyD88-/- mice, permeability was measured by tail-vein infusion of fluorescently labeled albumin. MyD88-/- wounds exhibited more than a 2-fold increase in permeability compared with wild-type wounds at 14 hours post-infection indicative of a break down in barrier function (Figure 5.8I). Histopathological and H&E image analysis of internal tissues of MyD88-/- mice confirmed that the cause of death was sepsis (Figure 5.10). MyD88-/- livers, for example, showed hepatocellular necrosis associated with rod shaped bacteria consistent with *P. aeruginosa* and hepatocellular necrosis associated with neutrophilic infiltration. MyD88-/- kidneys exhibited glomerular tuft emboli of rod-shaped bacteria consistent with *P. aeruginosa*, indicative of circulating bacteria and sepsis. MyD88-/- lungs showed thickened alveolar septa by congested blood vessels with circulating neutrophilia, while

the pancreas exhibited zymogen depletion in the exocrine pancreas acinar cells, indicative of hyporexia. Lastly, MyD88-/- thymus showed lymphocytolysis with increased number of tangible body macrophages, while the spleen exhibited lymphoid hyperplasia. Taken together, these studies demonstrate that lack of MyD88 signaling leads to *P. aeruginosa* dissemination due to breach in the vascular barrier, resulting in mortality by sepsis in less than 24 hours after infection.

MyD88 is required to contain *P. aeruginosa* regardless of initial inoculation abundance. To test the effect of initial bacterial inoculation on survival of MyD88-/- mice, wounds were inoculated with either live (10^4 CFU or 10^7 CFU) or heat-killed *P. aeruginosa* (Figure 5.11). Compared with wild-type mice inoculated with 10^7 CFU that succumbed to infection before 24 hours, those inoculated with 10^4 CFU survived up to ~48 hours, whereas ~50% of mice inoculated with heat-killed *P. aeruginosa* survived up to Day 3 post-infection. Mice from all groups exhibited equivalent numbers of PMN recruitment into the site of infection, indicating that survival is dictated by the time delay for *P. aeruginosa* to proliferate up to a critical level before dissemination into circulation.

Since lack of MyD88 signaling appears to cause a significant delay in PMN recruitment compared to wild-type infected wounds (Figure 5.12), we performed an experiment in which MyD88-/- mice were wounded. This was done to allow equivalent PMN recruitment into the wound site for 36 hours before inoculation with *P. aeruginosa*. Delaying the infection to allow for increased PMN recruitment, however, did not significantly enhance relative number of PMN in the wounds or change the survival probability of MyD88-/- mice (Figure 5.12). Following inoculation, MyD88-/- mice experienced a rapid rate of *P. aeruginosa* proliferation compared to no increases in wild-type mice (Figure 5.12A-B). MyD88-/- mice experienced 100% mortality within 16 hours after inoculation compared to 100% survival of wild-type mice (Figure 5.12E). To further investigate the relationship between PMN recruitment numbers, bacterial proliferation, and survival after PA infection, MyD88-/- mice were depleted of their circulating PMN via intraperitoneal administration of anti-Gr1 mAb one day prior to infection. Following 10 hours of infection, depleted MyD88-/- mice registered 50% fewer PMN at the site of infection compared to the non-depleted control-treated MyD88-/- mice (Figure 5.13A). By comparison, bacterial abundance at 10 hours after infection was nearly the same between PMN depleted and non-depleted mice (Figure 5.13B), which correlated with equivalent survival up to 16 hours (Figure 5.13C). Had the MyD88-/- PMN exhibited normal anti-bacterial capacity against *P. aeruginosa*, bacterial abundance would likely be higher in the IgG control non-depleted MyD88-/- mice, following the pattern observed in anti-Gr1 PMN-depleted wild-type mice (Figure 5.3). However, the observation that depleted and non-depleted mice

exhibited the same levels of *P. aeruginosa* abundance raises the possibility that PMN antibacterial functions are deficient in MyD88-/- mice.

To test the effect of key virulence factors in the MyD88-/- phenotype, MyD88-/- mice were dorsally wounded and inoculated with various *P. aeruginosa* mutants (Figure 5.14). The T3SS secretion system in *P. aeruginosa* is a key virulence regulator that induces host tissue toxicity and necrosis [165–169]. Similarly, nonplius adhesins are critical in *P. aeruginosa*'s ability to form biofilm and adhere to host surfaces [170–173]. We hypothesized that T3SS and nonplius adhesins must play a critical role in the ability of *P. aeruginosa* to evade the immune response, proliferate, and cause sepsis in mice. Therefore, MyD88-/- mice were inoculated with the *P. aeruginosa* ΔexsA mutant, which lacks a key gene necessary to initiate T3SS transcription [174–176]. Similarly, a second cohort of MyD88-/- mice were dorsally wounded and inoculated with the *P. aeruginosa* ΔfliF mutant that exhibits impaired motility and adhesion *in vitro* [172, 177–179]. Survival of mice infected with either ΔexsA or ΔfliF mutants was significantly prolonged compared with the wild-type PAO1F strain. However, all infected mice exhibited mortality by 36 hours post-infection (Figure 5.14) and only saline-inoculated mice survived for the duration of the study. This is consistent with published studies demonstrating that MyD88-/- epithelia was still susceptible to *P. aeruginosa* infection despite mutations in exsA expression [176]. Given the similarity in survival of MyD88-/- mice inoculated with either 10^4 or 10^7 CFU of wildtype xen41, it can be concluded that it is the capacity of *P. aeruginosa* to proliferate and breach the wound site that is primarily responsible for dissemination and mortality in MyD88-/- mice, due to reduced anti-bactericidal activity of the MyD88-/- PMN.

5.5: MyD88 Contributes to PMN Antibacterial Functions Elicited by P. aeruginosa

To mount a successful immune response, PMN must detect invading pathogens and reach the site of infection, where they perform a variety of antibacterial functions including ROS elaboration, phagocytosis, and NET formation. Histological analysis and imaging of wound tissue collected at 12-16 hours after wounding and infection of wild-type and MyD88-/- mice confirmed that PMN recruitment was robust in response to PA infection (Figure 5.15A-B). H&E staining revealed that PMN transmigrated from blood vessels into infected skin in MyD88-/- mice (Figure 5.15B). This motivated further analysis of PMN navigation to the site PA infection, since it was previously reported that PMN swarming is necessary to defeat bacteria, including *P. aeruginosa,* and involved LTB4 signals [181–185]. PMN were isolated from bone marrow of wild-type and MyD88-/- mice expressing the LysM-EGFP gene and then

exposed to basal media or LTB4 chemoattractant to activate PMN migration and swarming capacity. Although basal and LTB4-induced migratory speed was not significantly different between wild-type and MyD88-/- PMN, MyD88-/- PMN were less effective at directional chemotaxis as demonstrated by their lower angular bias in migration to the LTB4 source (Figure 5.16A). Migratory path maps of individual PMN resembled the patterns observed in H&E histological images of infected skin confirming that MyD88-/- PMN were more diffuse than wild-type due to defective swarming (Figure 5.16B).

We next determined the role of MyD88 signaling on phagocytosis and NETosis in bone marrow PMN isolated from wild-type or MyD88-/- mice. *In vitro* phagocytosis measurements revealed that MyD88-/- PMN were ~30% less efficient at engulfing *S. aureus* bioparticles than wild-type PMN (Figure 5.17A). Similarly, when exposed to live *P. aeruginosa* and stained with SYTOX, a marker for extracellular DNA (eDNA) released during NETosis, it revealed that MyD88-/- PMN were also less effective at producing NETs compared to wild-type (Figure 5.17B). The defects in phagocytosis and NETosis also correlated with higher levels of *P. aeruginosa* bioluminescence in wells containing MyD88-/- PMN than in those containing wild-type cells, indicative of impaired bacterial killing capacity. This motivated examination of the *in vivo* functional capacity of MyD88-/- mice. Production of reactive oxygen species (ROS) is a critical function for effective bacterial killing [186–188], and its elaboration within infected wounds was quantified by detection of luminol bioluminescence within infected wounds of MyD88-/- compared to wild-type mice (Figure 5.18A). Remarkably, we detected ~2-fold higher levels of ROS production at 12 hours following infection in MyD88-/- compared with wild-type mice. In order to assess the relative survival of PMN accessing the wound, PMN from MyD88-/- or wild-type LysM-EGFP mice were isolated and administered into the tail-vein of wild-type dark mice that had been depleted of circulating PMN by introduction of anti-Gr1 mAb 24 hours before infection with *P. aeruginosa*. Wounds of mice with the MyD88-/- PMN registered 2-fold higher EGFP fluorescence compared to mice that were infused with wild-type PMN (Figure 5.19A). This suggests that MyD88-/- PMN were able to reach the site of infection but were incapable of undergoing programmed cell death to levels observed in wild-type PMN, which is consistent with the data shown in Figure 5.7. H&E histological imaging of these wounds revealed that mice with MyD88-/- PMN appear to experience vascular congestion compared to wounds with wild-type PMN (Figure 5.19B). These images confirmed that while both MyD88-/- and wild-type PMN reached the site of infection, MyD88-/- survived for a longer period of time, which is consistent with the *in vitro* data shown in Figure 5.7.

To investigate whether the defect in killing and containment of *P. aeruginosa* was due to defective PMN, 2 hours before wounding and inoculation, infected MyD88-/- mice were adoptively transferred with a bolus of either wild-type or MyD88-/- PMN via tail vein injection. Following 12 hours of infection, mice that had received the wild-type PMN had ~25% less *P. aeruginosa* abundance than mice that had received PMN from MyD88-/- mice (Figure 5.20). Taken together, these studies suggest that PMN dependent migratory and anti-bacterial functions over the initial 12 hours, signaled at least in part via MyD88, are critical for host survival from *P. aeruginosa* infected wounds.

5.6: MyD88-Dependent Host Strategies to Contain P. aeruginosa are TLR4-Independent but Involve IL-1β-Dependent Mechanisms

Detection of *P. aeruginosa's* lipopolysaccharide (LPS) and virulence factors leads to activation of TLR4 and the NLRP3/NLRC4 inflammasome and activation of caspase-1 that initiates release of IL-1β [96, 189–191]. MyD88 is a common adaptor downstream of TLR2 activation that leads to IL-1β generation, previously shown to be necessary to control MRSA [93–95, 97]. To evaluate the role of TLR4 in the host response, TLR4-/- mice were dorsally wounded and infected with *P. aeruginosa.* In contrast to no survival of infected MyD88-/- mice, we observed a 50% probability of survival at 24 hours for TLR4-/- mice (Figure 5. 21A). Moreover, TLR4-/- mice were able to suppress bacterial colonization equivalent to wild-type mice and to levels significantly lower than MyD88-/- mice (Figure 5.21B). To evaluate the relative capacity to activate the inflammasome, IL-1β was measured in wild-type, MyD88-/-, and TLR4-/- wounds 14 hours after wounding and inoculation with *P. aeruginosa*. TLR4-/- and wild-type wounds contained equivalent concentrations of IL-1β, while MyD88-/- wounds produced ~6-fold less.

The process of IL-1β release from Gasdermin-D pores during inflammasome activation of PMNs is termed *pyroptosis* and is detected by Annexin V and Propidium Iodine staining [192–194]. PMN isolated from MyD88-/- mice were less pyroptotic than either TLR4-/- or wild-type PMN, the latter two exhibited equal frequencies of pyroptosis, consistent with the IL-1β wound measurements. To further examine the role of caspase-1 on host immunity against *P. aeruginosa*, an *in vitro* killing assay was performed using PMN from Cas1-/-, TLR4-/-, MyD88-/- , and wild-type mice (Figure 5.22). The results revealed higher levels of *P. aeruginosa* bioluminescence in wells containing Cas1-/- and MyD88-/- PMN, indicative of an inability to combat the bacteria *in vitro*. Wells containing TLR4-/- and wild-type PMN showed lower

and similar levels of bacterial abundance. This suggests that PMN ability to combat *P. aeruginosa* may be Caspase-1-dependent.

Systemic administration of the pan-caspase inhibitor Q-VD-OPH is another way to investigate the role of caspase activation on the immune response against *P. aeruginosa*. Previous studies using Q-VD-OPH, which irreversible blocks caspases 1, 3, 7, and 12 via covalent binding [195], was shown to enhance the immune response against MRSA and *P. aeruginosa* in wild-type mice, by suppressing immune cell apoptosis, pyroptosis, and necrosis [196]. However, when MyD88-/- mice were systemically administered Q-VD-OPH 4 hours before and at the time of wounding, no significant difference in survival, PMN recruitment, or bacterial dissemination was observed between control and Q-VD-OPH-administered animals (Figure 5.23A-C). This data suggest that caspase activity may be dispensable or already absent in MyD88-/- mice. That is, if caspase activity was necessary and active in MyD88-/- mice, then caspase-inhibited mice would fare worse in response to *P. aeruginosa* than non-inhibited mice. However, further *in vivo* studies using Cas-1-/- mice are required to demonstrate that the phenotype observed in MyD88-/- mice is directly correlated to Caspase-1 activation.

5.7: Discussion and Future Directions

This chapter explores the host mechanisms that regulate the immune response against *P. aeruginosa* infection in skin. They are an extension of previous studies using a similar mouse model of wounding and infection with *S. aureus,* observing the dynamics of PMN recruitment and bacterial abundance in wounds and their effect on host survival. In the context of PMN innate immunity via TLR, MyD88, and IL-1β signaling, we observed a very different early immune response to *S. aureus* compared with *P. aeruginosa* infection. *S. aureus*-infected wounds elicit lower numbers of PMN recruitment, which is consistent with previous studies demonstrating that the infection alters PMN recruitment dynamics via virulence factors that decrease PMN transmigratory capacity. It was previously shown that the host response to *S. aureus* involves immune regulation resulting in a prolonged PMN lifetime and local expansion by HSC that home to the wound in addition to PMN recruitment from circulation. In contrast, *P. aeruginosa* infection is characterized by rapid unimpeded PMN recruitment from circulation that is equivalent to uninfected wounds during the first 24 hours after infection. PMN numbers continue to rise to levels higher than those in saline-inoculated wounds when accounting for the fact that nearly 75% of PMN undergo cell death upon encountering *P. aeruginosa*. Of those that are recruited and survive in the wound, we estimated a half-life of ~3 days, a value less than *S. aureus* but twice that of PMN in

uninfected wounds. This rapid turnover of PMN produced in bone marrow and recruited and sustained in a *P. aeruginosa* is sufficient for 80-90% mouse survival in wild-type mice.

Pseudomonas aeruginosa is a gram-negative bacterium that, upon infecting skin wounds, typically forms biofilm to protect itself against the host's innate immune response, resulting in rapid pathogen replication and antibiotic resistance. As a result, as demonstrated by our studies, rapid and sufficient PMN recruitment is required to control the infection and avert systemic dissemination and sepsis. Wild-type mice depleted of circulating PMN a day before wounding and infection are unable to survive for more than 24 hours after inoculation, and their demise involves sepsis due to bacterial dissemination into circulation and to vital organs including lung and liver. Histopathological analysis revealed that the lungs of these animals were characterized by moderate intravascular neutrophilia with numerous migrating neutrophilic and small fibrin aggregates. Our studies also show that nearly 75% of PMN undergo rapid cell death upon encountering *P. aeruginosa*. This was shown with PMN from LysM-EGFP mice that were adoptively transferred directly into the wound or into the tail-vein of C57BL6 mice that were dorsally wounded and inoculated with either Saline or *P. aeruginosa*. *P. aeruginosa*-infected wounds showed 75% less PMN within hours after infection compared to saline wounds. Further measurements revealed that the remaining 25% PMN were able to prolong their lifetime for up to three days, as measured by exponential decay from the peak florescence. Overall, these studies show that emergency granulopoiesis in bone marrow and rapid release of PMN into circulation and migration to the site of bacterial insult is necessary to sustain numbers over the initial 6-12 hours of the infection is indispensable to control *P. aeruginosa* dissemination and host survival against infection.

Our studies demonstrate also that TLR4- and MyD88-deficient mice are more susceptible than wild-type mice to *P. aeruginosa* in an infected wound. Thus, an intact NLRP3 inflammasome response along with IL-1β production are critical for host survival. However, the severity of infection is far greater in MyD88-deficient mice compared with TLR4-deficient mice. MyD88-/- experience systemic and lethal bacterial proliferation within 16 hours after infection. At the time of death, MyD88-/- wounds show lower levels of IL-1β, while TLR4 and wild-type mice produce similar levels at that timepoint. These data suggest that inflammasome activation and IL-1 receptors that also signal via MyD88 significantly contribute to the early immune response against *P. aeruginosa*, which is primarily driven by PMN infiltration from circulation and activation in the wound. Interestingly, early recruitment and maintenance of PMN over the initial 18 hours is equivalent between wild-type and MyD88-/- wounds. This suggests that IL-1β and MyD88 signaling is dispensable for production in bone marrow and homing to the vasculature

surrounding the wound. However, we demonstrate that MyD88 is required for adequate PMN migration from microcirculation in the dermis and to the site of infection. Previously, it was reported that swarming of PMN is critical to controlling dissemination by facilitating contact with *P. aeruginosa* and activation of antibacterial functions such as phagocytosis and ROS production. However, the ancillary role of MyD88 on resident cells, including macrophages and dendritic cells remains unknown. Particularly in the context of facilitating PMN swarming, migration, and killing capacity and in mitigating vascular breach that enables pathogen dissemination.

Future studies should employ chimeric mice to further investigate the role of TLR4, IL-1, and MyD88 on myeloid and non-myeloid cells in response to *P. aeruginosa* in infected skin, in addition to the role of these signaling pathways on PMN recruited from bone marrow compared to skin resident cells. In lungs, for example, inflammation is more tightly regulated by alveolar macrophages, which are critical in mitigating tissue destruction. It has been shown that lung macrophages are better able to control *S. aureus* infection via a MyD88-independent mechanism but require MyD88 signaling to defeat *P. aeruginosa* in the lung [219]. Similarly, NF-kB activation on resident macrophages, which is downstream of MyD88 in the inflammasome signaling pathway, can act as a negative regulator of inflammasome activation and is necessary for regulation of the immune response. Lastly, in the skin, PMN swarming is an immune response known to involve complex signaling between resident cells and recruited PMN, but the timing of these events following infection remains elusive, yet is of high interest for controlling pathogen dissemination. Combined, these studies should guide the development of therapeutic approaches that tune not only the number of PMN at the site of infection but also their ability to mount an effective immune response via TLR priming and inflammasome activation.

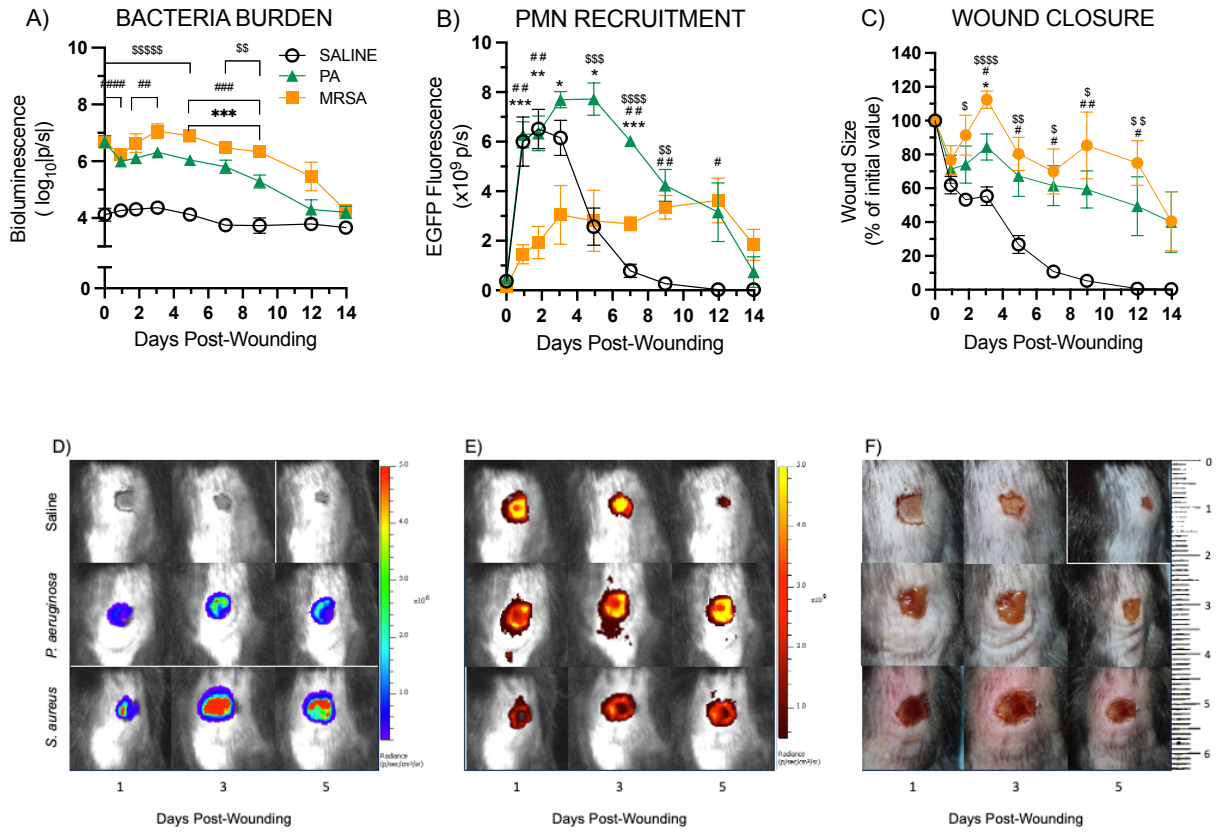

Figure 5.1: Host response to *S. aureus* and *P. aeruginosa* infection in wounded skin. LysM-EGFP mice were dorsally wounded and inoculated with either Saline or *P. aeruginosa* and imaged in an IVIS spectrum to measure A) bacterial abundance, B) PMN recruitment, and C) would closure over time. Representative D) bioluminescence, E) fluorescence, and F) photographs of mouse wounds depicting bacterial abundance, PMN recruitment, and wound closure respectively.
Data are derived from n=5 mice per group.
*, **, ***,**** denote p value ≤.05 ≤ 0.01, ≤ 0.001, and ≤ 0.0001, respectively.
* denotes S.a. vs P.a., # denotes Saline vs S.a., and $ denotes Saline vs P.a.
EGFP = Enhanced Green Fluorescent Protein
MRSA = Methicillin-Resistant *Staphylococcus aureus*
PA = *Pseudomonas aeruginosa*
PMN = Polymorphonuclear Leukocytes

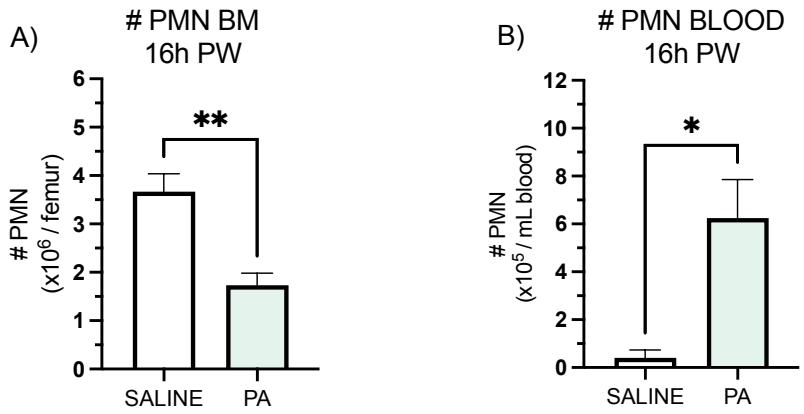

Figure 5.2: PMN enumeration in bone marrow and circulation at 16 hours post-wounding. *Pseudomonas aeruginosa* indices rapid PMN release out of bone marrow into circulation. LysM-EGFP mice were dorsally wounded and inoculated with either Saline or *P. aeruginosa* and the number of PMN in A) bone marrow and in B) circulation were quantified at 16 hours post-infection.
Data are derived from n=3 animals per group.
*, **, ***,**** denote p value ≤.05 ≤ 0.01, ≤ 0.001, and ≤ 0.0001respectively.
BM = Bone Marrow
PMN = Polymorphonuclear Leukocytes
PW = Post-Wounding

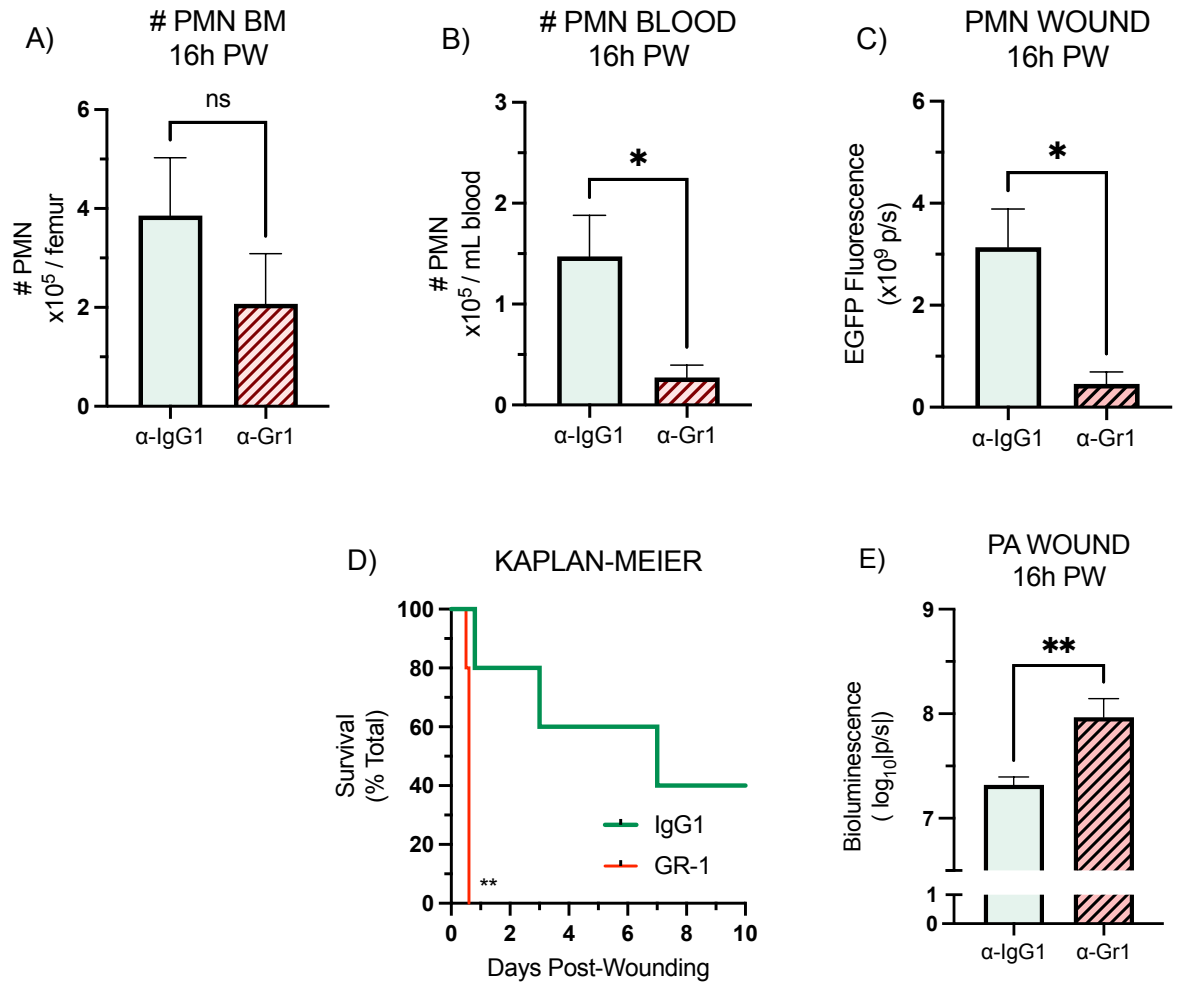

Figure 5.3: Effect of PMN depletion on animal survival and pathogen dissemination following wounding and inoculation with *P. aeruginosa*. LysM-EGFP mice were intraperitoneally administered either mAb anti-IgG1 (control cohort) or mAb anti-Gr1 antibody (PMN-depleted cohort) (0.1mg in 100uL injection) one day prior to being dorsally wounded and infected with *P. aeruginosa*. PMN were quantified in A) bone marrow and B) circulation at 16 hours after infection via flow cytometry. C) PMN were also measured at the site of infection via animal imaging using an IVIS Spectrum. D) Kaplan-Meier survival curve of non-depleted (IgG1) and PMN-depleted (Gr1) mice showing that depleted animals did not survive for more than 24 hours after infection. E) Bacterial abundance at the site of infection measured as bioluminescence flux using an IVIS Spectrum.
Data are derived from n=3-5 animals per group.
*, **, ***,**** denote p value ≤.05 ≤ 0.01, ≤ 0.001, and ≤ 0.0001, respectively.
IgG1 = Rat IgG1 kappa Isotype Control Antibody (eBRG1)
GR1 = Ly-6G/Ly-6C Monoclonal Antibody (RB6-8C5)
PA = *Pseudomonas aeruginosa*
PW = Post-Wounding

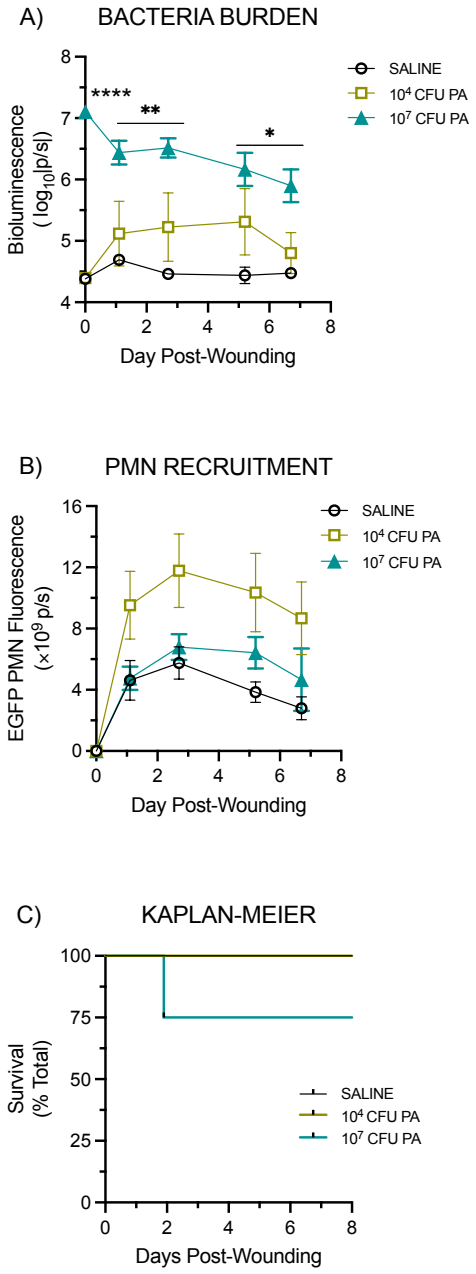

Figure 5.4: PMN number at the site of infection response inversely correlates with initial *P. aeruginosa* abundance. LysM-EGFP mice were dorsally wounded and inoculated with either Saline, 10^4, or 10^7 CFU of *P. aeruginosa* and imaged in an IVIS spectrum to measure A) bacterial abundance and B) PMN recruitment over time. C) Kaplan-Meier curve showing probability of survival for each group.
Data are derived from n=5 mice per group.
*, **, ***,**** denote p value ≤.05 ≤ 0.01, ≤ 0.001, and ≤ 0.0001, respectively between Saline and 10^7 groups.
CFU = Colony Forming Unit
EGFP = Enhanced Green Fluorescent Protein
PA = *Pseudomonas aeruginosa*
PMN = Polymorphonuclear Leukocytes

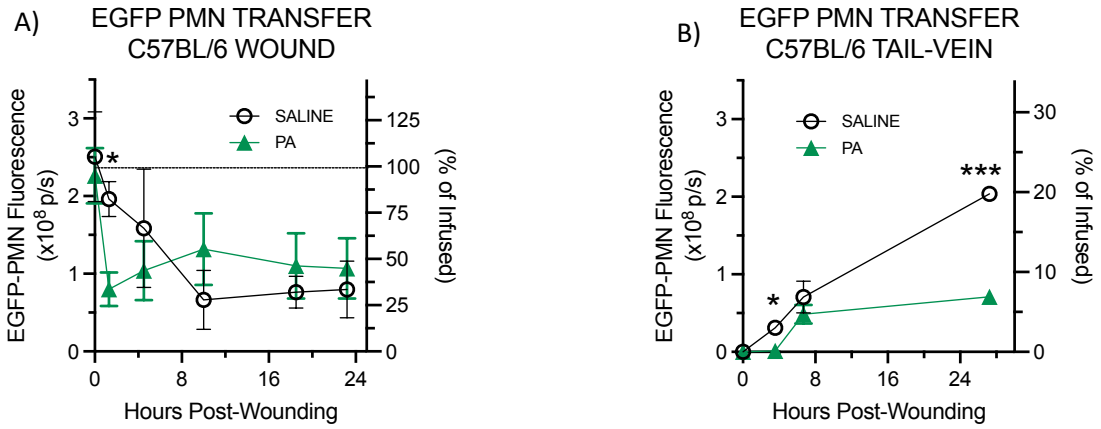

Figure 5.5: Pseudomonas aeruginosa decreases PMN numbers detected at the site of infection. A) Transfer of LysM-EGFP PMN into the wounds of C57BL6 mice right after wounding and inoculation with either Saline or PA. B) Transfer of LysM-EGFP PMN into the tail vein of C57BL6 two hours before wounding and inoculation with either Saline or PA. Data are derived from n=3 mice per group.
*, **, ***,**** denote p value ≤.05 ≤ 0.01, ≤ 0.001, and ≤ 0.0001 respectively.
EGFP = Enhanced Green Fluorescent Protein
PA = *Pseudomonas aeruginosa*
PMN = Polymorphonuclear Leukocytes

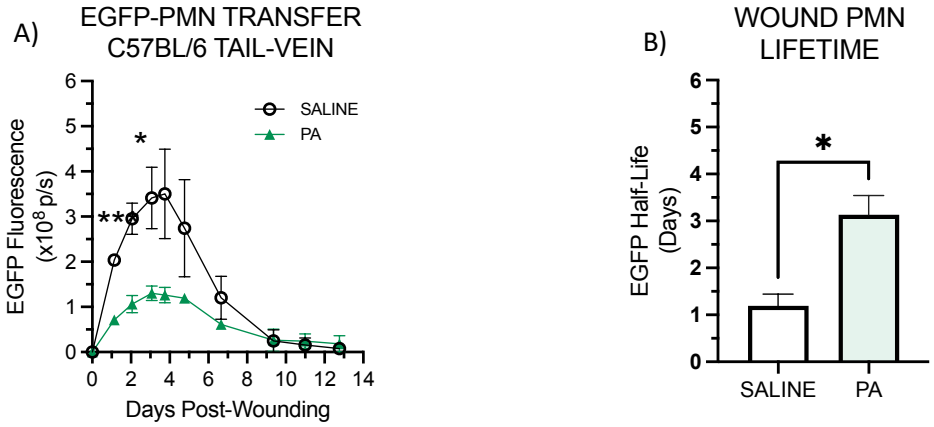

Figure 5.6: A viable subset of PMN that reach the wound site prolong their lifetime in response to *Pseudomonas aeruginosa*. A) Tail-vein adoptive transfer of WT PMN from LysM-EGFP mice into C57BL6 mice 2 hours before being wounded and inoculated with either saline or *Pseudomonas aeruginosa* (PA). B) PMN lifetime measured by half-life exponential decay from peak florescence in A. Data are derived from n=3 mice per group.
*, **, ***,**** denote p value ≤.05 ≤ 0.01, ≤ 0.001, and ≤ 0.0001 respectively.
EGFP = Enhanced Green Fluorescent Protein
PA = *Pseudomonas aeruginosa*
PMN = Polymorphonuclear Leukocytes

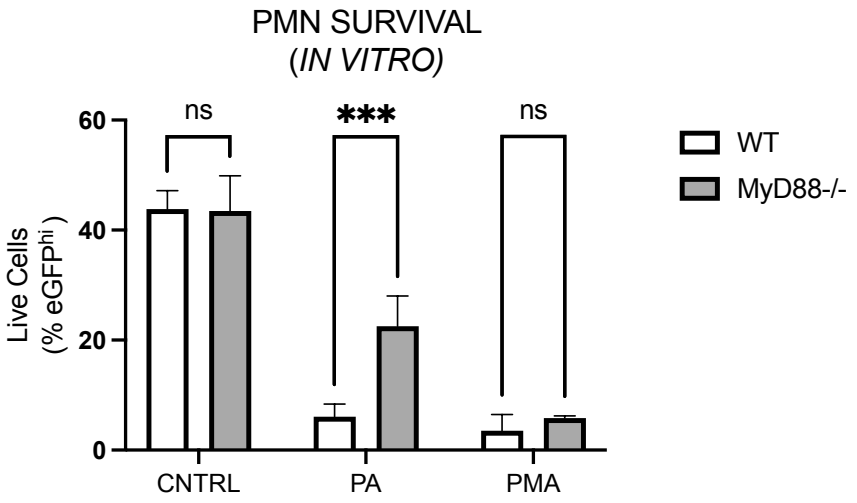

Figure 5.7: Changes in PMN viability induced by PA as a function of MyD88. Wild-type (WT) and MyD88-/- PMN from LysM-EGFP mice were cultured *in vitro* using basal media, media containing PA, or media containing PMA. Data are derived from n=3 replicates per group.
*, **, ***,**** denote p value ≤.05 ≤ 0.01, ≤ 0.001, and ≤ 0.0001 respectively.
CNTRL = control basal media
EGFP = Enhanced Green Fluorescent Protein
PA = *Pseudomonas aeruginosa*
PMA = Phorbol Myristate Acetate
PMN = Polymorphonuclear Leukocytes
WT = Wild-type

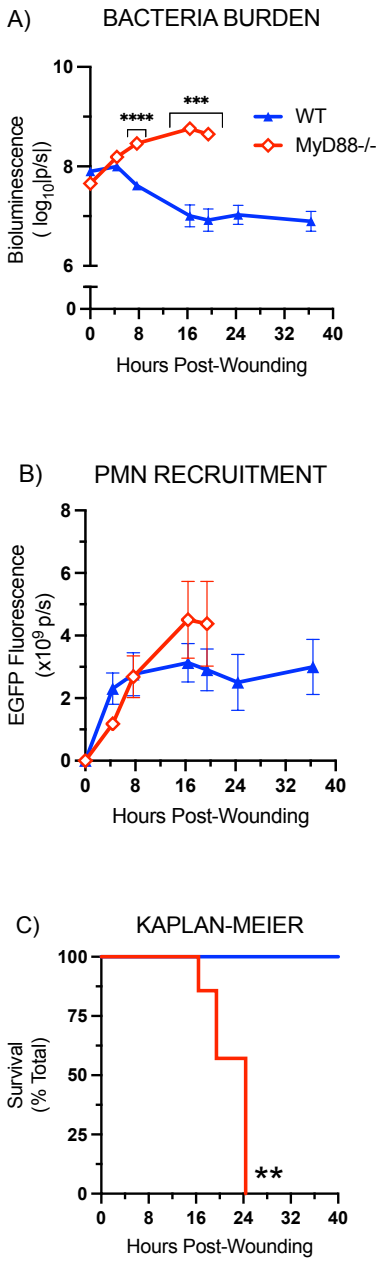

Figure 5.8: PA infection studies on MyD88-/- and wild-type mice. Wild-type and MyD88-/- mice that express eGFP in the lysosome gene (*lys*) were dorsally wounded and infected with PA. PMN recruitment (A) and bacterial abundance (A) were measured as a function of eGFP fluorescence and bioluminescence flux from the wound using an IVIS Spectrum. C) Mice were closely monitored to assess survival time following wounding and infection.
Data are derived from n=5-7 mice per group.
*, **, ***,**** denote p value ≤.05 ≤ 0.01, ≤ 0.001, and ≤ 0.0001 respectively.
EGFP = Enhanced Green Fluorescent Protein
PMN = Polymorphonuclear Leukocytes
WT = Wild-type

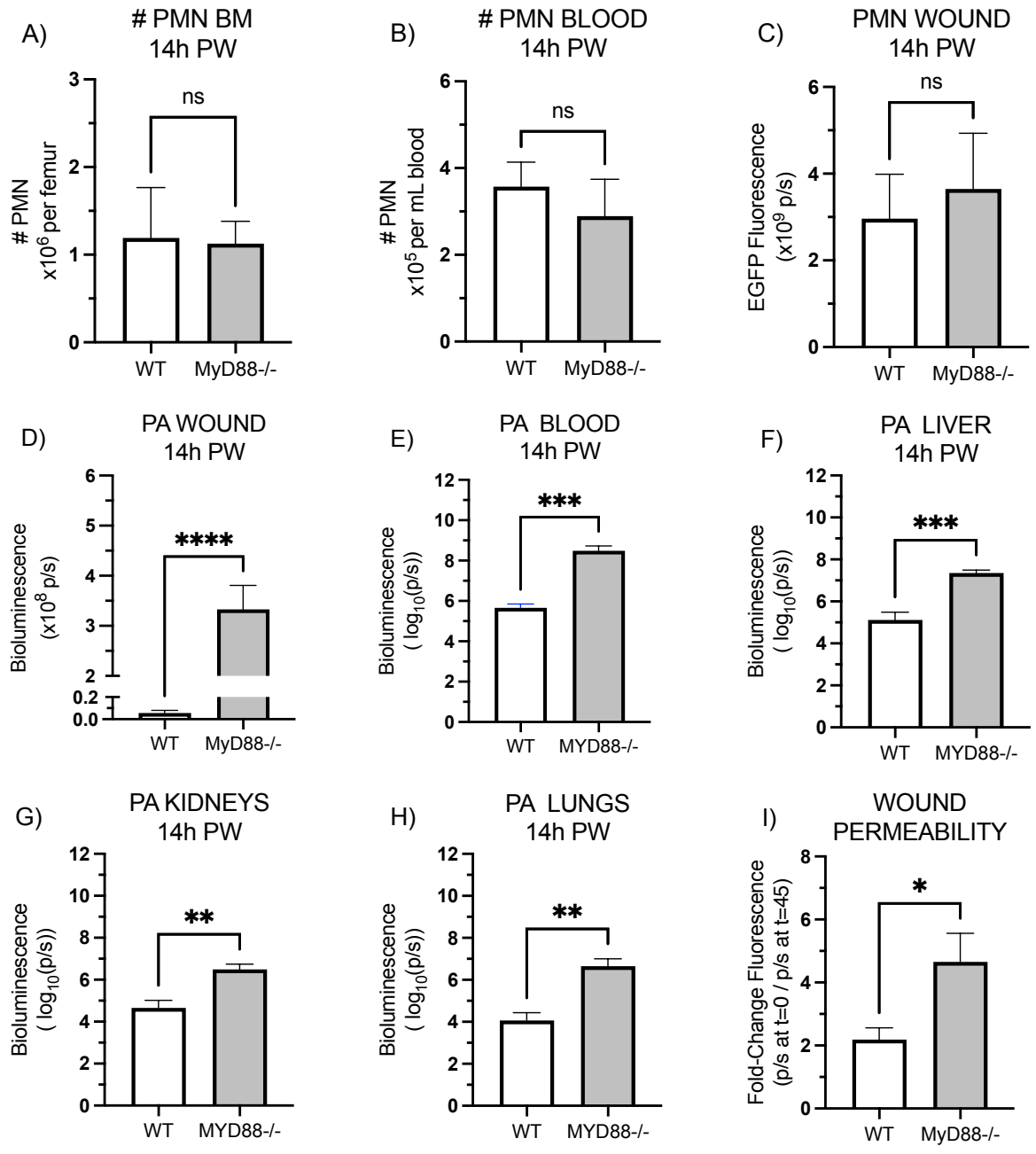

Figure 5.9: Effect of MyD88 absence on PMN recruitment and PA dissemination. A-C) PMN number in blood and at the site of infection in WT and MyD88-/- at 14h Post-wounding and PA infection. Measurements of PA abundance at wound site (D), in blood (E), and into vital tissues (F-H) at 14h post-wounding and infection. I) Vascular permeability measured as the change in BSA-Alexa680 fluorescence from t=0 to t=45 minutes after BSA-Alexa 680 administration into the tail vein of WT and MyD88-/- mice at 12-14h after wounding and inoculation with PA.

Data are derived from n=3-5 mice per group.

*, **, ***,**** denote p value ≤.05 ≤ 0.01, ≤ 0.001, and ≤ 0.0001 respectively.

BM = Bone Marrow | EGFP = Enhanced Green Fluorescent Protein | PA = *Pseudomonas aeruginosa*

PMN = Polymorphonuclear Leukocytes | PW = Post-Wounding | WT = Wild-type

A) LIVER

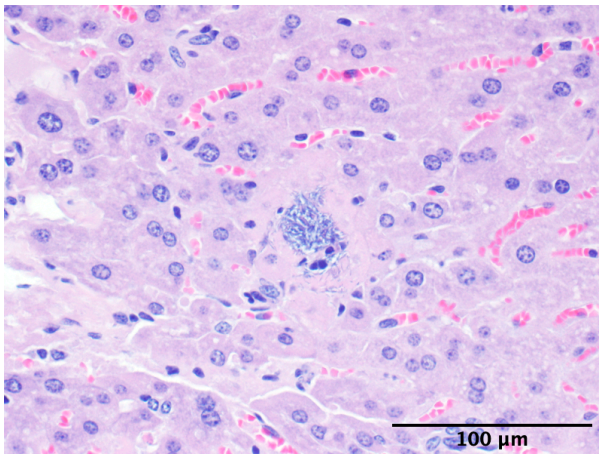

B) KIDNEY

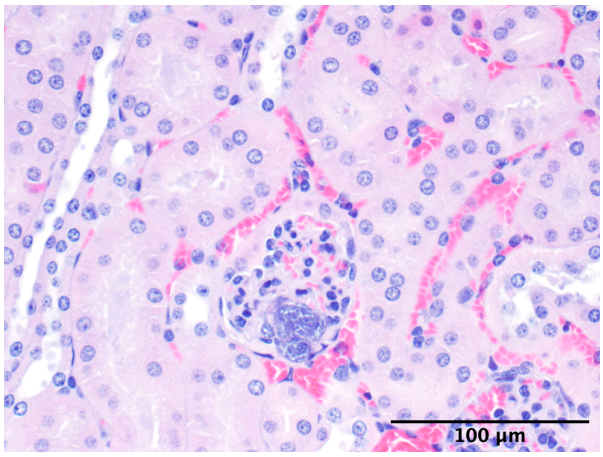

C) LUNG

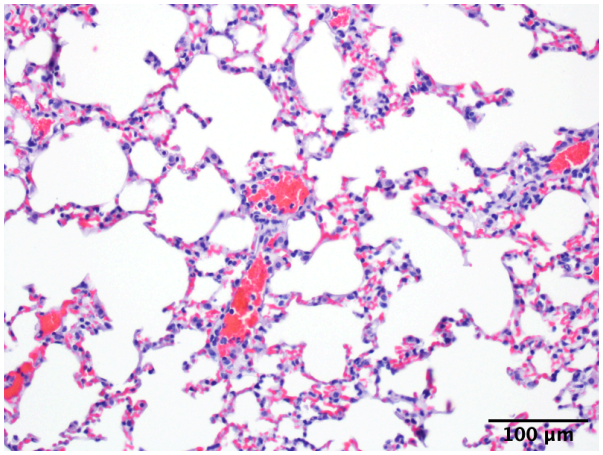

D) PANCREAS

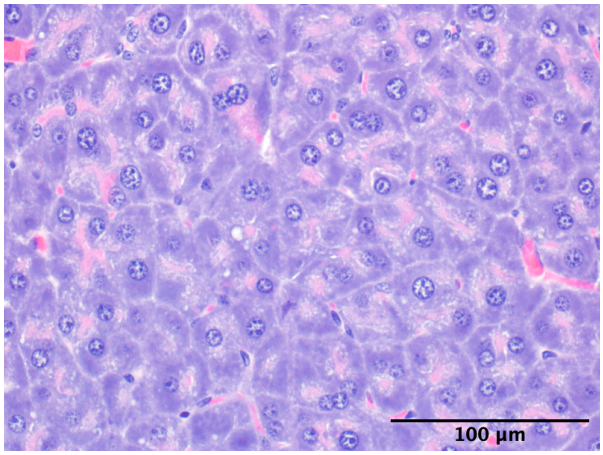

E) SPLEEN

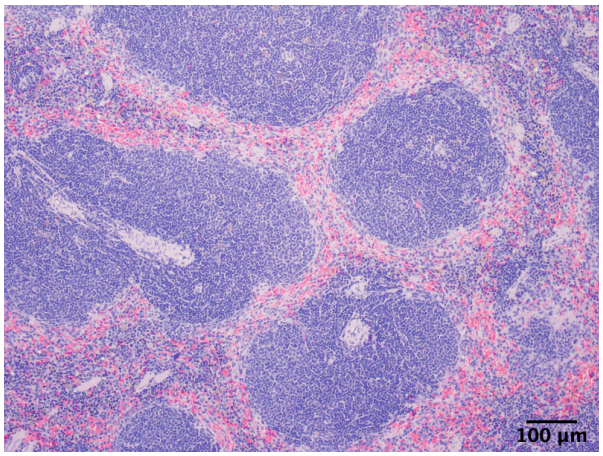

F) THYMUS

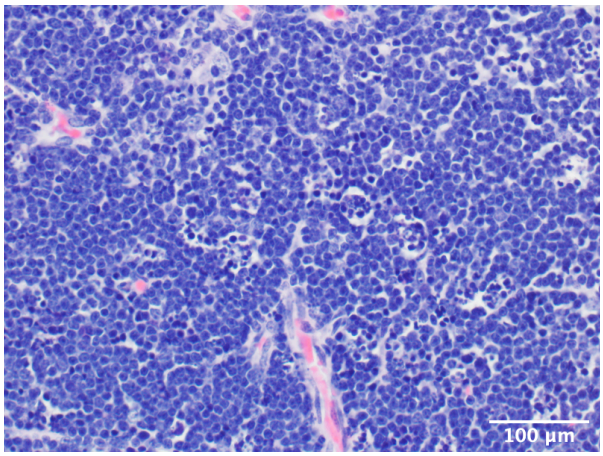

Figure 5.10: H&E from various tissues from MyD88-/- mice at 14h post wound infection with Pseudomonas.

A) Liver (40x) showing hepatocellular necrosis with associated rod-shaped bacteria consistent with *P. aeruginosa* and hepatocellular necrosis associated neutrophilic infiltration. B) Kidney (40x) exhibiting glomerular tuft emboli of rod-shaped bacteria consistent with *P. aeruginosa* indicating circulating bacteria and sepsis. C) Lung tissue (20x) with thickening alveolar septa by congested blood vessels with circulating neutrophilia. D) Pancreas (40x) showing zymogen depletion in the exocrine pancreas acinar cells indicating hyporexia. E) Spleen (10x) showing lymphoid hyperplasia. F) Thymus (40x) with lymphocytolysis and increased number of tangible body macrophages. Scale bars represent 100μm.

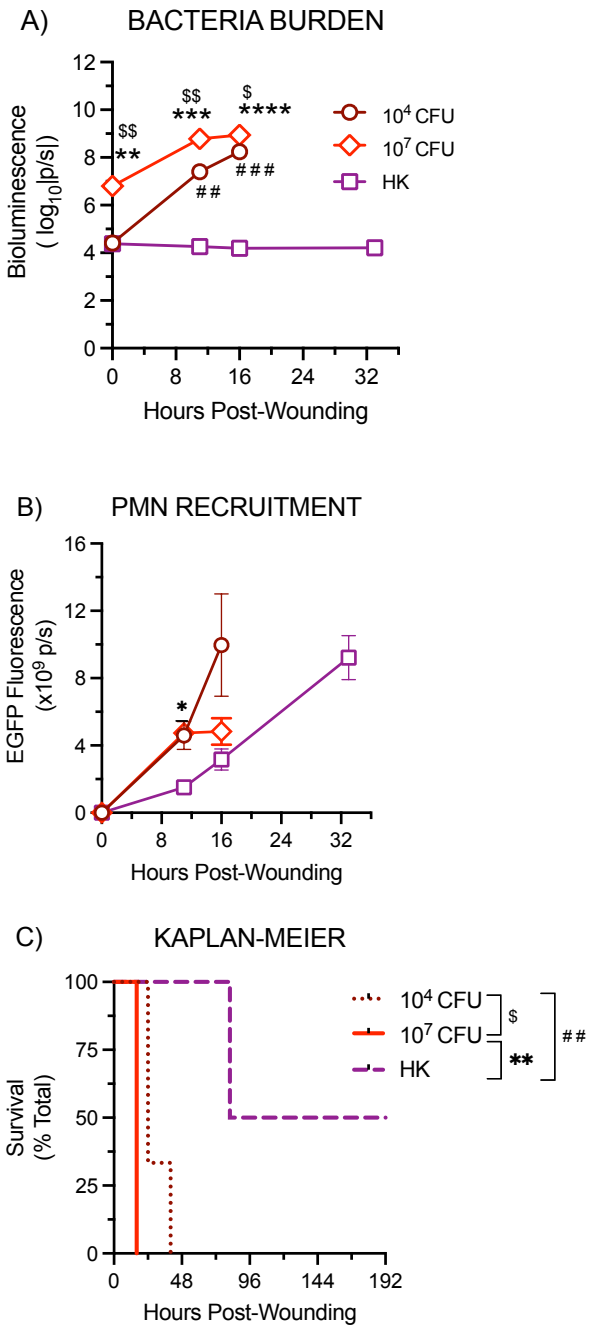

Figure 5.11: Effect of initial PA abundance on immune response in MyD88-/- mice. MyD88-/- mice were dorsally wounded and inoculated with either 10^4 CFU, 10^7 CFU, or HK PA. Mice were imaged to measure PMN recruitment (A) and bacterial abundance (B), and monitored to assess survival rates over time (C).
Data are derived from n=3-5 mice per group.
*, **, ***,**** denote p value ≤.05 ≤ 0.01, ≤ 0.001, and ≤ 0.0001 respectively.
CFU = Colony Forming Unit
EGFP = Enhanced Green Fluorescent Protein
HK = heat-killed (95 °C for 45 minutes)
PA = *Pseudomonas aeruginosa*
PMN = Polymorphonuclear Leukocytes
PA = *Pseudomonas aeruginosa*

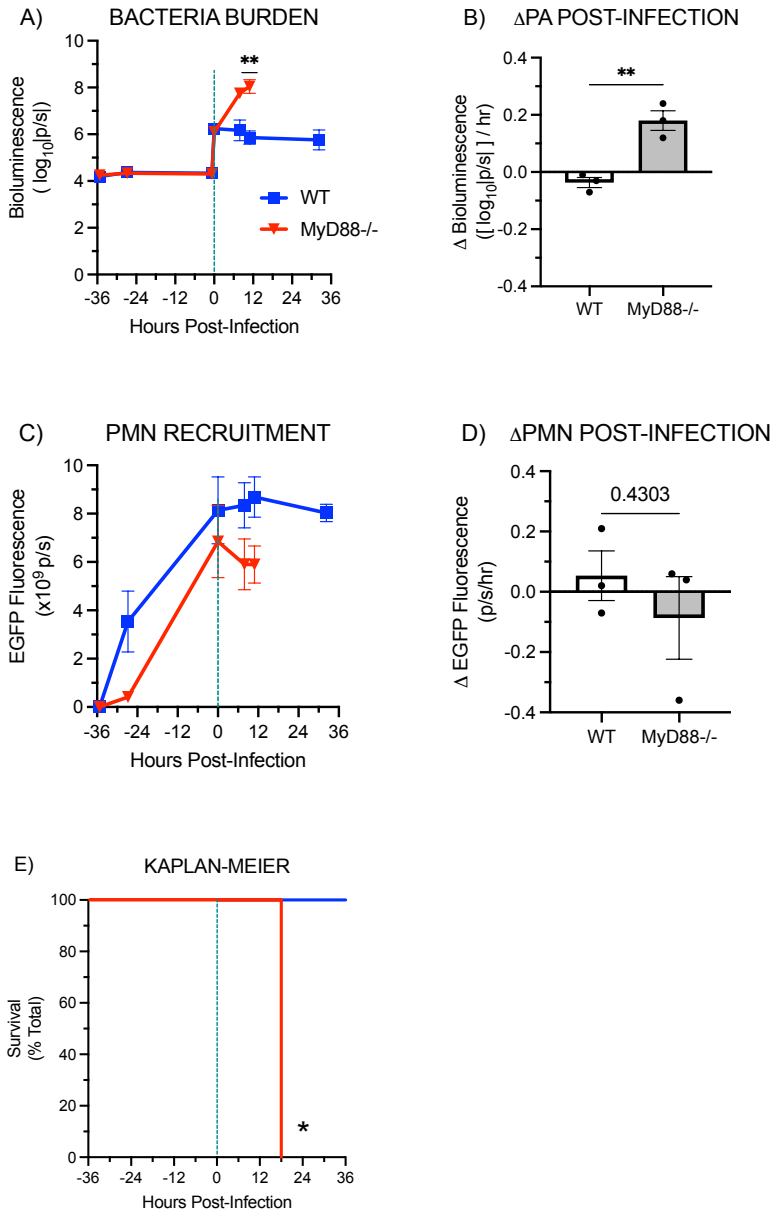

Figure 5.12: Effect of increasing PMN recruitment by delaying PA infection on MyD88-/- vs WT mice. WT and MyD88-/- mice were wounded 36 hours before infection with PA as a strategy to increase PMN number at the site of infection. A) Bioluminescence flux measured from the wound over time using an IVIS Spectrum. B) Rate of change in Bioluminescence from the wound following inoculation with PA. C) EGFP fluorescence flux measured from the wound using an IVIS Spectrum indicative of PMN recruitment over time. D) Rate of change in EGFP-PMN fluorescence following inoculation with PA. E) Survival curve of WT and MyD88-/- mice. t=0 denotes the time when PA was inoculated. Data are derived from n=3 mice per group.
*, **, ***,**** denote p value ≤.05 ≤ 0.01, ≤ 0.001, and ≤ 0.0001 respectively.
EGFP = Enhanced Green Fluorescent Protein
PA = *Pseudomonas aeruginosa*
PMN = Polymorphonuclear Leukocytes

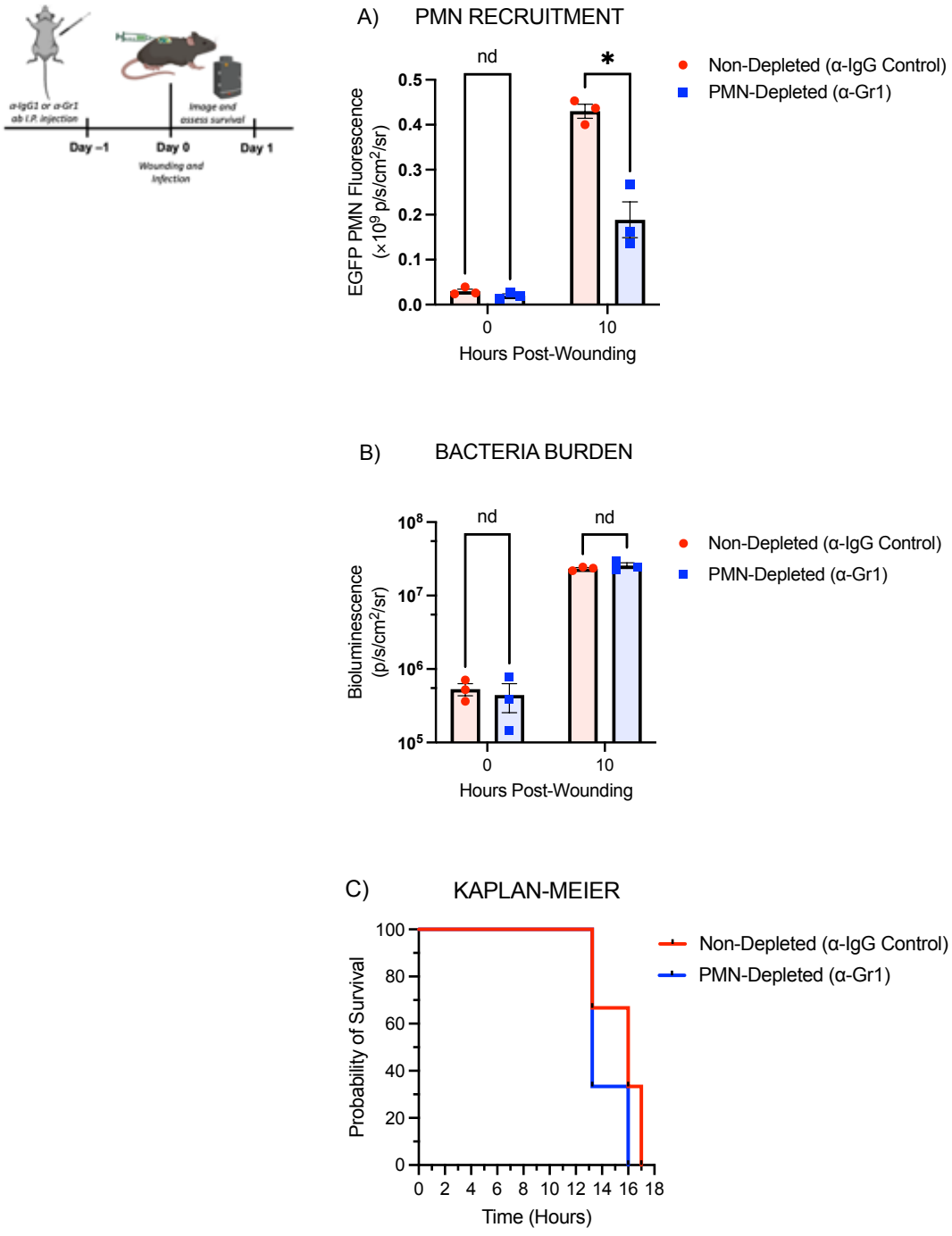

Figure 5.13: Effect of PMN depletion on MyD88-/- mouse response against PA. MyD88-/- mice were either deplete or not depleted of circulating PMN via anti-IgG1 or anti-Gr1 antibody administration one day before wounding and infection with PA. A) EGFP fluorescence flux measured from the wound using an IVIS Spectrum indicative of PMN recruitment at 0- and 10-hours post-wounding. B) Bioluminescence flux measured from the wound over time using an IVIS Spectrum. C) Survival curve of depleted and non-depleted MyD88-/- mice. Data are derived from n=3 mice per group.
*, **, ***,**** denote p value ≤.05 ≤ 0.01, ≤ 0.001, and ≤ 0.0001 respectively.
EGFP = Enhanced Green Fluorescent Protein
PA = *Pseudomonas aeruginosa*

PMN = Polymorphonuclear Leukocytes

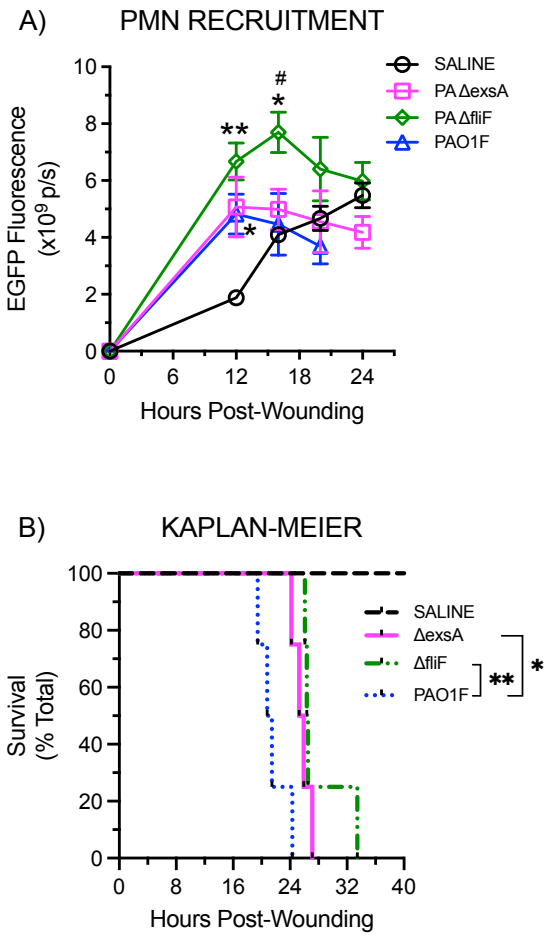

Figure 5.14: Effect of PA T3SS secretion system and fliF adhesins on MyD88-/- mouse response against PA.
MyD88-/- mice were wounded and inoculated with Saline, wild-type PAO1, or PA mutants lacking the T3SS system or fliF adhesins. A) EGFP fluorescence flux measured from the wound using an IVIS Spectrum indicative of PMN recruitment over time. B) Survival curve of MyD88-/- mice. Data are derived from n=3 mice per group.
*, **, ***,**** denote p value ≤.05 ≤ 0.01, ≤ 0.001, and ≤ 0.0001 respectively.
EGFP = Enhanced Green Fluorescent Protein
PA = *Pseudomonas aeruginosa*
PMN = Polymorphonuclear Leukocytes

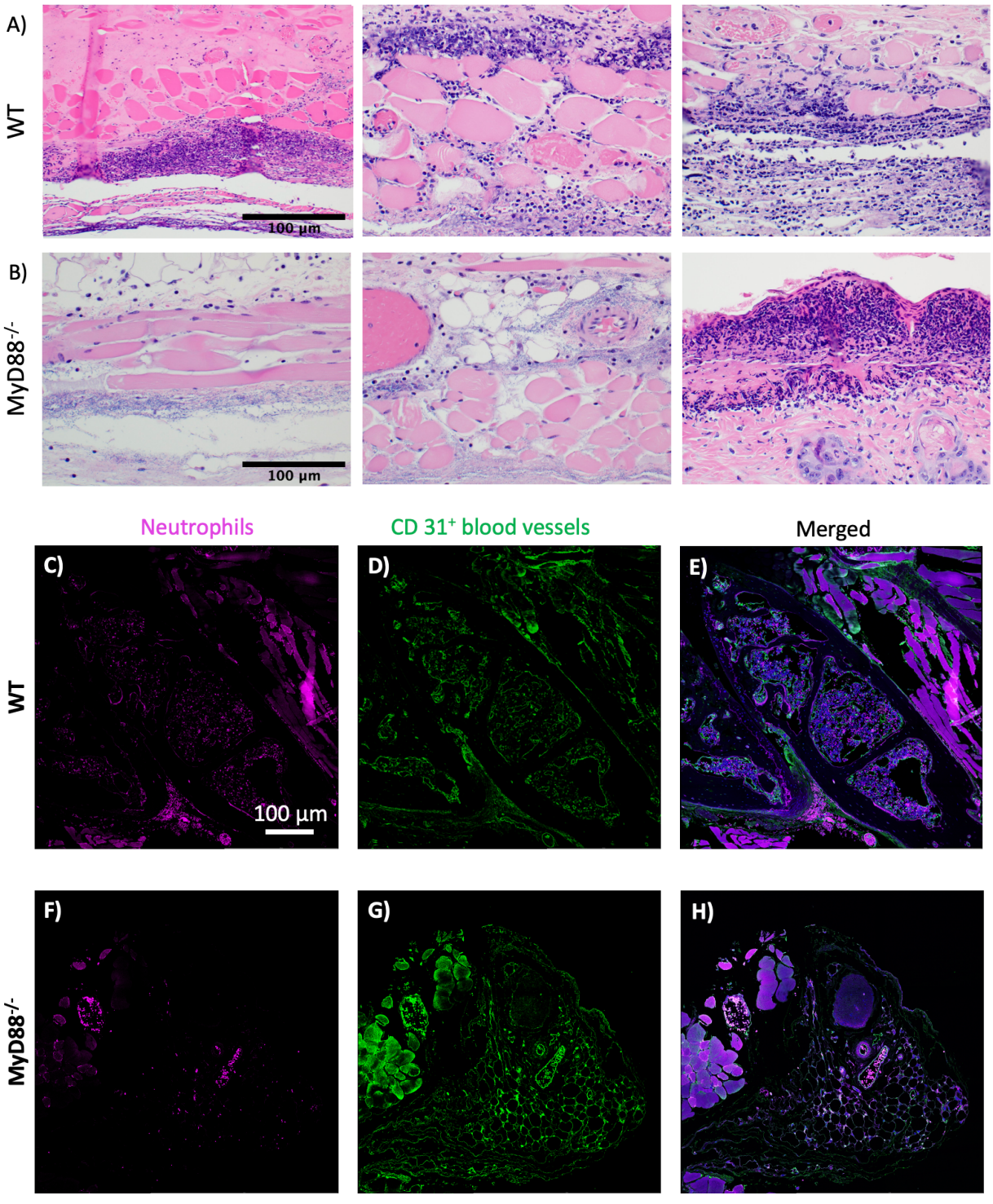
A)
WT
100 µm
B)
MyD88-/-
100 µm
Neutrophils
CD 31+ blood vessels
Merged
C)
D)
E)
WT
100 µm
F)
G)
H)
MyD88-/-

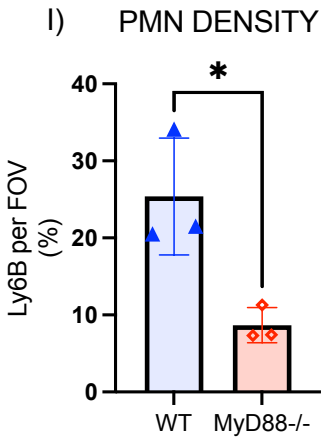

Figure 5.15: Tissue histology from WT and MyD88-/- wounds excised at 14h after infection with PA. AB) H&E staining of wound sections of WT and MyD88-/- mice. C) Ly6b staining on WT and MyD88-/- wound sections. D) CD31 staining on WT and MyD88-/- wound sections. E) Overlap of C and D. J) Measurement of percent Ly6b expression on each section. Data are derived from n=3 mice per group. Scale bars represent 100μm.
*, **, ***,**** denote p value ≤.05 ≤ 0.01, ≤ 0.001, and ≤ 0.0001 respectively.
PMN = Polymorphonuclear Leukocytes
WT = Wild-type

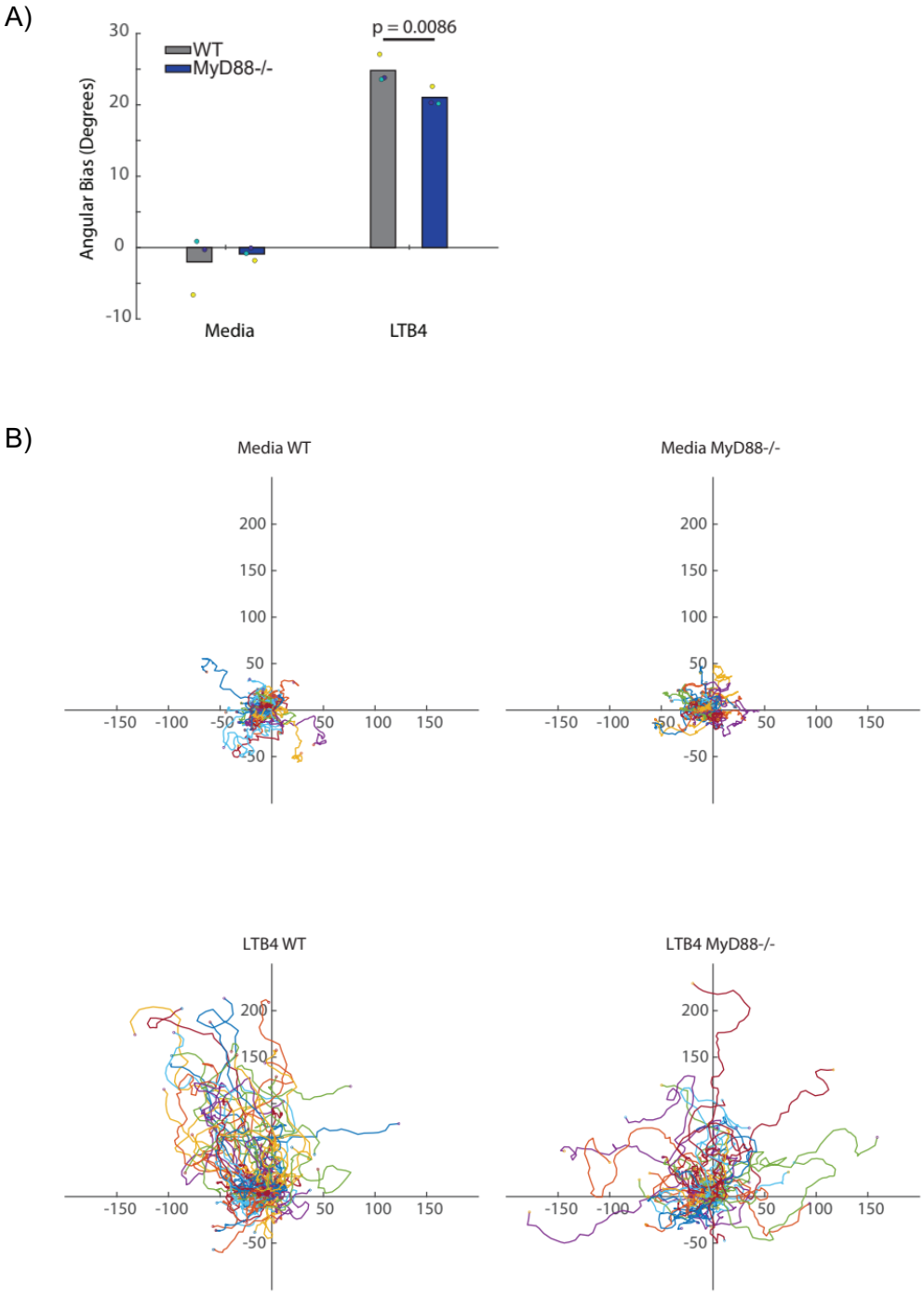

Figure 5.16: *In vitro* PMN chemotaxis assay as a function of MyD88. WT and MyD88-/- PMN from LysM-EGFP mice were isolated and evaluated for A) migratory speed and B) angular bias between wild-type and MyD88-/- PMN. C-F) Individual cell paths in response to basal media or LTB4 on WT and MyD88-/- PMN. Data are from n=3 independent experiments. Plots and statistical analysis performed in MATLAB (R2023b, Natick, Massachusetts: The MathWorks Inc.; 2023).
LTB4 = Leukotriene B4
WT = Wild-type

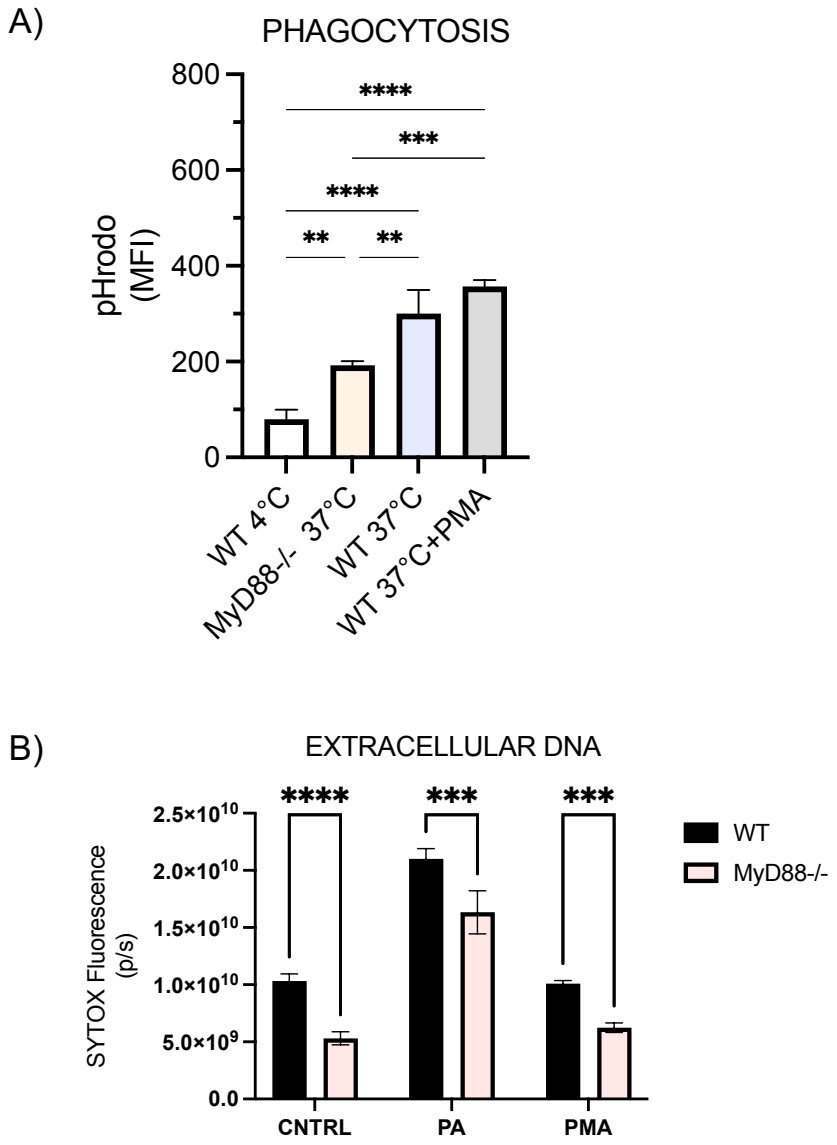

Figure 5.17: *In vitro* PMN functionality assays as a function of MyD88. WT and MyD88-/- PMN from LysM-EGFP mice were isolated and evaluated for A) phagocytosis and B) eDNA release (NETosis) capacity.
Data are derived from n=3 replicates per group.
*, **, ***,**** denote p value ≤.05 ≤ 0.01, ≤ 0.001, and ≤ 0.0001 respectively.
eDNA = Extracellular DNA
MFI = Mean Fluorescence Intensity
PA = *Pseudomonas aeruginosa*
PMA = Phorbol Myristate Acetate
PMN = Polymorphonuclear Leukocytes
WT = Wild-type

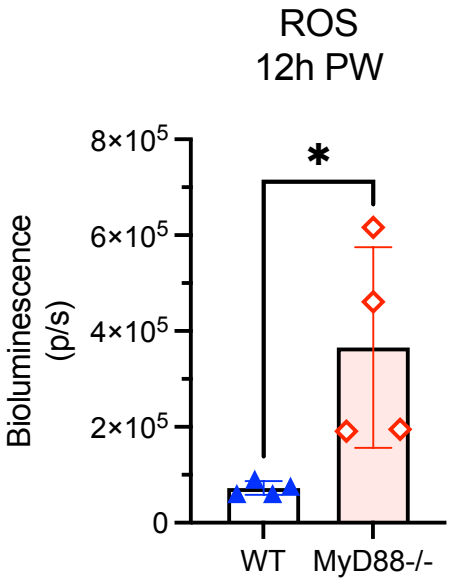

Figure 5.18: Measurement of ROS elaboration *in vivo*. WT and MyD88-/- mice received administration of Luminol into the site of infection 12 hours after wounding and inoculation with the non-bioluminescent *P. aeruginosa* PAO1 strain.
Data are derived from n=4 mice per group.
* denotes *p*-value ≤.05.
PW = Post-Wounding
ROS = Reactive Oxygen Species
WT = Wild-type

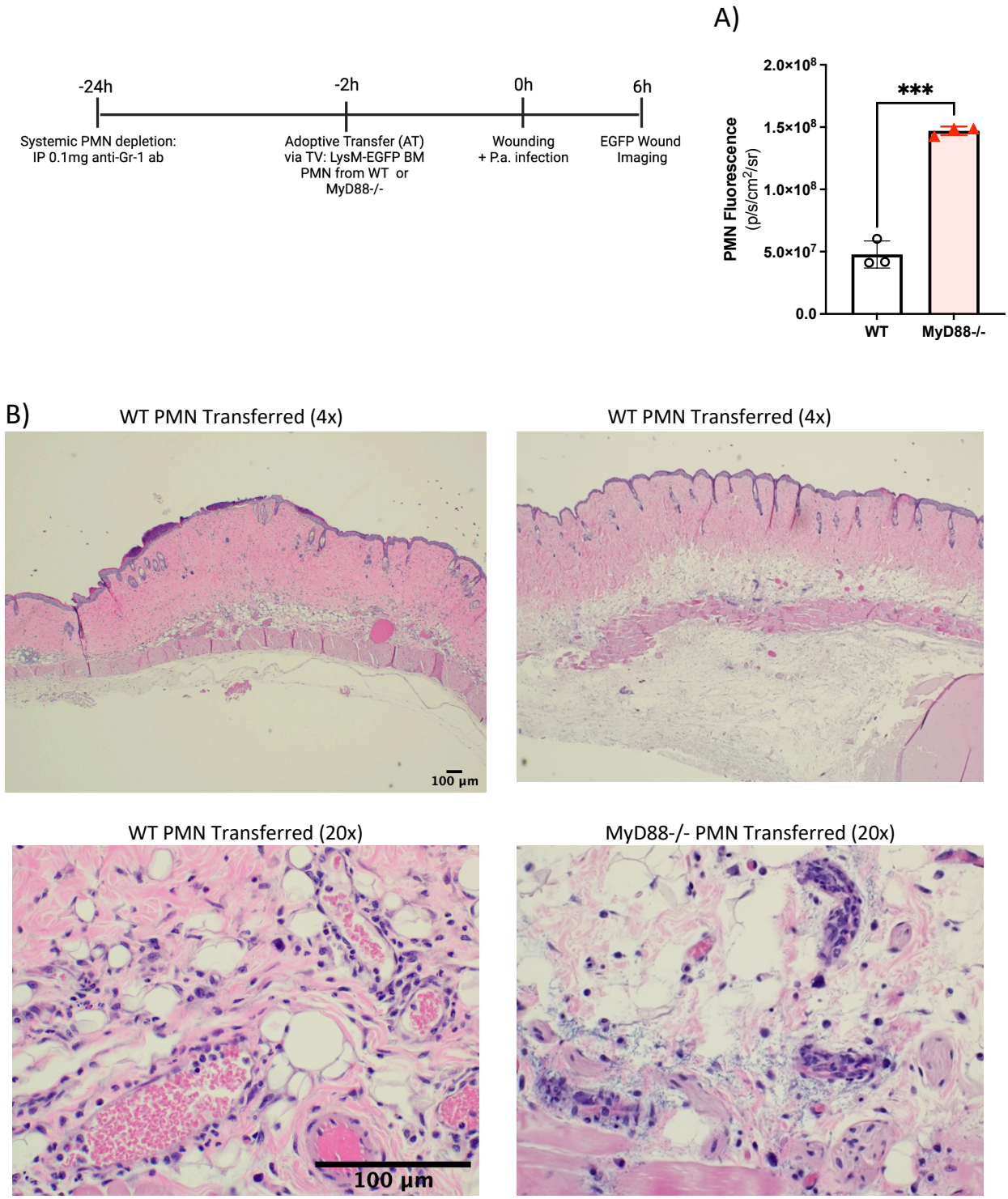

Figure 5.19: Adoptive transfer of WT or MyD88-/- PMN into C57BL6 mice depleted of their native PMN. A) MyD88-/- PMN *persist* longer than WT in PMN-depleted, P.a.-infected C57BL6 wounds. EGFP signal measured at 6 hours after infection. Data are derived from n=3 mice per group. B) H&E staining from wound tissue of P.a.-infected mice that received TV adoptive transfer of either WT of MyD88-/- PMN 2 hours before infection. Mice

carcasses were fixed and processed for tissue collection at 21 hours post-infection. The host response to infection is dramatically different when compared to wild-type AT. In the MyD88-/- AT mouse, the host response is predominantly edema and vascular congestion with pronounced bacterial colonization of the subcutis, dermal vessels and underlying muscle. In the WT AT mouse, the host response to infection is neutrophilic and focused on regions of epithelial barrier breach (erosion or ulceration). Images are derived from one representative mouse per group. Scale bars represent 100μm.
*, **, ***,**** denote *p*-value ≤.05 ≤ 0.01, ≤ 0.001, and ≤ 0.0001 respectively.
AT = Adoptive Transfer
PA = *Pseudomonas aeruginosa*
PMN = Polymorphonuclear Leukocytes
TV = Tail-Vein
WT = Wild-type

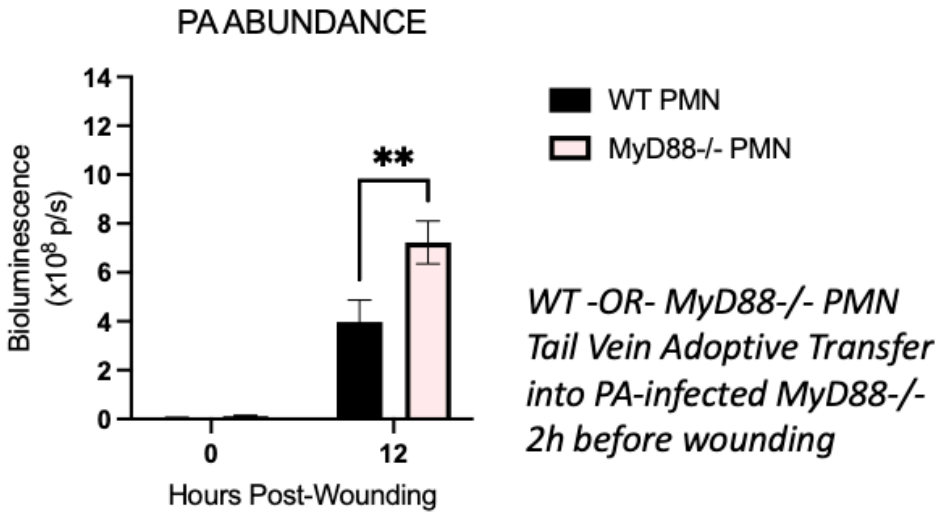

Figure 5.20: WT vs MyD88-/- PMN killing capacity against P. aeruginosa in MyD88-/- mouse wounds. WT or MyD88-/- PMN were isolated from LysM-EGFP mice and transferred via tail-vein into MyD88-/- mice. These mice were then wounded and infected with P. aeruginosa. Bacterial abundance was measured at 12 hours post-infection as a function of bioluminescence flux (p/s) using an IVIS Spectrum.
Data are derived from n=3 mice per group
** denotes *p*-value ≤ 0.01
PA = *Pseudomonas aeruginosa*
WT = Wild-type

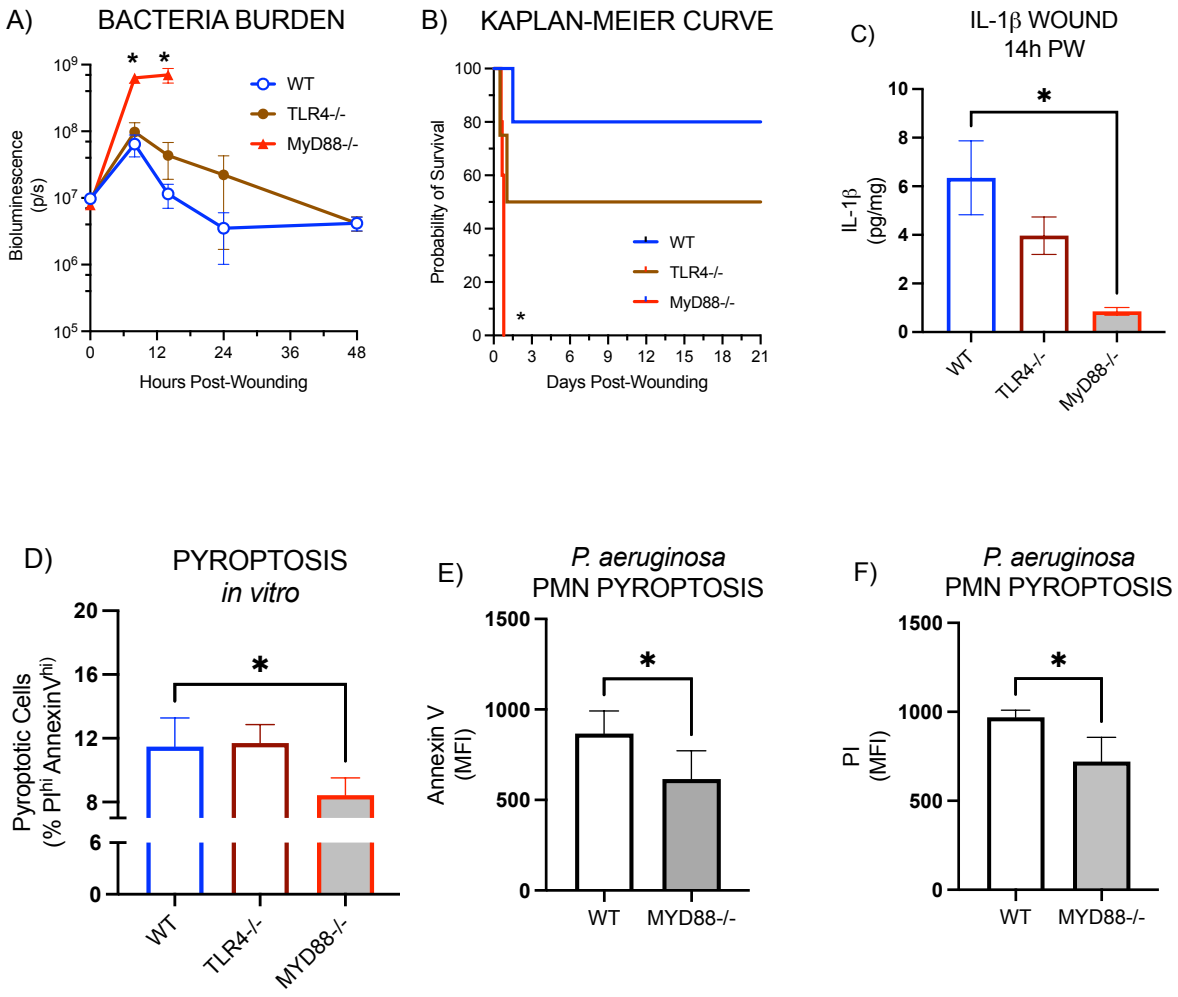

Figure 5.21: TLR4-/- mice have better survival and ability to contain bacteria than MyD88-/-. MyD88-/- defect does not seem to be LPS-detection-dependent. TLR4-/- wounds show similar IL-1β concentration as WT. Similarly, TLR4-/- show similar pyroptotic phenotype in response to HK-P.a. as WT. However, MyD88-/- are both deficient in IL-1β and less pyroptotic than WT in presence of P.a.
Data in A-C are derived from n=5 mice per group.
Data in D-F are derived from n=3 replicates per group.
*, **, ***,**** denote *p*-value ≤.05 ≤ 0.01, ≤ 0.001, and ≤ 0.0001 respectively.
MFI = Mean Fluorescence Intensity
PA = *Pseudomonas aeruginosa*

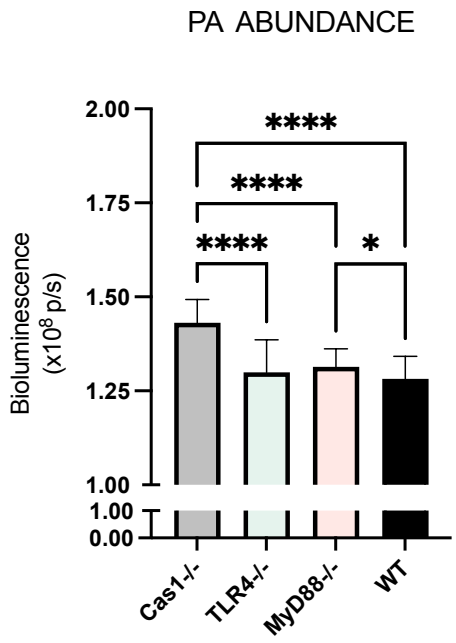

Figure 5.22: PMN killing capacity against P. aeruginosa as a function of Cas1, TLR4, and MyD88 activation.
MyD88-/- and Cas1-/- PMN showed the higher levels of P.a. abundance *in vitro,* suggestive of impaired killing capacity.
Data are derived from n=3 replicates per group.
*, **, ***,**** denote *p*-value ≤.05 ≤ 0.01, ≤ 0.001, and ≤ 0.0001 respectively.
PA = *Pseudomonas aeruginosa*

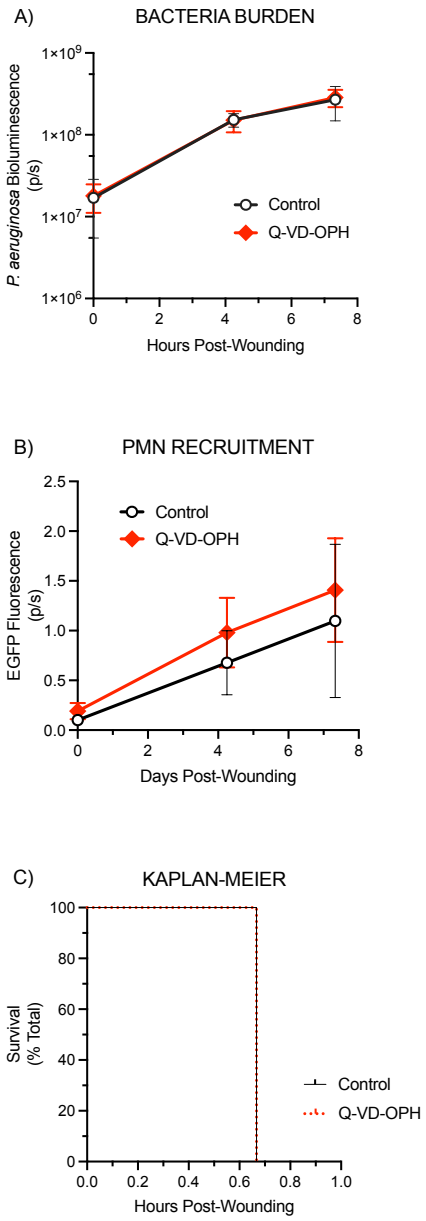

Figure 5.23: Effect of caspase inhibition on the immune response against P. aeruginosa in MyD88-/- mice.
MyD88-/- mice were administered either the Pan-caspase inhibitor Q-VD-OPH or vehicle control at 4h before and at 0h post- wounding and infection. After wounding, mice were scanned in an IVIS Spectrum to measure bacterial abundance (A) and PMN recruitment (B). C) Kaplan-Meier curve showing % survival.
Data are derived from n=2 mice per group.
*, **, ***,**** denote *p*-value ≤.05 ≤ 0.01, ≤ 0.001, and ≤ 0.0001 respectively.
PA = *Pseudomonas aeruginosa*

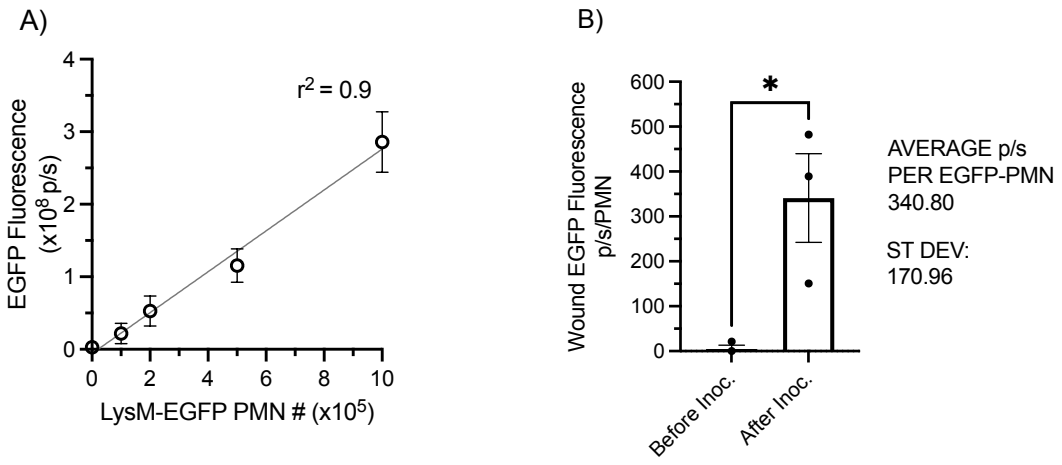

Supplemental Figure 5.1: Correlation between LysM-EGFP PMN number EGFP flux from a mouse wound.
PMN were isolated from LysM-EGFP mice bone marrow and a known number of PMN was directly transferred into the wounds of C57BL6 mice. Wounds were imaged for EGFP flux (p/s) before and after PMN inoculation. A) EGFP fluorescence emanating solely from the known number of LysM-EGFP PMN transferred into the wound (i.e. flux after inoculation minus flux before inoculation). Data are derived from n=3 mice per data point. B) Slope of the regression line shown in A, indicating EGFP fluorescence flux (p/s) per PMN.
*, **, ***,**** denote *p*-value ≤.05 ≤ 0.01, ≤ 0.001, and ≤ 0.0001respectively.
Inoc. = PMN Inoculation into 'dark' C57BL6 mouse wounds.

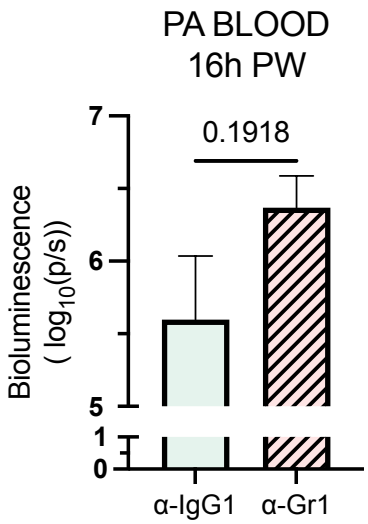

Supplemental Figure 5.2: *P. aeruginosa* detection in blood in non-depleted (α-IgG1) versus in PMN-depleted (α-Gr1) LysM-EGFP mice at 16 hours after being dorsally wounded and infected with P. aeruginosa.
Data are derived from n=3 mice per group.
p-value = 0.2 between non-depleted (α-IgG1) and depleted (α-Gr1) groups.
PA = *P. aeruginosa*
16h PW = 16 hours Post-Wounding

Detection of *P. aeruginosa* 16h PW

	α-IgG1 *(non-depleted)*	α-Gr1 *(PMN-depleted)*
Wound	+	+
Lung	–	+
Liver	–	+
Spleen	–	+

– No detection

\+ *P. aeruginosa* growth

Table 1: Mice depleted of circulating PMN a day before *P. aeruginosa* wound infection experience bacterial dissemination into lung, liver, and spleen. Thus, PMN are essential to contain *P. aeruginosa* in a wound during the early phase (first 24 hours) of the infection.
16h PW = 16 hours Post-Wounding
PMN = Polymorphonuclear Leukocytes

A)

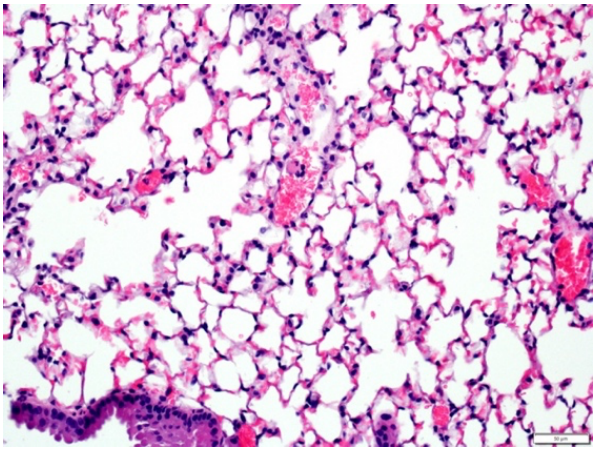

α-IgG1

NON-DEPLETED

B)

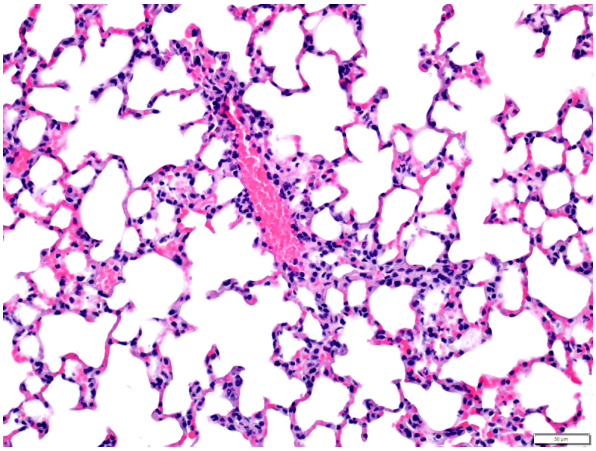

α-Gr1

PMN-DEPLETED

Supplemental Figure 5.3: H&E staining (20x) from lung tissue at 14 hours post-infection. Lungs of PMN-depleted mice infected with *P. aeruginosa* are characterized by moderate intravascular neutrophilia with numerous migrating neutrophilic and small fibrin aggregates.
Images obtained at 20x resolution and are derived from n=1 representative mouse from a group of 3-5.
Scale bars represent 50μm.
PMN = Polymorphonuclear Leukocytes

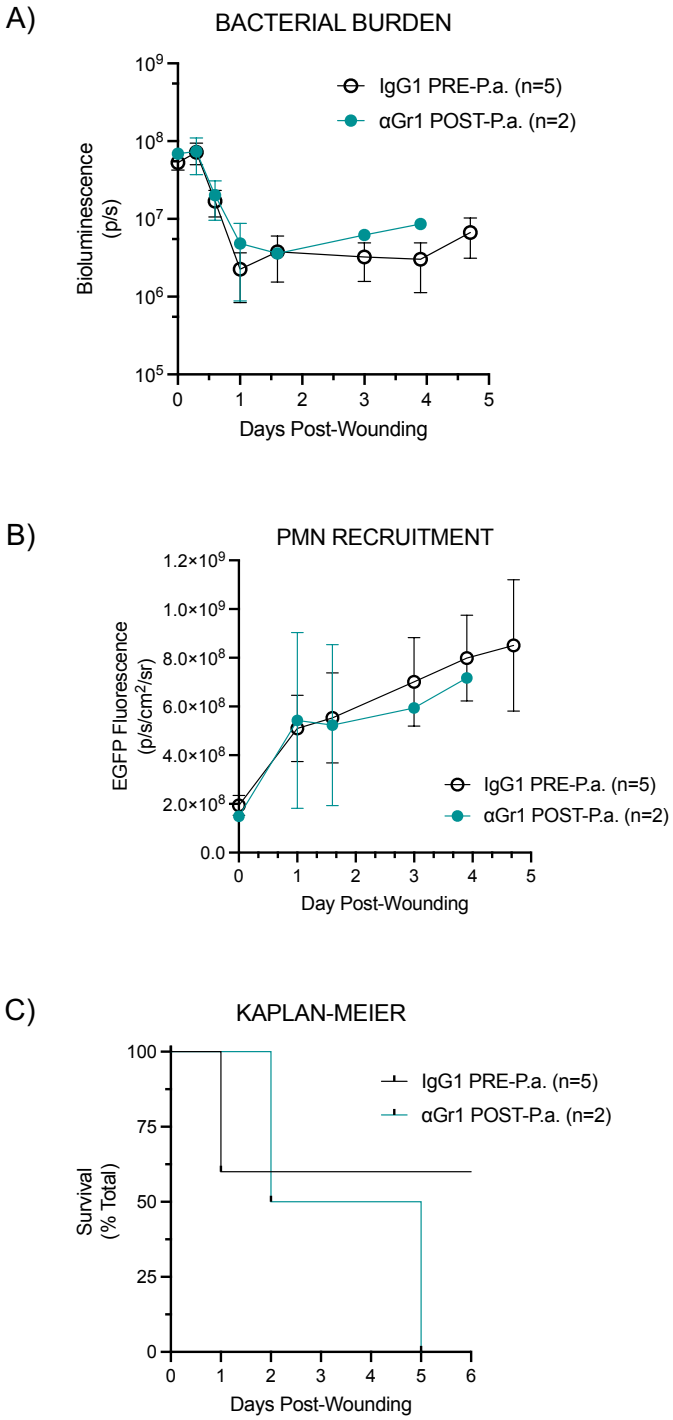

Supplemental Figure 5.4: A viable subset of PMN that reach the wound site prolong their lifetime in response to *Pseudomonas aeruginosa*. Mice were treated with mAb anti-IgG1 24 hours prior or with mAb anti-Gr1 24 hours after wounding and infection with *P. aeruginosa*. A) Bacterial abundance, B) PMN recruitment, and C) Survival were measured. From this stusy, it appears that a some PMN are prolong their lifetime in response to *P. aeruginosa* infection.
Data are derived from n=2-5 mice per group.
*, **, ***,**** denote *p*-value ≤.05 ≤ 0.01, ≤ 0.001, and ≤ 0.0001 respectively.
P.a. = *Pseudomonas aeruginosa* | PMN = Polymorphonuclear Leukocytes

CHAPTER 6: DISSERTATION SUMMARY AND FUTURE DIRECTIONS

Throughout their existence, organisms on Earth have developed strategies to keep harmful pathogens at bay and persist through the millennia. Mammals have evolved various adaptions of physical barriers to prevent microorganism infections. In addition, they are equipped with innate and adaptive immune mechanisms to quickly respond to and combat invading pathogens when physical barriers, such as the skin and gut, are breached. Innate responses are elicited within minutes after infection, while adaptive mechanisms can take days or a lifetime to develop and activate. Innate responses are considered less specific than adaptive responses because cells of the innate immune system employ similar defense mechanisms regardless of the particular nature of a virus or bacteria. While toll-like receptors help identify specific motifs found in pathogens, their activation follows predictable signaling pathways and elicits similar defense mechanisms. In the case of bacterial infections, TLR activation leads to transcription of NF-kB, which in turn results in production of pro-inflammatory cytokines and chemokines that coordinate a more tissue-specific set of events. These responses lead to the recruitment and increased production of polymorphonuclear leukocytes (PMN) to the site of infection. PMN function as a legion to launch a variety of antimicrobial functions, such as degranulation, ROS production, migration, phagocytosis, and NETosis. Furthermore, in an infected wound the total numbers and phenotypes of PMN are tuned to the nature of the insult, maximally enhancing the host's immune response against infections.

While antibiotics can be effective at eradicating infections, their ability to do so has diminished over time. This is because bacteria can evolve and develop mechanisms that evade the effects of antibiotics. In addition, the number of newly developed antibiotics has stalled over the past few decades due to economic and regulatory obstacles. As a result, multi-drug resistant bacterial strains are on the rise worldwide, which has resulted in increased hospitalizations and deaths. Two abundant causes of disease are infections caused by *S. aureus* and *P. aeruginosa*. Given the rise of antibiotic resistant infections caused by these strains, it is imperative to develop alternative approaches to antibiotics with which to combat infections with these bacteria. One approach is to enhance a host's innate immune system to combat bacteria by augmenting the numbers and antibacterial capacity of PMN.

This dissertation presents three strategies to enhance the immune response against infection. The first makes use of the antibacterial peptide RP557 demonstrating enhanced killing of *S. aureus* in diabetic mouse wounds. In addition, RP557 demonstrated synergistic antibacterial capacity *in vitro* by boosting

the activation of human PMNs. Future studies will explore the signaling pathways that govern this interaction and determine whether RP557 is effective at killing muti-pathogen virulent infections. The second strategy makes use of bone-marrow-like 3D structures designed to enhance myeloid progenitor differentiation and expansion of PMN with enhanced antibacterial function. Future studies will explore whether implantation of HSPCs within gelatin constructs can produce local PMN expansion on demand to enhance pathogen clearance from healthy and immunodeficient hosts. The third strategy aims to increase our understanding of TLR and inflammasome signaling during the innate immune response to gram negative bacteria. For that, a mouse model of *P. aeruginosa* infection was employed, uncovering the significance of early MyD88 inflammasome signaling in the PMN responses to infected wounds. MyD88 is shown to be critical in controlling pathogen growth and dissemination through enhancing an array of antibacterial functions in PMN. MyD88-/- PMN are deficient in NET formation, phagocytosis, migratory capacity and pyroptosis. They underwent rapid cell death in the presence of *P. aeruginosa*, a phenotype that was MyD88-dependent. MyD88 was shown to be critical also for PMN to demonstrate appropriate responses, such as swarming, a response necessary to contain the pathogen to the site of initial infection. Future studies will look at the direct link between capase-1 and caspase-11 in addition to Gasdermin-D specifically in PMN deficient in MyD88 combating *P. aeruginosa*.

REFERENCES

1. Taylor TA, Unakal CG. Staphylococcus aureus Infection. In: *StatPearls*. Treasure Island (FL): StatPearls Publishing; July 17, 2023.
2. Turner NA, Sharma-Kuinkel BK, Maskarinec SA, et al. Methicillin-resistant Staphylococcus aureus: an overview of basic and clinical research. *Nat Rev Microbiol*. 2019;17(4):203-218. doi:10.1038/s41579-018-0147-4
3. Pollitt EJG, Szkuta PT, Burns N, Foster SJ. Staphylococcus aureus infection dynamics. *PLoS Pathog*. 2018;14(6):e1007112. Published 2018 Jun 14. doi:10.1371/journal.ppat.1007112
4. David MZ, Daum RS. Treatment of Staphylococcus aureus Infections. *Curr Top Microbiol Immunol*. 2017;409:325-383. doi:10.1007/82_2017_42
5. Dayan GH, Mohamed N, Scully IL, et al. Staphylococcus aureus: the current state of disease, pathophysiology and strategies for prevention. *Expert Rev Vaccines*. 2016;15(11):1373-1392. doi:10.1080/14760584.2016.1179583
6. Tong SY, Davis JS, Eichenberger E, Holland TL, Fowler VG Jr. Staphylococcus aureus infections: epidemiology, pathophysiology, clinical manifestations, and management. *Clin Microbiol Rev*. 2015;28(3):603-661. doi:10.1128/CMR.00134-14
7. Wilson MG, Pandey S. Pseudomonas aeruginosa. In: *StatPearls*. Treasure Island (FL): StatPearls Publishing; August 8, 2023.
8. Qin S, Xiao W, Zhou C, et al. Pseudomonas aeruginosa: pathogenesis, virulence factors, antibiotic resistance, interaction with host, technology advances and emerging therapeutics. *Signal Transduct Target Ther*. 2022;7(1):199. Published 2022 Jun 25. doi:10.1038/s41392-022-01056-1
9. Reynolds D, Kollef M. The Epidemiology and Pathogenesis and Treatment of Pseudomonas aeruginosa Infections: An Update. *Drugs*. 2021;81(18):2117-2131. doi:10.1007/s40265-021-01635-6
10. Driscoll JA, Brody SL, Kollef MH. The epidemiology, pathogenesis and treatment of Pseudomonas aeruginosa infections. *Drugs*. 2007;67(3):351-368. doi:10.2165/00003495-200767030-00003
11. Bassetti M, Vena A, Croxatto A, Righi E, Guery B. How to manage *Pseudomonas aeruginosa* infections. *Drugs Context*. 2018;7:212527. Published 2018 May 29. doi:10.7573/dic.212527
12. Centers for Disease Control and Prevention. Deadly Staph Infections Still Threaten the U.S. Published March 5, 2019. Accessed March 2020. https://www.cdc.gov/media/releases/2019/p0305-deadly-staph-infections.html
13. Centers for Disease Control and Prevention. Pseudomonas aeruginosa in Healthcare Settings. Published 2019. Accessed March 2020. https://www.cdc.gov/hai/organisms/pseudomonas.html

14. Deusenbery C, Wang Y, Shukla A. Recent Innovations in Bacterial Infection Detection and Treatment. *ACS Infect Dis*. 2021;7(4):695-720. doi:10.1021/acsinfecdis.0c00890
15. Abushaheen MA, Muzaheed, Fatani AJ, et al. Antimicrobial resistance, mechanisms and its clinical significance. *Dis Mon*. 2020;66(6):100971. doi:10.1016/j.disamonth.2020.100971
16. Darby EM, Trampari E, Siasat P, et al. Molecular mechanisms of antibiotic resistance revisited [published correction appears in Nat Rev Microbiol. 2024 Feb 2;:]. *Nat Rev Microbiol*. 2023;21(5):280-295. doi:10.1038/s41579-022-00820-y
17. Hutchings MI, Truman AW, Wilkinson B. Antibiotics: past, present and future. *Curr Opin Microbiol*. 2019;51:72-80. doi:10.1016/j.mib.2019.10.008
18. Thompson T. The staggering death toll of drug-resistant bacteria. *Nature*. Published online January 31, 2022. doi:10.1038/d41586-022-00228-x
19. National Center for Emerging and Zoonotic Infectious Diseases (U.S.). Division of Healthcare Quality Promotion. COVID-19: U.S. Impact on Antimicrobial Resistance, Special Report 2022. CDC; 2022. Accessed March 9, 2023. https://dx.doi.org/10.15620/cdc:117915
20. Levin PA, Angert ER. Small but Mighty: Cell Size and Bacteria. *Cold Spring Harb Perspect Biol*. 2015;7(7):a019216. Published 2015 Jun 8. doi:10.1101/cshperspect.a019216
21. Chow J, Lee SM, Shen Y, Khosravi A, Mazmanian SK. Host-bacterial symbiosis in health and disease. *Adv Immunol*. 2010;107:243-274. doi:10.1016/B978-0-12-381300-8.00008-3
22. Davis CP. Normal Flora. In: Baron S, ed. *Medical Microbiology*. 4th ed. Galveston (TX): University of Texas Medical Branch at Galveston; 1996.
23. Steinert M, Hentschel U, Hacker J. Symbiosis and pathogenesis: evolution of the microbe-host interaction. *Naturwissenschaften*. 2000;87(1):1-11. doi:10.1007/s001140050001
24. Grubbs H, Kahwaji CI. Physiology, Active Immunity. In: *StatPearls*. Treasure Island (FL): StatPearls Publishing; August 14, 2023.
25. Medina KL. Overview of the immune system. *Handb Clin Neurol*. 2016;133:61-76. doi:10.1016/B978-0-444-63432-0.00004-9
26. Salmon JK, Armstrong CA, Ansel JC. The skin as an immune organ. *West J Med*. 1994;160(2):146-152.
27. Krishna S, Miller LS. Innate and adaptive immune responses against Staphylococcus aureus skin infections. *Semin Immunopathol*. 2012;34(2):261-280. doi:10.1007/s00281-011-0292-6
28. Lanier LL, Sun JC. Do the terms innate and adaptive immunity create conceptual barriers?. *Nat Rev Immunol*. 2009;9(5):302-303. doi:10.1038/nri2547
29. Zindel J, Kubes P. DAMPs, PAMPs, and LAMPs in Immunity and Sterile Inflammation. *Annu Rev Pathol*. 2020;15:493-518. doi:10.1146/annurev-pathmechdis-012419-032847
30. Dempsey PW, Vaidya SA, Cheng G. The art of war: Innate and adaptive immune responses. *Cell Mol Life Sci*. 2003;60(12):2604-2621. doi:10.1007/s00018-003-3180-y

31. Pietrocola G, Arciola CR, Rindi S, et al. Toll-like receptors (TLRs) in innate immune defense against Staphylococcus aureus. *Int J Artif Organs*. 2011;34(9):799-810. doi:10.5301/ijao.5000030
32. Askarian F, Wagner T, Johannessen M, Nizet V. Staphylococcus aureus modulation of innate immune responses through Toll-like (TLR), (NOD)-like (NLR) and C-type lectin (CLR) receptors. *FEMS Microbiol Rev*. 2018;42(5):656-671. doi:10.1093/femsre/fuy025
33. Askarian F, Wagner T, Johannessen M, Nizet V. Staphylococcus aureus modulation of innate immune responses through Toll-like (TLR), (NOD)-like (NLR) and C-type lectin (CLR) receptors. *FEMS Microbiol Rev*. 2018;42(5):656-671. doi:10.1093/femsre/fuy025
34. McIsaac SM, Stadnyk AW, Lin TJ. Toll-like receptors in the host defense against Pseudomonas aeruginosa respiratory infection and cystic fibrosis. *J Leukoc Biol*. 2012;92(5):977-985. doi:10.1189/jlb.0811410
35. Moser C, Jensen PØ, Thomsen K, et al. Immune Responses to *Pseudomonas aeruginosa* Biofilm Infections. *Front Immunol*. 2021;12:625597. Published 2021 Feb 22. doi:10.3389/fimmu.2021.625597
36. Fitzgerald KA, Kagan JC. Toll-like Receptors and the Control of Immunity. *Cell*. 2020;180(6):1044-1066. doi:10.1016/j.cell.2020.02.041
37. Satake H, Sasaki N. Comparative overview of toll-like receptors in lower animals. *Zoolog Sci*. 2010;27(2):154-161. doi:10.2108/zsj.27.154
38. Nie L, Cai SY, Shao JZ, Chen J. Toll-Like Receptors, Associated Biological Roles, and Signaling Networks in Non-Mammals. *Front Immunol*. 2018;9:1523. Published 2018 Jul 2. doi:10.3389/fimmu.2018.01523
39. Deguine J, Barton GM. MyD88: a central player in innate immune signaling. *F1000Prime Rep*. 2014;6:97. Published 2014 Nov 4. doi:10.12703/P6-97
40. Janssens S, Beyaert R. A universal role for MyD88 in TLR/IL-1R-mediated signaling. *Trends Biochem Sci*. 2002;27(9):474-482. doi:10.1016/s0968-0004(02)02145-x
41. Duan T, Du Y, Xing C, Wang HY, Wang RF. Toll-Like Receptor Signaling and Its Role in Cell-Mediated Immunity. *Front Immunol.* 2022;13:812774. doi:10.3389/fimmu.2022.812774
42. Yamamoto M, Sato S, Hemmi H, Hoshino K, Kaisho T, Sanjo H, Takeuchi O, Sugiyama M, Okabe M, Takeda K, Akira S. Role of adaptor TRIF in the MyD88-independent toll-like receptor signaling pathway. *Science.* 2003;301(5633):640–643. doi:10.1126/science.1087262
43. Takeda K, Akira S. TLR signaling pathways. *Semin Immunol.* 2004;16(1):3–9. doi:10.1016/j.smim.2003.10.003
44. Takeda K, Akira S. Microbial recognition by Toll-like receptors. *J Dermatol Sci.* 2004;34(2):73–82. doi:10.1016/j.jdermsci.2003.10.002
45. Takeda K, Akira S. Toll-like receptors in innate immunity. *Int Immunol.* 2005;17(1):1–14. doi:10.1093/intimm/dxh186
46. Takeda K, Akira S. Toll-like receptors. *Curr Protoc Immunol.* 2015;109:14.12.1–14.12.10. doi:10.1002/0471142735.im1412s109

47. Brikos C, O'Neill LA. Signalling of toll-like receptors. *Handb Exp Pharmacol.* 2008;(183):21–50. doi:10.1007/978-3-540-72167-3_2

48. Narayanan KB, Park HH. Toll/interleukin-1 receptor (TIR) domain-mediated cellular signaling pathways. *Apoptosis.* 2015;20(2):196–209. doi:10.1007/s10495-014-1073-1

49. Watters TM, Kenny EF, O'Neill LA. Structure, function and regulation of the Toll/IL-1 receptor adaptor proteins. *Immunol Cell Biol.* 2007;85(6):411–419. doi:10.1038/sj.icb.7100095

50. Park BS, Song DH, Kim HM, Choi BS, Lee H, Lee JO. The structural basis of lipopolysaccharide recognition by the TLR4-MD-2 complex. *Nature.* 2009;458(7242):1191–1195. doi:10.1038/nature07830

51. Sakai J, Cammarota E, Wright JA, Cicuta P, Gottschalk RA, Li N, Fraser IDC, Bryant CE. Lipopolysaccharide-induced NF-κB nuclear translocation is primarily dependent on MyD88, but TNFα expression requires TRIF and MyD88. *Sci Rep.* 2017;7(1):1428. doi:10.1038/s41598-017-01600-y

52. Kawai T, Akira S. Signaling to NF-kappaB by Toll-like receptors. *Trends Mol Med.* 2007;13(11):460–469. doi:10.1016/j.molmed.2007.09.002

53. Ciesielska A, Matyjek M, Kwiatkowska K. TLR4 and CD14 trafficking and its influence on LPS-induced pro-inflammatory signaling. *Cell Mol Life Sci.* 2021;78(4):1233–1261. doi:10.1007/s00018-020-03656-y

54. Piao W, Ru LW, Piepenbrink KH, Sundberg EJ, Vogel SN, Toshchakov VY. Recruitment of TLR adapter TRIF to TLR4 signaling complex is mediated by the second helical region of TRIF TIR domain. *Proc Natl Acad Sci USA.* 2013;110(47):19036–19041. doi:10.1073/pnas.1313575110

55. Kuzmich NN, Sivak KV, Chubarev VN, Porozov YB, Savateeva-Lyubimova TN, Peri F. TLR4 Signaling Pathway Modulators as Potential Therapeutics in Inflammation and Sepsis. *Vaccines.* 2017;5(4):34. doi:10.3390/vaccines5040034

56. Li X, Qin J. Modulation of Toll-interleukin 1 receptor mediated signaling. *J Mol Med (Berl).* 2005;83(4):258–266. doi:10.1007/s00109-004-0622-4

57. Zeytun A, Chaudhary A, Pardington P, Cary R, Gupta G. Induction of cytokines and chemokines by Toll-like receptor signaling: strategies for control of inflammation. *Crit Rev Immunol.* 2010;30(1):53–67. doi:10.1615/critrevimmunol.v30.i1.40

58. Beran O, Potměšil R, Holub M. Differences in Toll-like receptor expression and cytokine production after stimulation with heat-killed gram-positive and gram-negative bacteria. *Folia Microbiol (Praha).* 2011;56(2):138–142. doi:10.1007/s12223-011-0001-9

59. Prince LR, Whyte MK, Sabroe I, Parker LC. The role of TLRs in neutrophil activation. *Curr Opin Pharmacol.* 2011;11(4):397–403. doi:10.1016/j.coph.2011.06.007

60. Futosi K, Fodor S, Mócsai A. Neutrophil cell surface receptors and their intracellular signal transduction pathways. *Int Immunopharmacol.* 2013;17(3):638–650. https://doi.org/10.1016/j.intimp.2013.06.034

61. Sawyer DW, Donowitz GR, Mandell GL. Polymorphonuclear neutrophils: an effective antimicrobial force. Rev Infect Dis. 1989;11 Suppl 7:S1532-S1544. doi:10.1093/clinids/11.supplement_7.s1532

62. Németh T, Sperandio M, MV≥csai A. Neutrophils as emerging therapeutic targets. Nat Rev Drug Discov. 2020;19(4):253-275. doi:10.1038/s41573-019-0054-z

63. Rosales C. Neutrophil: A Cell with Many Roles in Inflammation or Several Cell Types?. *Front Physiol*. 2018;9:113. Published 2018 Feb 20. doi:10.3389/fphys.2018.00113

64. Panopoulos AD, Watowich SS. Granulocyte colony-stimulating factor: molecular mechanisms of action during steady state and 'emergency' hematopoiesis. *Cytokine.* 2008;42(3):277–288. doi:10.1016/j.cyto.2008.03.002

65. McCracken JM, Allen LA. Regulation of human neutrophil apoptosis and lifespan in health and disease. *J Cell Death.* 2014;7:15–23. doi:10.4137/JCD.S11038

66. Kobayashi SD, DeLeo FR. Role of neutrophils in innate immunity: a systems biology-level approach. *Wiley Interdiscip Rev Syst Biol Med.* 2009;1(3):309–333. doi:10.1002/wsbm.32

67. Witter AR, Okunnu BM, Berg RE. The Essential Role of Neutrophils during Infection with the Intracellular Bacterial Pathogen Listeria monocytogenes. *J Immunol.* 2016;197(5):1557–1565. doi:10.4049/jimmunol.1600599

68. Zeya HI, Spitznagel JK. Cationic proteins of polymorphonuclear leukocyte lysosomes. II. Composition, properties, and mechanism of antibacterial action. *J Bacteriol*. 1966;91(2):755-762. doi:10.1128/jb.91.2.755-762.1966

69. Kraus RF, Gruber MA. Neutrophils-From Bone Marrow to First-Line Defense of the Innate Immune System. *Front Immunol.* 2021;12:767175. doi:10.3389/fimmu.2021.767175

70. de Oliveira S, Rosowski EE, Huttenlocher A. Neutrophil migration in infection and wound repair: going forward in reverse. *Nat Rev Immunol.* 2016;16(6):378–391. doi:10.1038/nri.2016.49

71. Pérez-Figueroa E, Álvarez-Carrasco P, Ortega E, Maldonado-Bernal C. Neutrophils: Many Ways to Die. *Front Immunol.* 2021;12:631821. doi:10.3389/fimmu.2021.631821

72. Cappenberg A, Margraf A, Thomas K, Bardel B, McCreedy DA, Van Marck V, Mellmann A, Lowell CA, Zarbock A. L-selectin shedding affects bacterial clearance in the lung: a new regulatory pathway for integrin outside-in signaling. *Blood.* 2019;134(17):1445–1457. doi:10.1182/blood.2019000685

73. Ivetic A. A head-to-tail view of L-selectin and its impact on neutrophil behaviour. *Cell Tissue Res.* 2018;371(3):437–453. doi:10.1007/s00441-017-2774-x

74. Rahman I, Collado Sánchez A, Davies J, et al. L-selectin regulates human neutrophil transendothelial migration. *J Cell Sci.* 2021;134(3):jcs250340. doi:10.1242/jcs.250340

75. Borjesson DL, Simon SI, Hodzic E, Ballantyne CM, Barthold SW. Kinetics of CD11b/CD18 up-regulation during infection with the agent of human granulocytic ehrlichiosis in mice. *Lab Invest.* 2002;82(3):303–311. doi:10.1038/labinvest.3780424

76. Latger-Cannard V, Besson I, Doco-Lecompte T, Lecompte T. A standardized procedure for quantitation of CD11b on polymorphonuclear neutrophil by flow cytometry: potential application in infectious diseases. *Clin Lab Haematol.* 2004;26(3):177–186. doi:10.1111/j.1365-2257.2004.00599.x

77. Weirich E, Rabin RL, Maldonado Y, et al. Neutrophil CD11b expression as a diagnostic marker for early-onset neonatal infection. *J Pediatr.* 1998;132(3 Pt 1):445–451. doi:10.1016/s0022-3476(98)70018-6

78. Kobayashi SD, Malachowa N, DeLeo FR. Neutrophils and Bacterial Immune Evasion. *J Innate Immun.* 2018;10(5-6):432–441. doi:10.1159/000487756

79. Foster TJ. Immune evasion by staphylococci. *Nat Rev Microbiol.* 2005;3(12):948–958. doi:10.1038/nrmicro1289

80. de Vor L, Rooijakkers SHM, van Strijp JAG. Staphylococci evade the innate immune response by disarming neutrophils and forming biofilms. *FEBS Lett.* 2020;594(16):2556–2569. doi:10.1002/1873-3468.13767

81. Thay B, Wai SN, Oscarsson J. Staphylococcus aureus α-toxin-dependent induction of host cell death by membrane-derived vesicles. *PLoS One.* 2013;8(1):e54661. doi:10.1371/journal.pone.0054661

82. Ortines RV, Liu H, Cheng LI, et al. Neutralizing Alpha-Toxin Accelerates Healing of Staphylococcus aureus-Infected Wounds in Nondiabetic and Diabetic Mice. *Antimicrob Agents Chemother.* 2018;62(3):e02288-17. doi:10.1128/AAC.02288-17

83. Yipp BG, Petri B, Salina D, et al. Infection-induced NETosis is a dynamic process involving neutrophil multitasking in vivo. *Nat Med.* 2012;18(9):1386–1393. doi:10.1038/nm.2847

84. Yipp BG, Kubes P. NETosis: how vital is it?. *Blood.* 2013;122(16):2784–2794. doi:10.1182/blood-2013-04-457671

85. Papayannopoulos V. Neutrophil extracellular traps in immunity and disease. *Nat Rev Immunol.* 2018;18(2):134–147. doi:10.1038/nri.2017.105

86. Kaplan MJ, Radic M. Neutrophil extracellular traps: double-edged swords of innate immunity. *J Immunol.* 2012;189(6):2689–2695. doi:10.4049/jimmunol.1201719

87. Thanabalasuriar A, Scott BNV, Peiseler M, et al. Neutrophil Extracellular Traps Confine Pseudomonas aeruginosa Ocular Biofilms and Restrict Brain Invasion. *Cell Host Microbe.* 2019;25(4):526–536.e4. doi:10.1016/j.chom.2019.02.007

88. Skopelja-Gardner S, Theprungsirikul J, Lewis KA, et al. Regulation of Pseudomonas aeruginosa-Mediated Neutrophil Extracellular Traps. *Front Immunol.* 2019;10:1670. doi:10.3389/fimmu.2019.01670

89. Pieterse E, Rother N, Yanginlar C, Hilbrands LB, van der Vlag J. Neutrophils Discriminate between Lipopolysaccharides of Different Bacterial Sources and Selectively Release Neutrophil Extracellular Traps. *Front Immunol.* 2016;7:484. doi:10.3389/fimmu.2016.00484

90. Kim MH, Granick JL, Kwok C, et al. Neutrophil survival and c-kit(+)-progenitor proliferation in Staphylococcus aureus-infected skin wounds promote resolution. *Blood*. 2011;117(12):3343-3352. doi:10.1182/blood-2010-07-296970

91. Kim MH, Liu W, Borjesson DL, et al. Dynamics of neutrophil infiltration during cutaneous wound healing and infection using fluorescence imaging. *J Invest Dermatol*. 2008;128(7):1812-1820. doi:10.1038/sj.jid.5701223

92. Anderson LS, Reynolds MB, Rivara KR, Miller LS, Simon SI. A Mouse Model to Assess Innate Immune Response to Staphylococcus aureus Infection. *J Vis Exp*. 2019;(144):10.3791/59015. Published 2019 Feb 28. doi:10.3791/59015

93. Granick JL, Falahee PC, Dahmubed D, Borjesson DL, Miller LS, Simon SI. Staphylococcus aureus recognition by hematopoietic stem and progenitor cells via TLR2/MyD88/PGE2 stimulates granulopoiesis in wounds. *Blood*. 2013;122(10):1770-1778. doi:10.1182/blood-2012-11-466268

94. Falahee PC, Anderson LS, Reynolds MB, et al. α-Toxin Regulates Local Granulocyte Expansion from Hematopoietic Stem and Progenitor Cells in *Staphylococcus aureus*-Infected Wounds. *J Immunol*. 2017;199(5):1772-1782. doi:10.4049/jimmunol.1700649

95. Cho JS, Guo Y, Ramos RI, et al. Neutrophil-derived IL-1β is sufficient for abscess formation in immunity against Staphylococcus aureus in mice. *PLoS Pathog*. 2012;8(11):e1003047. doi:10.1371/journal.ppat.1003047

96. Karmakar M, Sun Y, Hise AG, Rietsch A, Pearlman E. Cutting edge: IL-1β processing during Pseudomonas aeruginosa infection is mediated by neutrophil serine proteases and is independent of NLRC4 and caspase-1. J Immunol. 2012;189(9):4231-4235. doi:10.4049/jimmunol.1201447

97. Miller LS, Cho JS. Immunity against Staphylococcus aureus cutaneous infections. *Nat Rev Immunol*. 2011;11(8):505-518. Published 2011 Jul 1. doi:10.1038/nri3010

98. Kinra M, Nampoothiri M, Arora D, Mudgal J. Reviewing the importance of TLR-NLRP3-pyroptosis pathway and mechanism of experimental NLRP3 inflammasome inhibitors. *Scand J Immunol*. 2022;95(2):e13124. doi:10.1111/sji.13124

99. Yazdi AS, Ghoreschi K. The Interleukin-1 Family. *Adv Exp Med Biol*. 2016;941:21-29. doi:10.1007/978-94-024-0921-5_2

100. Anderson MJ, den Hartigh AB, Fink SL. Molecular Mechanisms of Pyroptosis. *Methods Mol Biol*. 2023;2641:1-16. doi:10.1007/978-1-0716-3040-2_1

101. Sollberger G. Approaching Neutrophil Pyroptosis. *J Mol Biol*. 2022;434(4):167335. doi:10.1016/j.jmb.2021.167335

102. Liu L, Sun B. Neutrophil pyroptosis: new perspectives on sepsis. *Cell Mol Life Sci*. 2019;76(11):2031-2042. doi:10.1007/s00018-019-03060-1

103. Chauhan D, Demon D, Vande Walle L, et al. GSDMD drives canonical inflammasome-induced neutrophil pyroptosis and is dispensable for NETosis. *EMBO Rep*. 2022;23(10):e54277. doi:10.15252/embr.202154277

104. Spel L, Martinon F. Gasdermin D opens the way for NETs. *Nat Rev Rheumatol*. 2018;14(12):690-692. doi:10.1038/s41584-018-0124-3

105. Zheng F, Ma L, Li X, et al. Neutrophil Extracellular Traps Induce Glomerular Endothelial Cell Dysfunction and Pyroptosis in Diabetic Kidney Disease. *Diabetes*. 2022;71(12):2739-2750. doi:10.2337/db22-0153

106. Li P, Li M, Lindberg MR, Kennett MJ, Xiong N, Wang Y. PAD4 is essential for antibacterial innate immunity mediated by neutrophil extracellular traps. J Exp Med. 2010;207(9):1853-1862. doi:10.1084/jem.20100239

107. Rohrbach AS, Slade DJ, Thompson PR, Mowen KA. Activation of PAD4 in NET formation. Front Immunol. 2012;3:360. Published 2012 Nov 29. doi:10.3389/fimmu.2012.00360

108. Shao S, Fang H, Dang E, et al. Neutrophil Extracellular Traps Promote Inflammatory Responses in Psoriasis via Activating Epidermal TLR4/IL-36R Crosstalk. Front Immunol. 2019;10:746. Published 2019 Apr 5. doi:10.3389/fimmu.2019.00746

109. Plaut RD, Mocca CP, Prabhakara R, Merkel TJ, Stibitz S. Stably luminescent Staphylococcus aureus clinical strains for use in bioluminescent imaging. *PLoS One*. 2013;8(3):e59232. doi:10.1371/journal.pone.0059232

110. Schmidtchen A, Puthia M. Rapid *in vitro* and *in vivo* Evaluation of Antimicrobial Formulations Using Bioluminescent Pathogenic Bacteria. *Bio Protoc*. 2022;12(2):e4302. Published 2022 Jan 20. doi:10.21769/BioProtoc.4302

111. Berlanga-Acosta JA, Guillén-Nieto GE, Rodríguez-Rodríguez N, et al. Cellular Senescence as the Pathogenic Hub of Diabetes-Related Wound Chronicity. *Front Endocrinol (Lausanne)*. 2020;11:573032. Published 2020 Sep 16. doi:10.3389/fendo.2020.573032

112. Rodríguez-Rodríguez N, Martínez-Jiménez I, García-Ojalvo A, et al. Wound Chronicity, Impaired Immunity and Infection in Diabetic Patients. *MEDICC Rev*. 2021;24(1):44-58. Published 2021 Sep 17. doi:10.37757/MR2021.V23.N3.8

113. Graves DT, Kayal RA. Diabetic complications and dysregulated innate immunity. *Front Biosci*. 2008;13:1227-1239. doi:10.2741/2757.

114. Tsalamandris S, Antonopoulos AS, Oikonomou E, Papamikroulis GA, Vogiatzi G, Papaioannou S, Tousoulis D. The Role of Inflammation in Diabetes: Current Concepts and Future Perspectives. *Eur Cardiol*. 2019;14:50-59. doi:10.15420/ecr.2018.33.1.

115. Trostrup H, Laulund ASB, Moser C. Insights into Host-Pathogen Interactions in Biofilm-Infected Wounds Reveal Possibilities for New Treatment Strategies. *Antibiotics*. 2020;9:396. doi:10.3390/antibiotics9070396.

116. Ozturk AM, Tasbakan M, Metin DY, et al. A neglected causative agent in diabetic foot infection: A retrospective evaluation of 13 patients with fungal etiology. *Turk J Med Sci*. 2019;49:81-86. doi:10.3906/sag-1809-74.

117. Lin CW, Armstrong DG, Lin CH, et al. Nationwide trends in the epidemiology of diabetic foot complications and lower-extremity amputation over an 8-year period. *BMJ Open Diabetes Res Care*. 2019;7:e000795. doi:10.1136/bmjdrc-2019-000795.

118. Armstrong DG, Galiano RD, Orgill DP, et al. Multi-centre prospective randomised controlled clinical trial to evaluate a bioactive split thickness skin allograft vs standard of care in the treatment of diabetic foot ulcers. *Int Wound J.* 2022;19:932-944. doi:10.1111/iwj.13759.

119. Atashgah RB, Ghasemi A, Raoufi M, et al. Restoring Endogenous Repair Mechanisms to Heal Chronic Wounds with a Multifunctional Wound Dressing. *Mol Pharm*. 2021;18:3171-3180. doi:10.1021/acs.molpharmaceut.1c00400.

120. Woodburn KW, Jaynes JM, Clemens LE. Evaluation of the Antimicrobial Peptide, RP557, for the Broad-Spectrum Treatment of Wound Pathogens and Biofilm. *Front Microbiol*. 2019;10:1688. doi:10.3389/fmicb.2019.01688.

121. Woodburn KW, Jaynes JM, Clemens LE. Designed Antimicrobial Peptides Against Trauma-Related Cutaneous Invasive Fungal Wound Infections. *J Fungi*. 2020;6:184. doi:10.3390/jof6030184.

122. Mangoni ML, McDermott AM, Zasloff M. Antimicrobial peptides and wound healing: Biological and therapeutic considerations. *Exp Dermatol*. 2016;25:167-173. doi:10.1111/exd.12929.

123. Zasloff M. Antimicrobial peptides in health and disease. *N Engl J Med*. 2002;347:1199-1200. doi:10.1056/NEJMe020106347/15/1199.

124. Gordon YJ, Romanowski EG, McDermott AM. A review of antimicrobial peptides and their therapeutic potential as anti-infective drugs. *Curr Eye Res*. 2005;30:505-515. doi:10.1080/02713680590968637.

125. Torres-Castro I, Arroyo-Camarena UD, Martinez-Reyes CP, et al. Human monocytes and macrophages undergo M1-type inflammatory polarization in response to high levels of glucose. *Immunol Lett*. 2016;176:81-89. doi:10.1016/j.imlet.2016.06.001.

126. Clemens LE, Jaynes J, Lim E, et al. Designed Host Defense Peptides for the treatment of Bacterial Keratitis. *Investig Opthamology Vis Sci*. 2017;58:6273-6281.

127. Woodburn KW, Clemens LE, Jaynes J, et al. Designed Antimicrobial Peptides for Recurrent Vulvovaginal Candidiasis Treatment. *Antimicrob Agents Chemother*. 2019;63:e02690-18. doi:10.1128/AAC.02690-18.

128. Clemens LE, Woodburn K, Jaynes J, et al. Evaluation of Novel Antimicrobial Peptides as Topical Anti-Infectives with Broad Spectrum Activity Against Combat-Related Bacterial and Fungal Wound Infections. *Proceedings of the Military Health Sciences Research Symposium*, Kissimmee, FL, USA, 15-18 August 2016.

129. Clemens LE, Woodburn K. Topically Applied Antimicrobial Peptides Eradicate Polymicrobial Infections in a Porcine Combat Wound Infection Model. *Proceedings of the Military Health Sciences Research Symposium*, Orlando, FL, USA, 20-23 August 2018.

130. Brinkmann V, Reichard U, Goosmann C, et al. Neutrophil extracellular traps kill bacteria. *Science.* 2004;303:1532-1535. doi:10.1126/science.1092385.

131. Kishimoto TK, Jutila MA, Butcher EC. Identification of a human peripheral lymph node homing receptor: A rapidly down-regulated adhesion molecule. *Proc Natl Acad Sci* USA. 1990;87:2244-2248. doi:10.1073/pnas.87.6.2244.

132. Chen S, Li R, Cheng C, et al. Pseudomonas aeruginosa infection alters the macrophage phenotype switching process during wound healing in diabetic mice. *Cell Biol Int.* 2018;42:877-889. doi:10.1002/cbin.10955.

133. Liu H, Duan Z, Tang J, et al. A short peptide from frog skin accelerates diabetic wound healing. *FEBS J*. 2014;281:4633-4643. doi:10.1111/febs.12968.

134. Wilkinson HN, Hardman MJ. Wound senescence: A functional link between diabetes and ageing? *Exp Dermatol.* 2021;30:68-73. doi:10.1111/exd.14082.

135. Wilkinson HN, Clowes C, Banyard KL, et al. Elevated Local Senescence in Diabetic Wound Healing Is Linked to Pathological Repair via CXCR2. *J Investig Dermatol*. 2019;139:1171-1181.e1176. doi:10.1016/j.jid.2019.01.005.

136. Deng P, Shi H, Pan X, et al. Worldwide Research Trends on Diabetic Foot Ulcers (2004-2020): Suggestions for Researchers. *J Diabetes Res.* 2022;2022:7991031. doi:10.1155/2022/7991031.

137. Alven S, Peter S, Mbese Z, Aderibigbe BA. Polymer-Based Wound Dressing Materials Loaded with Bioactive Agents: Potential Materials for the Treatment of Diabetic Wounds. *Polymers.* 2022;14:724. doi:10.3390/polym14040724.

138. Roy R, Zayas J, Singh SK, et al. Overriding impaired FPR chemotaxis signaling in diabetic neutrophil stimulates infection control in murine diabetic wound. *eLife.* 2022;11:e72071. doi:10.7554/eLife.72071.

139. Pratama V, Risni HW, Yunir E, Sauriasari R. A Systematic Review of Randomized Controlled Trials of Antibiotic Use in Diabetic Foot Ulcer Infections: Focus on Clinical Cure. *Infect Chemother*. 2022;54:125-139. doi:10.3947/ic.2021.0144.

140. Vestergaard M, Frees D, Ingmer H. Antibiotic Resistance and the MRSA Problem. *Microbiol Spectr*. 2019;7(2):10.1128/microbiolspec.GPP3-0057-2018. doi:10.1128/microbiolspec.GPP3-0057-2018

141. Mahadik BP, Bharadwaj NA, Ewoldt RH, Harley BA. Regulating dynamic signaling between hematopoietic stem cells and niche cells via a hydrogel matrix. *Biomaterials*. 2017;125:54-64. doi:10.1016/j.biomaterials.2017.02.013

142. Gilchrist AE, Lee S, Hu Y, Harley BAC. Soluble Signals and Remodeling in a Synthetic Gelatin-Based Hematopoietic Stem Cell Niche. *Adv Healthc Mater*. 2019;8(20):e1900751. doi:10.1002/adhm.201900751

143. Faust N, Varas F, Kelly LM, Heck S, Graf T. Insertion of enhanced green fluorescent protein into the lysozyme gene creates mice with green fluorescent granulocytes and macrophages. Blood. 2000;96(2):719-726.

144. Parks WC, Wilson CL, López-Boado YS. Matrix metalloproteinases as modulators of inflammation and innate immunity. *Nat Rev Immunol*. 2004;4(8):617-629. doi:10.1038/nri1418

145. Wysoczynski M, Reca R, Lee H, Wu W, Ratajczak J, Ratajczak MZ. Defective engraftment of C3aR-/- hematopoietic stem progenitor cells shows a novel role of the C3a-C3aR axis in bone marrow homing. *Leukemia*. 2009;23(8):1455-1461. doi:10.1038/leu.2009.73

146. Pluen A, Netti PA, Jain RK, Berk DA. Diffusion of macromolecules in agarose gels: comparison of linear and globular configurations. *Biophys J*. 1999;77(1):542-552. doi:10.1016/S0006-3495(99)76911-0

147. van Donkelaar CC, Chao G, Bader DL, Oomens CW. A reaction-diffusion model to predict the influence of neo-matrix on the subsequent development of tissue-engineered cartilage. *Comput Methods Biomech Biomed Engin*. 2011;14(5):425-432. doi:10.1080/10255842.2011.554409

148. Hasty KA, Hibbs MS, Kang AH, Mainardi CL. Secreted forms of human neutrophil collagenase. *J Biol Chem*. 1986;261(12):5645-5650.

149. Markart P, Korfhagen TR, Weaver TE, Akinbi HT. Mouse lysozyme M is important in pulmonary host defense against Klebsiella pneumoniae infection. *Am J Respir Crit Care Med*. 2004;169(4):454-458. doi:10.1164/rccm.200305-669OC

150. Kolaczkowska E, Kubes P. Neutrophil recruitment and function in health and inflammation. *Nat Rev Immunol*. 2013;13(3):159-175. doi:10.1038/nri3399

151. Cappenberg A, Kardell M, Zarbock A. Selectin-Mediated Signaling-Shedding Light on the Regulation of Integrin Activity in Neutrophils. *Cells*. 2022;11(8):1310. Published 2022 Apr 12. doi:10.3390/cells11081310

152. Dixit N, Simon SI. Chemokines, selectins and intracellular calcium flux: temporal and spatial cues for leukocyte arrest. *Front Immunol*. 2012;3:188. Published 2012 Jul 10. doi:10.3389/fimmu.2012.00188

153. Pineault N, Abu-Khader A. Advances in umbilical cord blood stem cell expansion and clinical translation. *Exp Hematol*. 2015;43(7):498-513. doi:10.1016/j.exphem.2015.04.011

154. Heltmann-Meyer S, Steiner D, Müller C, et al. Gelatin methacryloyl is a slow degrading material allowing vascularization and long-term use*in vivo*. *Biomed Mater*. 2021;16(6):10.1088/1748-605X/ac1e9d. Published 2021 Sep 6. doi:10.1088/1748-605X/ac1e9d

155. Sansbury BE, Spite M. Resolution of Acute Inflammation and the Role of Resolvins in Immunity, Thrombosis, and Vascular Biology. *Circ Res*. 2016;119(1):113-130. doi:10.1161/CIRCRESAHA.116.307308

156. Cirves E, Vargas A, Wheeler EE, Leach JK, Simon SI, Gonzalez-Fernandez T. Neutrophil Granulopoiesis Optimized Through Ex Vivo Expansion of Hematopoietic Progenitors in Engineered 3D Gelatin Methacrylate Hydrogels. *Adv Healthc Mater*. Published online February 12, 2024. doi:10.1002/adhm.202301966

157. Vargas A, Garcia G, Rivara K, Woodburn K, Clemens LE, Simon SI. A Designed Host Defense Peptide for the Topical Treatment of MRSA-Infected Diabetic Wounds. *Int J Mol Sci*. 2023;24(3):2143. Published 2023 Jan 21. doi:10.3390/ijms24032143

158. Rada B. Interactions between Neutrophils and Pseudomonas aeruginosa in Cystic Fibrosis. Pathogens. 2017;6(1):10. Published 2017 Mar 9. doi:10.3390/pathogens6010010

159. Pachori P, Gothalwal R, Gandhi P. Emergence of antibiotic resistance Pseudomonas aeruginosa in intensive care unit; a critical review. Genes Dis. 2019;6(2):109-119. Published 2019 Apr 17. doi:10.1016/j.gendis.2019.04.001

160. Ruffin M, Brochiero E. Repair Process Impairment by Pseudomonas aeruginosa in Epithelial Tissues: Major Features and Potential Therapeutic Avenues. Front Cell Infect Microbiol. 2019;9:182. Published 2019 May 31. doi:10.3389/fcimb.2019.00182

161. Arora SK, Neely AN, Blair B, Lory S, Ramphal R. Role of motility and flagellin glycosylation in the pathogenesis of Pseudomonas aeruginosa burn wound infections. Infect Immun. 2005;73(7):4395-4398. doi:10.1128/IAI.73.7.4395-4398.2005

162. Declercq J, De Leeuw E, Lambrecht BN. Inflammasomes and IL-1 family cytokines in SARS-CoV-2 infection: from prognostic marker to therapeutic agent. *Cytokine*. 2022;157:155934. doi:10.1016/j.cyto.2022.155934

163. Banerjee SK, Chatterjee A, Gupta S, Nagar A. Activation and Regulation of NLRP3 by Sterile and Infectious Insults. *Front Immunol*. 2022;13:896353. Published 2022 May 12. doi:10.3389/fimmu.2022.896353

164. van Loo G, Bertrand MJM. Death by TNF: a road to inflammation. *Nat Rev Immunol*. 2023;23(5):289-303. doi:10.1038/s41577-022-00792-3

165. Horna G, Ruiz J. Type 3 secretion system of Pseudomonas aeruginosa. *Microbiol Res*. 2021;246:126719. doi:10.1016/j.micres.2021.126719

166. Selim H, Radwan TEE, Reyad AM. Regulation of T3SS synthesis, assembly and secretion in Pseudomonas aeruginosa. *Arch Microbiol*. 2022;204(8):468. Published 2022 Jul 10. doi:10.1007/s00203-022-03068-5

167. Minns MS, Liboro K, Lima TS, et al. NLRP3 selectively drives IL-1β secretion by Pseudomonas aeruginosa infected neutrophils and regulates corneal disease severity. *Nat Commun*. 2023;14(1):5832. Published 2023 Sep 20. doi:10.1038/s41467-023-41391-7

168. Goldufsky J, Wood SJ, Jayaraman V, et al. Pseudomonas aeruginosa uses T3SS to inhibit diabetic wound healing. *Wound Repair Regen*. 2015;23(4):557-564. doi:10.1111/wrr.12310

169. Grandjean T, Boucher A, Thepaut M, et al. The human NAIP-NLRC4-inflammasome senses the Pseudomonas aeruginosa T3SS inner-rod protein. *Int Immunol*. 2017;29(8):377-384. doi:10.1093/intimm/dxx047

170. O'Toole GA. Microtiter dish biofilm formation assay. *J Vis Exp*. 2011;(47):2437. Published 2011 Jan 30. doi:10.3791/2437

171. Prince A. Adhesins and receptors of Pseudomonas aeruginosa associated with infection of the respiratory tract. *Microb Pathog*. 1992;13(4):251-260. doi:10.1016/0882-4010(92)90035-m

172. Arora SK, Ritchings BW, Almira EC, Lory S, Ramphal R. Cloning and characterization of Pseudomonas aeruginosa fliF, necessary for flagellar assembly and bacterial adherence to mucin. *Infect Immun*. 1996;64(6):2130-2136. doi:10.1128/iai.64.6.2130-2136.1996

173. Tan RM, Kuang Z, Hao Y, Lau GW. Type IV pilus of Pseudomonas aeruginosa confers resistance to antimicrobial activities of the pulmonary surfactant protein-A. *J Innate Immun*. 2014;6(2):227-239. doi:10.1159/000354304

174. Lee EJ, Cowell BA, Evans DJ, Fleiszig SM. Contribution of ExsA-regulated factors to corneal infection by cytotoxic and invasive Pseudomonas aeruginosa in a murine scarification model. *Invest Ophthalmol Vis Sci*. 2003;44(9):3892-3898. doi:10.1167/iovs.02-1302

175. Kumar NG, Nieto V, Kroken AR, et al. Pseudomonas aeruginosa Can Diversify after Host Cell Invasion to Establish Multiple Intracellular Niches. *mBio*. 2022;13(6):e0274222. doi:10.1128/mbio.02742-22

176. Sullivan AB, Tam KP, Metruccio MM, Evans DJ, Fleiszig SM. The importance of the Pseudomonas aeruginosa type III secretion system in epithelium traversal depends upon conditions of host susceptibility. *Infect Immun*. 2015;83(4):1629-1640. doi:10.1128/IAI.02329-14

177. Arora SK, Ritchings BW, Almira EC, Lory S, Ramphal R. Cloning and characterization of Pseudomonas aeruginosa fliF, necessary for flagellar assembly and bacterial adherence to mucin. *Infect Immun*. 1996;64(6):2130-2136. doi:10.1128/iai.64.6.2130-2136.1996

178. Boll JM, Hendrixson DR. A regulatory checkpoint during flagellar biogenesis in Campylobacter jejuni initiates signal transduction to activate transcription of flagellar genes. *mBio*. 2013;4(5):e00432-13. Published 2013 Sep 3. doi:10.1128/mBio.00432-13

179. Goodier RI, Ahmer BM. SirA orthologs affect both motility and virulence. *J Bacteriol*. 2001;183(7):2249-2258. doi:10.1128/JB.183.7.2249-2258.2001

180. Köhler T, Curty LK, Barja F, van Delden C, Pechère JC. Swarming of Pseudomonas aeruginosa is dependent on cell-to-cell signaling and requires flagella and pili. *J Bacteriol*. 2000;182(21):5990-5996. doi:10.1128/JB.182.21.5990-5996.2000

181. Brown L, Yipp BG. Neutrophil swarming: Is a good offense the best defense?. *iScience*. 2023;26(9):107655. Published 2023 Aug 17. doi:10.1016/j.isci.2023.107655

182. Song Z, Bhattacharya S, Clemens RA, Dinauer MC. Molecular regulation of neutrophil swarming in health and disease: Lessons from the phagocyte oxidase. *iScience*. 2023;26(10):108034. Published 2023 Sep 26. doi:10.1016/j.isci.2023.108034

183. Poplimont H, Georgantzoglou A, Boulch M, et al. Neutrophil Swarming in Damaged Tissue Is Orchestrated by Connexins and Cooperative Calcium Alarm Signals. *Curr Biol*. 2020;30(14):2761-2776.e7. doi:10.1016/j.cub.2020.05.030

184. Lämmermann T, Afonso PV, Angermann BR, et al. Neutrophil swarms require LTB4 and integrins at sites of cell death in vivo. *Nature*. 2013;498(7454):371-375. doi:10.1038/nature12175

185. Kienle K, Glaser KM, Eickhoff S, et al. Neutrophils self-limit swarming to contain bacterial growth in vivo. *Science*. 2021;372(6548):eabe7729. doi:10.1126/science.abe7729

186. El-Benna J, Hurtado-Nedelec M, Marzaioli V, Marie JC, Gougerot-Pocidalo MA, Dang PM. Priming of the neutrophil respiratory burst: role in host defense and inflammation. *Immunol Rev*. 2016;273(1):180-193. doi:10.1111/imr.12447

187. Dahlgren C, Karlsson A, Bylund J. Intracellular Neutrophil Oxidants: From Laboratory Curiosity to Clinical Reality. *J Immunol*. 2019;202(11):3127-3134. doi:10.4049/jimmunol.1900235

188. Anselmi NK, Bynum K, Kay JG, Visser MB. Analysis of Neutrophil Responses to Biological Exposures. *Curr Protoc*. 2023;3(6):e827. doi:10.1002/cpz1.827

189. O'Brien M, Moehring D, Muñoz-Planillo R, et al. A bioluminescent caspase-1 activity assay rapidly monitors inflammasome activation in cells. *J Immunol Methods*. 2017;447:1-13. doi:10.1016/j.jim.2017.03.004

190. Talley S, Kalinina O, Winek M, et al. A Caspase-1 Biosensor to Monitor the Progression of Inflammation In Vivo. *J Immunol*. 2019;203(9):2497-2507. doi:10.4049/jimmunol.1900619

191. Downs KP, Nguyen H, Dorfleutner A, Stehlik C. An overview of the non-canonical inflammasome. *Mol Aspects Med*. 2020;76:100924. doi:10.1016/j.mam.2020.100924

192. Shi J, Gao W, Shao F. Pyroptosis: Gasdermin-Mediated Programmed Necrotic Cell Death. *Trends Biochem Sci*. 2017;42(4):245-254. doi:10.1016/j.tibs.2016.10.004

193. Kovacs SB, Miao EA. Gasdermins: Effectors of Pyroptosis. *Trends Cell Biol*. 2017;27(9):673-684. doi:10.1016/j.tcb.2017.05.005

194. Fan X, Li Q, Wang Y, et al. Non-canonical NF-κB contributes to endothelial pyroptosis and atherogenesis dependent on IRF-1. *Transl Res*. 2023;255:1-13. doi:10.1016/j.trsl.2022.11.001

195. Keoni CL, Brown TL. Inhibition of Apoptosis and Efficacy of Pan Caspase Inhibitor, Q-VD-OPh, in Models of Human Disease. *J Cell Death*. 2015;8:1-7. Published 2015 Apr 8. doi:10.4137/JCD.S23844

196. Alphonse MP, Rubens JH, Ortines RV, et al. Pan-caspase inhibition as a potential host-directed immunotherapy against MRSA and other bacterial skin infections. *Sci Transl Med*. 2021;13(601):eabe9887. doi:10.1126/scitranslmed.abe9887

197. Zughaier SM, Zimmer SM, Datta A, Carlson RW, Stephens DS. Differential induction of the toll-like receptor 4-MyD88-dependent and -independent signaling pathways by endotoxins [published correction appears in Infect Immun. 2006 May;74(5):3077]. Infect Immun. 2005;73(5):2940-2950. doi:10.1128/IAI.73.5.2940-2950.2005

198. Akdis CA, Arkwright PD, BrvºggenMC, et al. Type 2 immunity in the skin and lungs. Allergy. 2020;75(7):1582-1605. doi:10.1111/all.14318

199. Nagareddy PR, Sreejit G, Abo-Aly M, et al. NETosis Is Required for S100A8/A9-Induced Granulopoiesis After Myocardial Infarction. Arterioscler Thromb Vasc Biol. 2020;40(11):2805-2807. doi:10.1161/ATVBAHA.120.314807

200. Zhang H, Niesel DW, Peterson JW, Klimpel GR. Lipoprotein release by bacteria: potential factor in bacterial pathogenesis. Infect Immun. 1998;66(11):5196-5201. doi:10.1128/IAI.66.11.5196-5201.1998

201. Moreira-Teixeira L, Stimpson PJ, Stavropoulos E, et al. Type I IFN exacerbates disease in tuberculosis-susceptible mice by inducing neutrophil-mediated lung inflammation and NETosis. Nat Commun. 2020;11(1):5566. Published 2020 Nov 4. doi:10.1038/s41467-020-19412-6

202. Chen T, Li Y, Sun R, et al. Receptor-Mediated NETosis on Neutrophils. Front Immunol. 2021;12:775267. Published 2021 Nov 4. doi:10.3389/fimmu.2021.775267

203. Han J. MyD88 beyond Toll. Nat Immunol. 2006;7(4):370-371. doi:10.1038/ni0406-370

204. Wu DC, Chan WW, Metelitsa AI, Fiorillo L, Lin AN. Pseudomonas skin infection: clinical features, epidemiology, and management. Am J Clin Dermatol. 2011;12(3):157-169. doi:10.2165/11539770-000000000-00000

205. Law SM, Gray RD. Neutrophil extracellular traps and the dysfunctional innate immune response of cystic fibrosis lung disease: a review. J Inflamm (Lond). 2017;14:29. Published 2017 Dec 28. doi:10.1186/s12950-017-0176-1

206. Fujitani S, Sun HY, Yu VL, Weingarten JA. Pneumonia due to Pseudomonas aeruginosa: part I: epidemiology, clinical diagnosis, and source. Chest. 2011;139(4):909-919. doi:10.1378/chest.10-0166

207. Boxio R, Bossenmeyer-Pourié C, Steinckwich N, Dournon C, Nüsse O. Mouse bone marrow contains large numbers of functionally competent neutrophils. *J Leukoc Biol*. 2004;75(4):604-611. doi:10.1189/jlb.0703340

208. Kuhns DB, Priel DAL, Chu J, Zarember KA. Isolation and Functional Analysis of Human Neutrophils. Curr Protoc Immunol. 2015;111:7.23.1-7.23.16. Published 2015 Nov 2. doi:10.1002/0471142735.im0723s111

209. Aslam M. Introducing Kolmogorov-Smirnov Tests under Uncertainty: An Application to Radioactive Data. ACS Omega. 2019;5(1):914-917. Published 2019 Dec 31. doi:10.1021/acsomega.9b03940

210. Lampariello F. On the use of the Kolmogorov-Smirnov statistical test for immunofluorescence histogram comparison. Cytometry. 2000;39(3):179-188. doi:10.1002/(SICI)1097-0320(20000301)39:3<179::AID-CYTO2>3.0.CO;2-I

211. Li P, Li M, Lindberg MR, Kennett MJ, Xiong N, Wang Y. PAD4 is essential for antibacterial innate immunity mediated by neutrophil extracellular traps. J Exp Med. 2010;207(9):1853-1862. doi:10.1084/jem.20100239

212. Martinod K, Witsch T, Farley K, Gallant M, Remold-O'Donnell E, Wagner DD. Neutrophil elastase-deficient mice form neutrophil extracellular traps in an experimental model of deep vein thrombosis. J Thromb Haemost. 2016;14(3):551-558. doi:10.1111/jth.13239

213. Bergsbaken T, Fink SL, Cookson BT. Pyroptosis: host cell death and inflammation. Nat Rev Microbiol. 2009;7(2):99-109. doi:10.1038/nrmicro2070

214. Glatman Zaretsky A, Engiles JB, Hunter CA. Infection-induced changes in hematopoiesis. J Immunol. 2014;192(1):27-33. doi:10.4049/jimmunol.1302061

215. Boiko JR, Borghesi L. Hematopoiesis sculpted by pathogens: Toll-like receptors and inflammatory mediators directly activate stem cells. Cytokine. 2012;57(1):1-8. doi:10.1016/j.cyto.2011.10.005

216. Zhang X, Karatepe K, Chiewchengchol D, et al. Bacteria-Induced Acute Inflammation Does Not Reduce the Long-Term Reconstitution Capacity of Bone Marrow Hematopoietic Stem Cells. Front Immunol. 2020;11:626. Published 2020 Apr 16. doi:10.3389/fimmu.2020.00626

217. Pascutti MF, Erkelens MN, Nolte MA. Impact of Viral Infections on Hematopoiesis: From Beneficial to Detrimental Effects on Bone Marrow Output. Front Immunol. 2016;7:364. Published 2016 Sep 16. doi:10.3389/fimmu.2016.00364

218. Takizawa H, Boettcher S, Manz MG. Demand-adapted regulation of early hematopoiesis in infection and inflammation. Blood. 2012;119(13):2991-3002. doi:10.1182/blood-2011-12-380113

219. Skerrett SJ, Liggitt HD, Hajjar AM, Wilson CB. Cutting edge: myeloid differentiation factor 88 is essential for pulmonary host defense against Pseudomonas aeruginosa but not Staphylococcus aureus. *J Immunol*. 2004;172(6):3377-3381. doi:10.4049/jimmunol.172.6.3377

220. Sweere JM, Ishak H, Sunkari V, et al. The Immune Response to Chronic *Pseudomonas aeruginosa* Wound Infection in Immunocompetent Mice. *Adv Wound Care (New Rochelle)*. 2020;9(2):35-47. doi:10.1089/wound.2019.1039

221. Takizawa H, Manz MG. Impact of inflammation on early hematopoiesis and the microenvironment. Int J Hematol. 2017;106(1):27-33. doi:10.1007/s12185-017-2266-5

222. Kovtonyuk LV, Fritsch K, Feng X, Manz MG, Takizawa H. Inflamm-Aging of Hematopoiesis, Hematopoietic Stem Cells, and the Bone Marrow Microenvironment. Front Immunol. 2016;7:502. Published 2016 Nov 14. doi:10.3389/fimmu.2016.00502

223. Kovtonyuk LV, Caiado F, Garcia-Martin S, et al. IL-1 mediates microbiome-induced inflammaging of hematopoietic stem cells in mice. Blood. 2022;139(1):44-58. doi:10.1182/blood.2021011570

224. Sims JE, Smith DE. The IL-1 family: regulators of immunity. Nat Rev Immunol. 2010;10(2):89-102. doi:10.1038/nri2691

225. PV•lsson-McDermott EM, O'Neill LA. Signal transduction by the lipopolysaccharide receptor, Toll-like receptor-4. Immunology. 2004;113(2):153-162. doi:10.1111/j.1365-2567.2004.01976.x

226. Schultz MJ, Rijneveld AW, Florquin S, Edwards CK, Dinarello CA, van der Poll T. Role of interleukin-1 in the pulmonary immune response during Pseudomonas aeruginosa pneumonia. Am J Physiol Lung Cell Mol Physiol. 2002;282(2):L285-L290. doi:10.1152/ajplung.00461.2000

227. Huszczynski SM, Lam JS, Khursigara CM. The Role of Pseudomonas aeruginosa Lipopolysaccharide in Bacterial Pathogenesis and Physiology. Pathogens. 2019;9(1):6. Published 2019 Dec 19. doi:10.3390/pathogens9010006

228. Wang G, Sweren E, Liu H, et al. Bacteria induce skin regeneration via IL-1Œ≤ signaling. Cell Host Microbe. 2021;29(5):777-791.e6. doi:10.1016/j.chom.2021.03.003

229. Feng CG, Scanga CA, Collazo-Custodio CM, et al. Mice lacking myeloid differentiation factor 88 display profound defects in host resistance and immune responses to Mycobacterium avium infection not exhibited by Toll-like receptor 2 (TLR2)- and TLR4-deficient animals. J Immunol. 2003;171(9):4758-4764. doi:10.4049/jimmunol.171.9.4758

230. Ma Z, Liu J, Wu W, et al. The IL-1R/TLR signaling pathway is essential for efficient CD8+ T-cell responses against hepatitis B virus in the hydrodynamic injection mouse model. Cell Mol Immunol. 2017;14(12):997-1008. doi:10.1038/cmi.2017.43

231. Liu T, Zhang L, Joo D, Sun SC. NF-ŒʃB signaling in inflammation. Signal Transduct Target Ther. 2017;2:17023-. doi:10.1038/sigtrans.2017.23

232. Lu YC, Yeh WC, Ohashi PS. LPS/TLR4 signal transduction pathway. Cytokine. 2008;42(2):145-151. doi:10.1016/j.cyto.2008.01.006

233. Picard C, Puel A, Bonnet M, et al. Pyogenic bacterial infections in humans with IRAK-4 deficiency. Science. 2003;299(5615):2076-2079. doi:10.1126/science.1081902

234. Church D, Elsayed S, Reid O, Winston B, Lindsay R. Burn wound infections. Clin Microbiol Rev. 2006;19(2):403-434. doi:10.1128/CMR.19.2.403-434.2006

235. Kroken AR, Gajenthra Kumar N, Yahr TL, et al. Exotoxin S secreted by internalized Pseudomonas aeruginosa delays lytic host cell death. *PLoS Pathog*. 2022;18(2):e1010306. Published 2022 Feb 7. doi:10.1371/journal.ppat.1010306

236. Schindelin, J., Arganda-Carreras, I., Frise, E., Kaynig, V., Longair, M., Pietzsch, T., … Cardona, A. (2012). Fiji: an open-source platform for biological-image analysis. *Nature Methods*, *9*(7), 676–682. doi:10.1038/nmeth.2019